ZESZYTY NAUKOWE
POLITECHNIKI RZESZOWSKIEJ

SCIENTIFIC LETTERS
OF RZESZOW UNIVERSITY OF TECHNOLOGY

MECHANIKA

Rocznik
Tom 39
zeszyt 94 (2022)

WYDZIAŁ
BUDOWY MASZYN
I LOTNICTWA
POLITECHNIKI RZESZOWSKIEJ

Wydano za zgodą Rektora

p-ISSN 0209-2689
e-ISSN 2300-5211

Wersja elektroniczna czasopisma jest wersją pierwotną

Redakcja czasopisma: Politechnika Rzeszowska, Wydział Budowy Maszyn i Lotnictwa
al. Powstańców Warszawy 8, 35-959 Rzeszów (e-mail: tomtrz@prz.edu.pl)
http://oficyna.prz.edu.pl/pl/zeszyty-naukowe/mechanika

Wydawca: Oficyna Wydawnicza Politechniki Rzeszowskiej
al. Powstańców Warszawy 12, 35-959 Rzeszów
http://oficyna.prz.edu.pl

SPIS TREŚCI

ZESZYTY NAUKOWE POLITECHNIKI RZESZOWSKIEJ – MECHANIKA
SCIENTIFIC LETTERS OF RZESZOW UNIVERSITY OF TECHNOLOGY – MECHANICS
94 (2022), s. 5-22

Stanisław ANTAS[1]

METODA OBLICZEŃ PARAMETRÓW STOPNIA TURBINY CHŁODZONEJ W PROJEKCIE KONCEPCYJNYM ZESPOŁU

Streszczenie: W pracy przedstawiono podstawowe rodzaje układów chłodzenia turbin lotniczych silników przepływowych oraz zasadnicze metody chłodzenia łopatek wieńców stopnia turbiny. W głównej części artykułu zaprezentowano metodę wyznaczania parametrów strumienia w przekrojach wyjściowych wieńców stopnia turbiny chłodzonej, polegającej na wykonaniu w pierwszym etapie obliczeń parametrów termicznych i kinematycznych strumienia oraz geometrycznych na średnicy średniej w stopniu niechłodzonym. Drugi etap metody obejmuje korektę parametrów spalin oraz parametrów geometrycznych profili wieńca dyszowego i wirnikowego w stopniu chłodzonym. Metoda może być stosowana w trakcie realizacji projektu koncepcyjnego stopnia osiowej turbiny chłodzonej, a oparto ją na równaniu zachowania energii, równaniu ciągłości przepływu, równaniu Eulera, pierwszej zasadzie termodynamiki oraz definicjach współczynników używanych w teorii maszyn wirnikowych. Końcowa część pracy zawiera zalecenia dotyczące parametrów geometrycznych profili wieńców chłodzonych oraz wnioski.

Słowa kluczowe: turbina osiowa, metoda obliczeń, stopień chłodzony

Nomenklatura

b – cięciwa profilu
c – prędkość bezwzględna
d – grubość spływu łopatki
D – średnica
i – entalpia statyczna
k – wykładnik izentropy
l – praca właściwa
$\dot{m}$ – strumień masy
R – indywidualna stała gazowa
t – podziałka palisady

[1] Autor do korespondencji/Corresponding author: Stanisław Antas, Politechnika Rzeszowska, Katedra Inżynierii Lotniczej i Kosmicznej, al. Powstańców Warszawy 8, 35-959 Rzeszów, e-mail: santas@prz.edu.pl, ORCID ID: 0000-0001-6241-7061

T – temperatura statyczna
u – prędkość obwodowa
w – prędkość względna
α – kąt kierunkowy prędkości bezwzględnej
θ – współczynnik efektywności chłodzenia wieńca stopnia
π – spręż/rozpręż
ρ – reakcyjność
τ – względne zużycie paliwa
φ – współczynnik strat prędkości bezwzględnej w wieńcu dyszowym
ψ - współczynnik strat prędkości względnej w wieńcu wirnikowym
ν – względny strumień masy czynnika

Indeksy

$/_{KS}$ – dotyczy parametru komory spalania
$/_{S}$ – dotyczy parametru sprężarki
$/_{T}$ – dotyczy parametru turbiny
$/_{TS}$ – dotyczy parametru turbiny wytwornicowej
$/_{chł}$ – dotyczy parametru związanego z chłodzeniem
$/_{g}$ – dotyczy parametru związanego z gardzielą wieńca
$/_{m}$ – dotyczy parametru materiału łopatki
$/_{M}$ – dotyczy parametru mieszaniny spalin i powietrza
$/_{st}$ – dotyczy parametru stopnia
$/_{śr}$ – dotyczy parametru na średnicy średniej
$/_{u}$ – dotyczy parametru upustu
$/_{w}$ – dotyczy parametru względnego
$/_{0,1,2}$ – dotyczy parametru związanego z odpowiednim przekrojem kontrolnym
$/'$ – dotyczy parametru spalin
$/^{*}$ – dotyczy parametru spiętrzenia

1. Wprowadzenie

Od początku rozwoju konstrukcyjnego turbin silników lotniczych obserwuje się tendencję do podwyższania temperatury spiętrzenia spalin T_0^* przed ich wieńcami dyszowymi tzn. na wlocie do turbiny wytwornicowej – rys. 1.

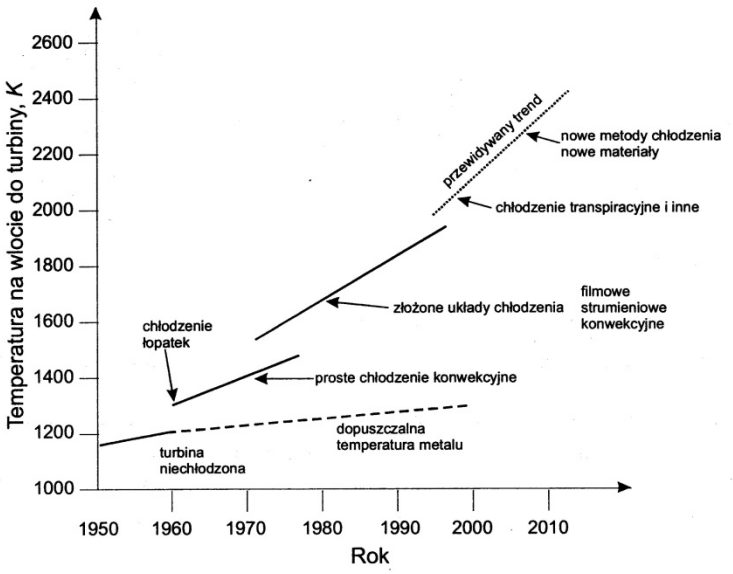

Rys. 1. Zmiany temperatury spiętrzenia spalin na wlocie do turbiny w latach (Nowak, 2011)
Fig. 1. Changes of gas stagnation temperature at the turbine inlet in the years (Nowak, 2011)

W produkowanych seryjnie współczesnych silnikach lotniczych temperatura spiętrzenia spalin na wylocie komory spalania zawiera się zwykle w przedziale wartości $T_0^*=1100 \ldots 2000$ *K*. Niestety wytwarzane obecnie stopy żarowytrzymałe oraz nadstopy niklu i kobaltu stosowane na elementy składowe turbin nie wytrzymują temperatur roboczych znacznie przewyższających 1200 K. Stąd przy temperaturze spalin $T_0^*>1200$ *K* wynika konieczność chłodzenia najbardziej nagrzewających się podzespołów, a mianowicie łopatek wieńców dyszowych i wirnikowych, tarcz nośnych wirników i części kadłubów (Antas & Wolański, 1989; Kułagin i in., 2009).

Układy chłodzenia turbin mogą być podzielone na zamknięte i otwarte (Łokaj i in., 1979). W układach zamkniętych ciekły lub gazowy czynnik chłodzący pobiera ciepło od elementów chłodzonych, które następnie oddawane jest w chłodnicy powietrznej lub paliwowej. W układach otwartych chłodziwem jest powietrze sprężone, które następnie jest kierowane do kanału przepływowego turbiny. Takie układy dzięki swojej prostocie konstrukcyjnej uzyskały szerokie zastosowanie w turbinach lotniczych, chociaż bardziej złożone konstrukcyjnie, o zwiększonych kosztach wytwarzania, układy zamknięte mogą także zapewniać intensywne chłodzenie łopatek ($T_0^* \leq 2000$ *K*).

Elementy kadłubów turbin są chłodzone powietrzem pobieranym zza wentylatora lub sprężarki niskiego ciśnienia, natomiast wieńce dyszowe oraz części ich wirników chłodzone są powietrzem upuszczanym za jednym ze środkowych stopni sprężarki, a najczęściej za ostatnim jej stopniem lub powietrzem wtórnym

pobieranym z osłony komory spalania. Powietrze chłodzące może być odprowadzane z kanału przepływowego silnika otworami równomiernie rozmieszczonymi na obwodzie kadłubów sprężarek lub komór spalania do kolektorów, z których przewodami rurowymi jest kierowane do odpowiednich miejsc w kadłubach turbin oraz wieńców dyszowych lub pobierane jest przez otwory w wirniku i przepływając przez przestrzenie wewnętrzne dociera do elementów wirników turbin – rys. 2.

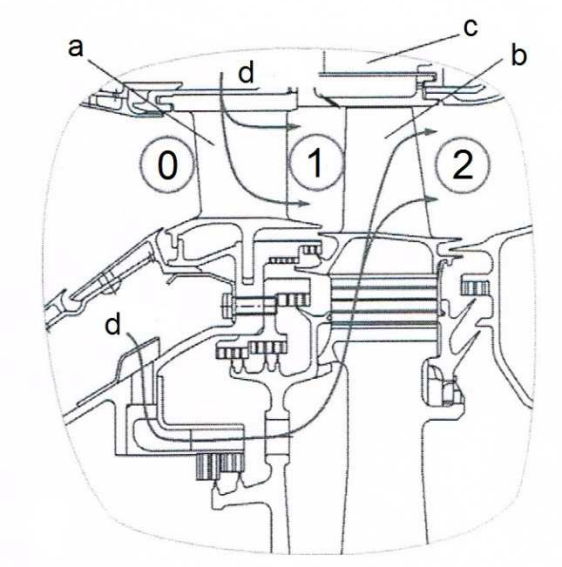

Rys. 2. Schemat konstrukcji kanału przepływowego jednostopniowej turbiny z chłodzeniem wewnętrznym łopatek: a – wieniec dyszowy, b – wieniec wirnikowy, c – kadłub turbiny, d – powietrze chłodzące; 0, 1, 2 – charakterystyczne przekroje stopnia – na podstawie Inoziemcew i in. (2008)

Fig. 2. Diagram of the flow channel structure of a single-stage turbine with internal blade cooling: a – nozzle rim, b – rotor rim, c – turbine housing, d – cooling air; 0, 1, 2 – characteristic cross sections of the turbine stage – prepared on the basis of Inoziemcew et al. (2008)

2. Metody chłodzenia łopatek

W lotniczych silnikach turbinowych w zależności od mechanizmu zastosowanego do chłodzenia wyróżnia się dwie główne metody chłodzenia łopatek tj.: zewnętrzną i wewnętrzną.

Zewnętrzna metoda chłodzenia łopatek polega na odprowadzaniu ciepła od łopatek do tarcz wirnika poprzez przewodzenie. Chłodzenie takie jest efektem mechanicznego styku powierzchni zamków łopatek z powierzchniami wrębów na zamki łopatek wykonanych w tarczy, która jest dla łopatek „chłodnicą". Temperatury tarcz w części wieńcowej sięgają wartości 850…950 K, zaś w części

centralnej 500…650 K. Chłodzenie takie jest stosowane przede wszystkim w turbinach o małych rozmiarach łopatek tj. o długości rzędu 30…40 mm i małych grubościach gdzie trudno jest zastosować wewnętrzne sposoby chłodzenia. Taki sposób chłodzenia umożliwia obniżenie temperatury przyzamkowej części łopatki o 50…60 K (Łokaj i in., 1979; Szczeciński i in., 1984).

Wewnętrzna metoda chłodzenia łopatek wykorzystuje głównie następujące sposoby chłodzenia:

- chłodzenie konwekcyjne, w którym powietrze chłodzące przepływa przez walcowe wewnętrzne kanały chłodzące łopatki od jej stopki ku wierzchołkowi (rys. 3 a) lub z przepływem poprzecznym czynnika w kanałach chłodzących wkładki - deflektora w ich wnętrzu i jego wypływem otworami na krawędzi spływu (rys. 3. b).Wymieniony rodzaj chłodzenia jest konstrukcyjnie i technologicznie prosty, a jego zastosowanie jest efektywne do poziomu temperatury spalin $T_0^*=1450 \ldots 1500$ *K.* Należy zauważyć, że chłodzenie konwekcyjne łopatek wieńca wirnika turbiny zastosowano już w pierwszym produkowanym seryjnie niemieckim silniku odrzutowym Jumo 004B.
- chłodzenie konwekcyjno-błonowe (błonkowe, filmowe, warstwowe, z owiewem) polegające na wytworzeniu wokół profilu cienkiej błony powietrza wypływającego przez szereg otworów na ściance łopatki, które owiewa ją od zewnątrz, oddzielając gorące spaliny od powierzchni łopatki. Jednocześnie, powietrze przepływające przez kanały wnętrza łopatki chłodzą je drogą konwekcji - rys. 3 c. Wykorzystanie tego sposobu chłodzenia jest celowe dla zakresu temperatur spalin $T_0^*=1500 \ldots 1600$ *K;*
- chłodzenie transpiracyjne (z powłoką porowatą) polega na wykorzystaniu powłoki porowatej na powierzchni łopatki. Powietrze chłodzące doprowadzane jest rowkami podłużnymi w rdzeniu łopatki, a następnie przez pory powłoki przedostaje się do warstwy przyściennej izolującej materiał łopatki przed wpływem wysokiej temperatury spalin-rys. 3d. Chłodzenie tego typu wydaje najbardziej perspektywicznym i efektywnym dla temperatur spalin $T_0^*=1800 \ldots 2200$ *K*, stanowiąc odmianę chłodzenia błonowego o równomiernym wypływie czynnika.

Chłodzenie transpiracyjne współcześnie nie znajduje szerszego zastosowania ze względu na brak dostatecznie niezawodnych materiałów ceramicznych oraz problemów natury eksploatacyjnej, związanych z zatykaniem się kanalików. Odmianą tej metody jest chłodzenie efuzyjne, w którym powietrze chłodzące przepływa przez mikrokanaliki o rozmiarze rzędu 10 μm, wykonane w powłoce metalowej na powierzchni łopatki. Szczegółowy przegląd mechanizmów chłodzenia wewnętrznego łopatek turbin podano w pracach Nowak (2011), Farokhi (2014), Lakshminarayana (1996) oraz Madejski (1988).

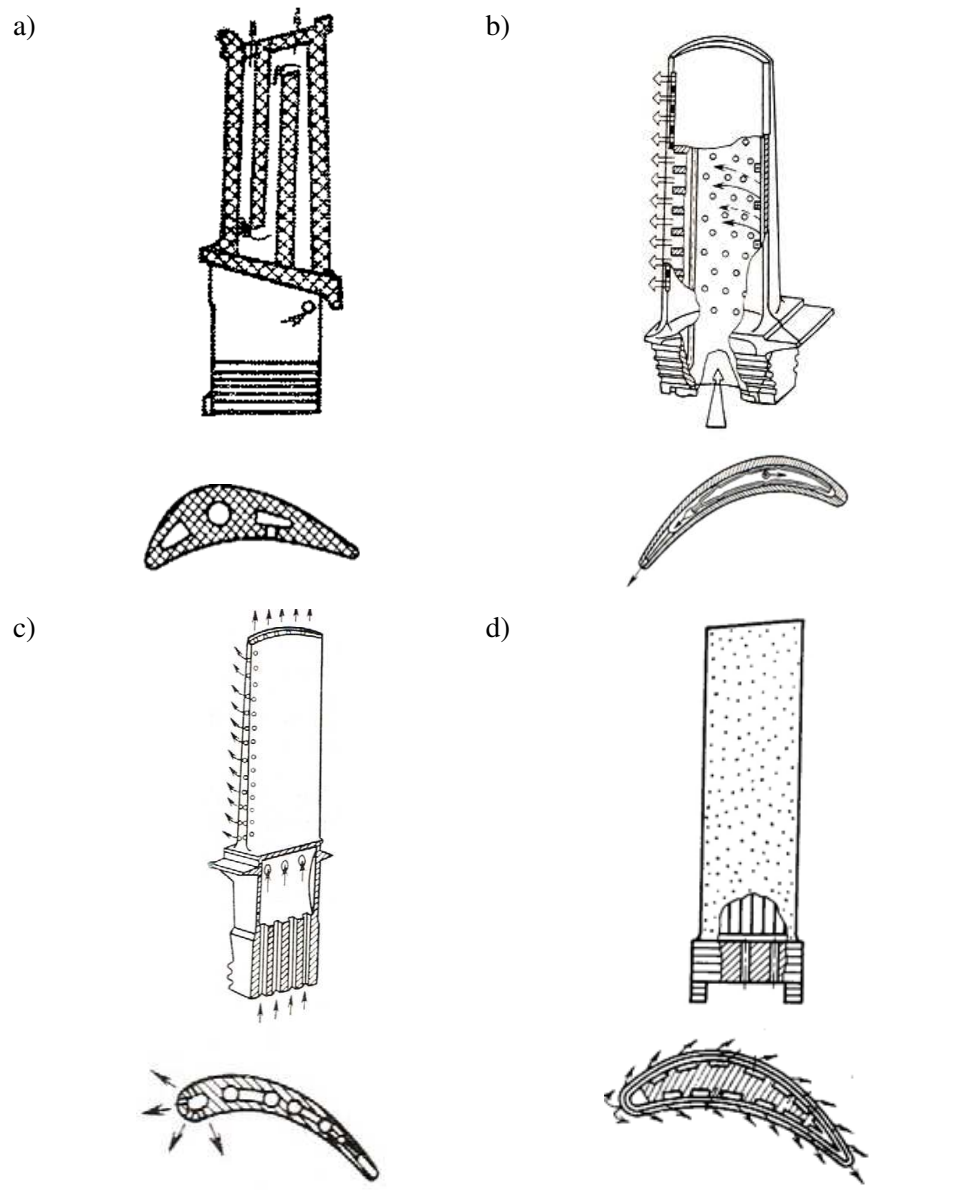

Rys. 3. Zasadnicze mechanizmy chłodzenia wewnętrznego łopatek: a – chłodzenie konwekcyjne z kanałami wzdłużnymi (Kopeliew & Tichonov, 1974), b – chłodzenie konwekcyjne z deflektorem (Kopeliew, 1983), c – chłodzenie konwekcyjno-błonowe (Nieczajew & Fiedorow, 1977), d – chłodzenie transpiracyjne (Łokaj i in., 1979)

Fig. 3. The main internal cooling mechanisms of the blades: a – convection cooling with longitudinal channels (Kopeliew & Tichonov, 1974), b – convective cooling with a deflector (Kopeliew, 1983), c – convection film cooling (Nieczajew & Fiedorow, 1977), d – transpiration cooling (Łokaj et al., 1979)

Współcześnie najczęściej stosuje się złożone układy chłodzenia łopatek, stanowiące kombinacje kilku mechanizmów chłodzenia jednocześnie (Sieniawski, 1995).

3. Parametry strumienia na wylocie wieńców

Sumaryczna ilość powietrza, które należy odprowadzić ze sprężarki lub osłony komory spalania i skierować do układu chłodzenia równa jest sumie strumieni powietrza niezbędnych do obniżenia temperatury poszczególnych elementów składowych kanału przepływowego turbiny. W praktyce inżynierskiej wielkość tę przyjęto charakteryzować względnym strumieniem masy powietrza odprowadzanego w celu chłodzenia turbiny (Ziricki i in., 1971):

$$\nu_{chł} = \frac{\dot{m}_{chł}}{\dot{m}_1} \tag{1}$$

gdzie: $\dot{m}_{chł}$ - strumień masy powietrza chłodzącego,
$\dot{m}_1$ - strumień masy powietrza na wejściu do sprężarki w zakresie startowym.

Lub według autorów pracy Kopielew i Tichonow (1974):

$$\nu'_{chł} = \frac{\dot{m}_{chł}}{(\dot{m}_g)_{TS}} \tag{2}$$

gdzie: strumień masy spalin przepływających przez przekrój minimalny wieńca dyszowego pierwszego stopnia turbiny wytwornicowej $(\dot{m}_g)_{TS}$:

$$\dot{m}'_0 = (\dot{m}_g)_{TS} = \dot{m}_1(1 - \nu_{uS} - \nu_{uKS})(1 + \tau) \tag{3}$$

gdy: względna wartość strumienia masy powietrza odprowadzanego ze sprężarki $\nu_{uS} = 0$, wówczas względna wartość strumienia masy powietrza odprowadzanego z osłony komory spalania (na potrzeby chłodzenia turbiny):

$$\nu_{uKS} = \frac{\dot{m}_{uKS}}{\dot{m}_1} \tag{4}$$

jest równa $\nu_{chł}$, bowiem: $\dot{m}_{chł} = \dot{m}_{uKS}$, zatem relację (3) można zapisać następująco:

$$\dot{m}'_0 = (\dot{m}_g)_{TS} = \dot{m}_1 (1 - \nu_{chł}) (1 + \tau) \tag{5}$$

Podstawiając powyższą zależność do reguły (3) otrzymuje się:

$$\nu'_{chł} = \frac{\dot{m}_{chł}}{\dot{m}_1 (1 - \nu_{chł}) (1 + \tau)} \tag{6}$$

stąd, po uwzględnieniu formuły definicyjnej (1) uzyskuje się:

$$\nu'_{ch\text{ł}} = \frac{\nu_{ch\text{ł}}}{(1-\nu_{ch\text{ł}})\,(1+\tau)} \tag{7}$$

gdzie: $\tau = 0{,}01 \div 0{,}02$- względne zużycie paliwa w głównej komorze spalania

Ponieważ mianownik powyższej równości: $(1-\nu_{ch\text{ł}})\,(1+\tau) \cong 1$ zatem można przyjmować

$$\nu'_{ch\text{ł}} \cong \nu_{ch\text{ł}} \tag{8}$$

Im mniejsza wartość $\nu_{ch\text{ł}}$ do uzyskania zadanego poziomu temperatur, tym ekonomiczniejszy układ chłodzenia. W pierwszym przybliżeniu, wartość $\nu_{ch\text{ł}}$ dla silników o dużym resursie ($R_S > 3000h$) można określić na podstawie ogólnych (statystycznych) zaleceń (Antas & Wolański, 1989; Łokaj i in., 1979):

1. Wieńce łopatek mogą być niechłodzone, jeśli temperatura spiętrzenia spalin przed wieńcem dyszowym wynosi odpowiednio: $T_0^* \leq 1270\ K$, zaś przed wieńcem łopatek wirnikowych $T_{1w}^* \leq 1170\ K$, gdzie temperaturę spiętrzenia spalin w ruchu względnym przed wieńcem wirnika określa relacja (Kułagin i in., 2005):

$$T_{1w}^* = T_2^* + \frac{u_{2sr}^2}{2\dfrac{k'R'}{k'-1}} \tag{9}$$

gdzie:
T_2^* - temperatura spiętrzenia spalin w ruchu bezwzględnym na wylocie wirnika stopnia,
u_{2sr} – prędkość obwodowa na średnicy średniej w przekroju wyjściowym wirnika stopnia turbiny.

lub według relacji (Biełusow i in., 2003):

$$T_{1w}^* = T_{2w}^* = T_2^* - \frac{c_2^2 - w_2^2}{2\dfrac{k'R'}{k'-1}} \tag{10}$$

Ciągły postęp w inżynierii materiałów na łopatki turbin pozwala na podnoszenie wymienionych powyżej granicznych wartości temperatur spiętrzenia spalin T_0^* oraz T_{1w}^* o około 5…10 K rocznie (Pawlenko i Wołow, 2007).

2. W przypadku temperatury spiętrzenia spalin na wlocie stopnia turbiny $T_0^* < 1250\ K$ chłodzenie zamków łopatek wirnikowych i tarczy wirnika wymaga $\nu_{ch\text{ł}} \cong 0{,}5\%$.

3. Podwyższenie temperatury spiętrzenia spalin przed wieńcem łopatkowym o
   $\Delta T^* = 100\ K$ ponad wartości podane w p. 1 wymaga:
   - przy wewnętrznym chłodzeniu konwekcyjnym- 0,8 – 1,2 %;
   - przy chłodzeniu błonkowym – 0,6 – 0.9 %,
   - przy chłodzeniu transpiracyjnym (efuzyjnym) – 0,4 – 0,6 % strumienia masy powietrza dopływającego do sprężarki $\dot{m}_1$w warunkach startowych, dla każdego chłodzonego wieńca.

Zazwyczaj przy $T_0^* \leq 1350\ K$ chłodzi się wyłącznie wieniec dyszowy pierwszego stopnia, przy $T_0^* \leq 1500\ K$ – trzy wieńce łopatkowe (tj. dyszowy i wirnikowy pierwszego stopnia oraz dyszowy drugiego stopnia), natomiast, gdy $T_0^* > 1600\ K$ – cztery (i więcej) kolejne wieńce łopatkowe.

Ilustrację graficzną powyższych zaleceń stanowi rys. 4, na którym zaznaczono wartości $\nu_{chł}$ dla prototypowych i seryjnych silników lotniczych z chłodzeniem wewnętrznym łopatek turbinowych. Wykres sporządzono na podstawie danych statystycznych lotniczych silników turbinowych wszystkich typów w przedziale temperatur spiętrzenia spalin przed turbiną $T_0^* = 1300 \div 1800\ K$ i spręży $\pi_0^* = 12 \div 28$.

Z wykresu 4 opracowanego na podstawie (Łokaj i in., 1985) odczytuje się sumaryczną wartość $\nu_{chł}$, która zgodnie z przyjętą temperaturą spiętrzenia spalin T_0^* odpowiada wymaganemu rodzajowi chłodzenia jej elementów składowych.

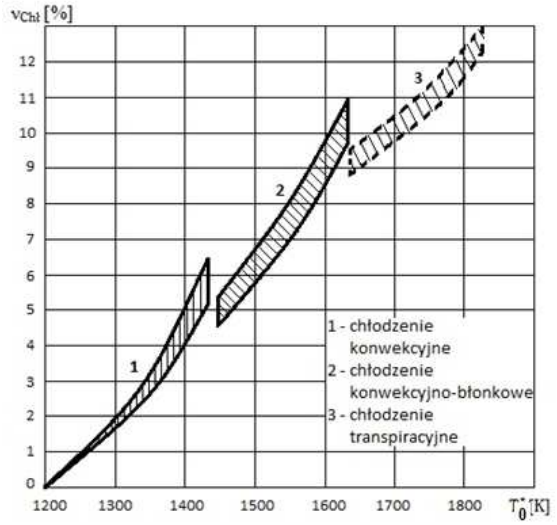

Rys. 4. Zależność względnego natężenia przepływu powietrza potrzebnego do chłodzenia wieńców turbiny od sposobu ich chłodzenia i wymaganej temperatury spalin przed turbiną

Fig. 4. The dependence of the relative air flow rate needed to cool the turbine rims based on the method of their cooling and the required gas temperature at inlet of the turbine

Po dobraniu wartości temperatury spiętrzenia spalin przed turbiną wytwornicową T_0^* z rys. 4 określa się wartość $\nu_{chł}$, a następnie ze wzoru (1) wyznacza się sumaryczny strumień masy powietrza upuszczanego ze sprężarki, niezbędnego do chłodzenia wszystkich elementów turbiny.

Dla zakresu temperatur spiętrzenia spalin $T_0^* = 1250 \div 1650\ K$ przebiegi przedstawione na powyższym rysunku można w przybliżeniu aproksymować relacją (Pawlenko i Wołow, 2007):

$$\nu_{chł} \cong 0{,}0285\ (T_0^* - 1250) \tag{11}$$

W przypadku chłodzenia transpiracyjnego sumaryczny względny strumień powietrza chłodzącego wieńce turbiny dla przedziału temperatur spiętrzenia spalin $T_0^* = 1650 \div 1850\ K$ aproksymuje formuła:

$$\nu_{chł} \cong 0{,}000175\ (T_0^* - 1650) + 0.095 \tag{12}$$

Konstruując silniki o zwiększonym resursie oraz silniki o małej przepustowości ($\dot{m}_1 < 10 \div 20\ kg/s$), szczególnie śmigłowe i śmigłowcowe, wartości $\nu_{chł}$ odczytane z rys. 4 należy zwiększyć ok. 1,5 razy.

W przypadkach większej ilości sumarycznej chłodzącego powietrza $\nu_{chł} > 5\%$, projektant winien uwzględnić również spadek sprawności izentropowej chłodzonej turbiny o około 2÷4,0 %.

Względny strumień masy powietrza odprowadzanego w celu chłodzenia elementów turbiny $\nu_{chł}$ jest miarą jakości zastosowanego układu chłodzenia. Im ten współczynnik jest niższy, tym wyższa jest sprawność wytwarzania energii w turbinie przy zadanej temperaturze spalin T_0^* na jej wlocie. Zmiany wartości sprawności turbin wytwornicowych η_T^* w zależności od temperatury spiętrzenia spalin na jej wlocie - T_0^* według badań firmy Rolls-Royce ilustruje rys. 5. Należy zauważyć, że turbiny wytwornicowe (wysokiego ciśnienia) cywilnych lotniczych silników turbinowych wykonuje się zarówno jako jednostopniowe (wysoko obciążone z rozprężem w parametrach spiętrzenia$\pi_T^* = \pi_{st}^* = 2{,}4 \div 4{,}5$ sięgając wartości 5,4) (Antas, 2006) jak i dwustopniowe (nisko obciążone) z rozprężem stopnia w parametrach spiętrzenia $\pi_{st}^* = 1{,}7 \div 2{,}2$ (2,5) oraz stosunkiem ciśnień spiętrzenia spalin w turbinie $\pi_T^* = 4{,}0 \div 5{,}5$ (Inoziemcew i in., 2008).

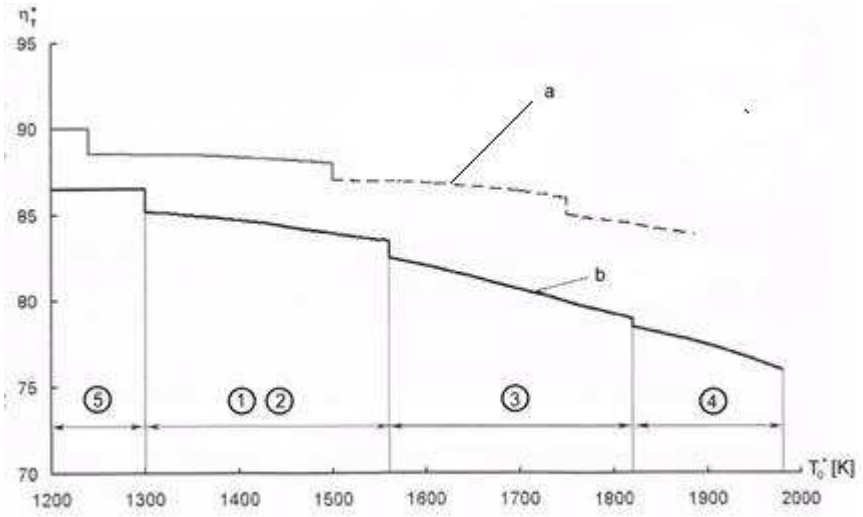

Rys. 5. Wpływ mechanizmów chłodzenia wewnętrznego łopatek wieńców turbiny wytwornicowej na jej sprawność: a – turbiny nisko obciążone, b – turbiny wysoko obciążone, 1 – chłodzenie konwekcyjne z kanałami wzdłużnymi, 2 – chłodzenie konwekcyjne z deflektorem, 3 – chłodzenie konwekcyjno-błonowe, 4 – chłodzenie transpiracyjne, 5 – turbiny niechłodzone – na podstawie Inoziemcew i in. (2008)

Fig. 5. Influence of the internal cooling mechanisms of the rim blades of gas-generator turbine on its efficiency: a – low-loaded turbines, b – highly-loaded turbines, 1 – convection cooling with longi-tudinal channels, 2 – convection cooling with a deflector, 3 – convection film cooling, 4 – transpiration cooling , 5 – uncooled turbines – prepared on the basis of Inoziemcew et al. (2008)

Drugi parametr oceny jakości chłodzenia stanowi współczynnik efektywności chłodzenia wieńca stopnia, traktowany jako bezwymiarowa temperatura łopatki. Jego wartość dla wieńców dyszowych określa zależność definicyjna:

$$\Theta_{0,1} = \frac{T_0^* - T_{m0,1}}{T_0^* - T_{ch\text{ł}}^*} \tag{13}$$

natomiast dla wieńców wirnikowych:

$$\Theta_{1,2} = \frac{T_{1w}^* - T_{m1,2}}{T_{1w}^* - T_{ch\text{ł}}^*} \tag{14}$$

gdzie:

T_0^* – temperatura spiętrzenia spalin w ruchu bezwzględnym przed wieńcem dyszowym,

T_{1w}^* – temperatura spiętrzenia spalin w ruchu względnym przed wieńcem wirnikowym,

$T_{m0,1}$, $T_{m1,2}$ – odpowiednio: temperatura statyczna materiału łopatki wieńca dyszowego i wirnikowego,

$T^*_{chł}$ – temperatura spiętrzenia czynnika chłodzącego, którą zwykle przyjmuje się równą temperaturze spiętrzenia powietrza w przekroju wyjściowym sprężarki – T^*_{2S} zarówno w odniesieniu do wieńca dyszowego jak i wirnikowego.

Dysponowanie statystyczną zależnością przebiegów wartości współczynnika efektywności chłodzenia wieńca (rys. 6) w zależności od wybranego rodzaju chłodzenia wewnętrznego łopatki wieńca turbiny i względnego strumienia masy powietrza chłodzącego umożliwia wyznaczenie temperatury materiału łopatki wieńca dyszowego:

$$T_{m0,1} = T^*_0 - \Theta_{0,1}(T^*_0 - T^*_{chł}) \tag{15}$$

oraz wirnikowego:

$$T_{m1,2} = T^*_{1w} - \Theta_{1,2}(T^*_{1w} - T^*_{chł}) \tag{16}$$

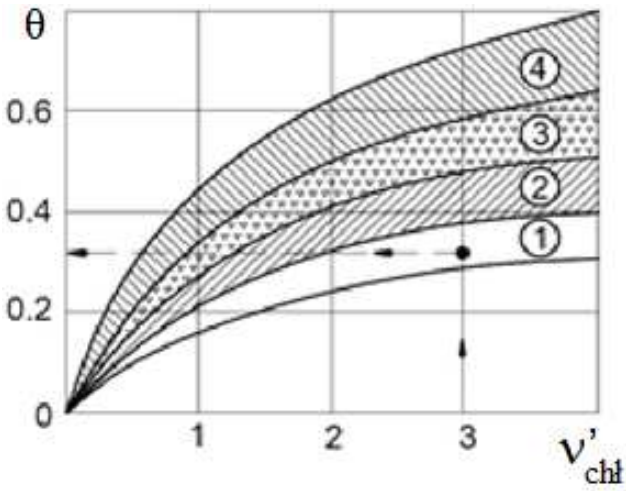

Rys. 6. Współczynnik efektywności chłodzenia wieńca w funkcji względnego strumienia masy powietrza chłodzącego wyrażonego w procentach dla różnych mechanizmów chłodzenia wieńca stopnia turbiny: 1 – chłodzenie konwekcyjne z kanałami wzdłużnymi, 2 – chłodzenie konwekcyjne z deflektorem, 3 – chłodzenie konwekcyjno-błonowe, 4 – chłodzenie transpiracyjne – na podstawie Kułagin i in. (2005)

Fig. 6. Coefficient of rim cooling efficiency as a function of the relative cooling air mass flow expressed as a percentage for various cooling mechanisms of the rim of the turbine stage: 1 – convection cooling with longitudinal channels, 2 – convection cooling with a deflector, 3 – convection film cooling, 4 – transpiration cooling – prepared on the basis of Kułagin et al. (2005)

Możliwe jest również określenie strumienia masy mieszaniny spalin i powietrza chłodzącego w przekrojach kontrolnych obliczanego stopnia turbiny:

– w przekroju wyjściowym (1-1) wieńca dyszowego:

$$\dot{m}_1' = \dot{m}_0' + \dot{m}_{ch\text{ł}0,1} \tag{17}$$

lub:

$$\dot{m}_1' = \dot{m}_0'\left(1 + \nu_{ch\text{ł}0,1}'\right) \tag{18}$$

– w przekroju wyjściowym (2-2) wieńca wirnikowego:

$$\dot{m}_2' = \dot{m}_1' + \dot{m}_{ch\text{ł}1,2} \tag{19}$$

oraz:

$$\dot{m}_2' = \dot{m}_0'\left(1 + \nu_{ch\text{ł}0,1}'\right)\left(1 + \nu_{ch\text{ł}1,2}'\right) \tag{20}$$

gdzie: $\dot{m}_0' = \left(\dot{m}_g\right)_{TS}$ – strumień masy spalin na wlocie wieńca dyszowego (z obliczeń termogazodynamicznych silnika).

$\nu_{ch\text{ł}0,1}'$, $\nu_{ch\text{ł}1,2}'$– odpowiednio: względny strumienia masy powietrza chłodzącego wieniec dyszowy i wirnikowy,

$\dot{m}_{ch\text{ł}0,1}$, $\dot{m}_{ch\text{ł}1,2}$ – odpowiednio: strumień masy powietrza chłodzącego wieniec dyszowy i wirnikowy,

Na rys. 6 przedstawiono przebiegi $\theta = f(\nu_{ch\text{ł}}')$ dla zasadniczych, omówionych wcześniej mechanizmów chłodzenia wieńców łopatek stopnia. Zwykle wartości względnego strumienia masy powietrza chłodzącego jeden wieniec łopatek stopnia zawiera się w przedziale 1,5–2,5%.

Kładąc, że ciepło właściwe mieszaniny spalin i powietrza za chłodzonym wieńcem stopnia jest praktycznie równe ciepłu właściwemu spalin strumienia głównego, wówczas temperatury spiętrzenia mieszaniny w odpowiednich przekrojach kontrolnych stopnia chłodzonego określają relacje (Mamaje i in., 1984):

– za wieńcem dyszowym:

$$T_{1M}^* = T_1^*\left(1 - \nu_{ch\text{ł}0,1}'\right) + \frac{i_{2S}^*}{i_1^*}\, T_1^* \nu_{ch\text{ł}0,1}' \tag{21}$$

gdzie:

T_1^* - temperatura spiętrzenia spalin w przekroju wylotowym wieńca dyszowego dla stopnia niechłodzonego,

i_{2S}^* - entalpia spiętrzenia powietrza w przekroju wyjściowym sprężarki,

i_1^* - entalpia spiętrzenia spalin w przekroju wylotowym wieńca dyszowego dla stopnia niechłodzonego.

– za wieńcem wirnikowym:

$$T_{2M}^{*} = T_{2}^{*}\left(1 - \nu'_{ch\text{ł}1,2}\right) + \frac{i_{2S}^{*}}{i_{2}^{*}}\, T_{2}^{*}\nu'_{ch\text{ł}1,2} \tag{22}$$

W zależności powyższej oznaczono przez:

T_2^* - temperaturę spiętrzenia spalin w przekroju wylotowym wieńca wirnikowego dla stopnia niechłodzonego,

i_2^* - entalpia spiętrzenia spalin w przekroju wylotowym wieńca wirnikowego dla stopnia niechłodzonego.

Zagadnienie szczegółowej analizy parametrów mieszaniny spalin oraz powietrza chłodzącego w stopniu turbiny chłodzonej przedstawiono w pracach Young & Wilcock (2002a, 2002b).

W przypadku chłodzenia wieńców stopnia turbiny, ze względu na dodatkowe straty energii związane z ich chłodzeniem, zmianie ulegają wartości współczynnika strat prędkości w wieńcu dyszowym $\varphi_{ch\text{ł}}$ i wirnikowym $\psi_{ch\text{ł}}$ (w stosunku do ich wartości w stopniu niechłodzonym tj. φ i ψ).

W chłodzeniu konwekcyjnym wieńców stopnia wartości $\varphi_{ch\text{ł}}$ oraz $\psi_{ch\text{ł}}$ można określać z zależności (Mamajew i in., 1984; Łokaj & Salnikow, 1979):

$$\varphi_{ch\text{ł}} = \varphi - (0{,}005 \div 0{,}007) \tag{23}$$

$$\psi_{ch\text{ł}} = \psi - (0{,}004 \div 0{,}006) \tag{24}$$

W przypadku chłodzenia konwekcyjno-błonowego (Biełousow i in., 2003; Łokaj & Salnikow, 1979):

$$\varphi_{ch\text{ł}} = \varphi - (0{,}013 \div 0{,}017) \tag{25}$$

$$\psi_{ch\text{ł}} = \psi - (0{,}008 \div 0{,}01) \tag{26}$$

W obliczeniach projektowych stopni turbiny wynika konieczność wprowadzenia korekty parametrów czynnika wynikająca z doprowadzenia do kanału przepływowego powietrza chłodzącego poszczególne wieńce. Pierwszy etap obliczeń projektu koncepcyjnego takich stopni ma analogiczny przebieg jak dla stopni niechłodzonych (Kopielew & Tichonow, 1974; Ziricki i in., 1971). W rezultacie tych obliczeń wyznacza się w odpowiednich przekrojach kontrolnych stopnia wartości temperatur spiętrzenia: $T_0^* = T_1^*$ oraz T_2^*, a także ciśnień spiętrzenia: p_0^*, p_1^*, p_2^* oraz parametrów kinematycznych i geometrycznych odpowiadających procesowi rozprężania spalin w stopniu niechłodzonym.

Po przeprowadzeniu tych obliczeń, wykonuje się drugi etap obliczeń parametrów strumienia na średnicy średniej wprowadzając wartości skorygowane parametrów spalin w stopniu chłodzonym: $\dot{m}_1'$, $\dot{m}_2'$, T_{1M}^*, T_{2M}^*, $\varphi_{ch\text{ł}}$, $\psi_{ch\text{ł}}$, które

należy wykorzystać do korekty wartości prędkości krytycznych dźwięku, liczb Lavala λ_1 i λ_2 oraz ciśnień spiętrzenia w przekrojach kontrolnych (1-1) i (2-2).

Temperatura spiętrzenia w ruchu względnym spalin jest wówczas określana z zależności (9) i (10) – skorygowanych:

$$T^*_{1wch\text{ł}} = T^*_{1M} - \frac{c_1^2 - w_1^2}{2\dfrac{k'R'}{k'-1}} \tag{27}$$

$$T^*_{2wch\text{ł}} = T^*_{2M} - \frac{c_2^2 - w_2^2}{2\dfrac{k'R'}{k'-1}} \tag{28}$$

4. Uwagi końcowe i wnioski

Potrzeba wykonania we wnętrzu łopatek chłodzonych kanałów niezbędnych dla obiegu powietrza chłodzącego wymaga także zmiany ich parametrów geometrycznych, które w odniesieniu do parametrów geometrycznych łopatek niechłodzonych mają następujące wartości (Dżygadło i in., 1982):

- gęstość palisady:

$$\left(\frac{b}{t}\right)_{ch\text{ł}} = (1{,}1 \div 1{,}2)\frac{b}{t} \tag{29}$$

- względna grubość profilu:

$$(\bar{c}_m)_{ch\text{ł}} = (1{,}2 \div 1{,}3)\bar{c}_m \tag{30}$$

dla wieńca dyszowego (Pawlenko & Wołow, 2007):

$$\left(\bar{c}_{m0,1}\right)_{ch\text{ł}} = 0{,}15 \div 0{,}2 \tag{31}$$

dla wieńca wirnikowego:

$$\left(\bar{c}_{m1,2}\right)_{ch\text{ł}} = 0{,}2 \div 0{,}25 \tag{32}$$

- względna grubość spływu łopatki:

$$\left(\bar{d}_2\right)_{ch\text{ł}} = \left(\frac{d_2}{a_g}\right)_{ch\text{ł}} \tag{33}$$

dla wieńca dyszowego i wirnikowego:

$$\left(\bar{d}_{2\,0,1}\right)_{ch\text{ł}} = \left(\bar{d}_{2\,1,2}\right)_{ch\text{ł}} = 0,1 \div 0,15 \tag{34}$$

Należy podkreślić, że w projekcie koncepcyjnym turbiny chłodzonej obliczenia chłodzonego stopnia można traktować jako korektę pierwszego przybliżenia tzn. obliczeń stopnia niechłodzonego z takimi samymi wartościami parametrów (l_{est}, D_{sr}, u_{sr}, ρ_{st}, α_1, α_2 i in.) (Mamaje i in., 1984; Biełousow i in., 2003).W projekcie wstępnym turbiny ze stopniami chłodzonymi dokonuje się dokładniejszej analizy wymiany ciepła w wybranych konfiguracjach kanałów wewnętrznych i elementach konstrukcyjnych łopatek z uwzględnieniem mechanizmów chłodzenia i wstępną oceną wartości sprawności stopnia oraz względnego strumienia masy powietrza odprowadzanego w celu chłodzenia wieńców stopnia według algorytmów podanych w pracach Kopielew (1984), Łokaj & Salnikow (1979) oraz Ziricki i in. (1971).

W projekcie technicznym turbiny obliczenia stopnia chłodzonego mają na celu odpowiedni dobór kanałów układu chłodzenia, co jest związane z przeprowadzeniem procesu optymalizacji (sprawności, strumienia czynnika chłodzącego i in.) mającym na celu wybór takiej konfiguracji układu, która zapewnia spełnienie kryteriów ekonomiczno-wytrzymałościowych. Wymaga to przeprowadzenia bardzo złożonych obliczeń sprzężonych cieplno-przepływowych, które polegają na równoczesnym rozwiązywaniu pola przepływu czynnika (gazu roboczego w kanale międzyłopatkowym i czynnika chłodzącego w kanałach chłodzących) oraz pola temperatury w materiale łopatki przy użyciu metod numerycznych podanych w pracach Nowak (2011), Je-Chin i in. (2001) oraz Okita i in. (2017).

Należy zauważyć, że cykl rozwojowy silnika z chłodzonymi łopatkami turbinowymi jest długi i kosztowny oraz związany z dużym ryzykiem. Duże są również koszty produkcji silnika i trudna jego eksploatacja.

Literatura

Antas, S. (2006). *Ocena wpływu wybranych metod modyfikacji maszyn wirnikowych turbinowych silników śmigłowych i śmigłowcowych na zapas statecznej pracy sprężarki* (praca habilitacyjna). Oficyna Wydawnicza Politechniki Rzeszowskiej.

Antas, S., & Wolański, P. (1989). *Obliczenia termogazodynamiczne lotniczych silników turbinowych*. Wydawnictwa Politechniki Warszawskiej.

Biełousow, A.N., Musatkin, N.F., & Radko, W.M. (2003). *Teoria i rasczet awiacionnych łopatocznych maszin*. Samarskij Gos. Aerokosm. Inst.

Dżygadło, Z. i in. (1982). *Zespoły wirnikowe silników turbinowych*. Wydawnictwa Komunikacji i Łączności.

Farokhi, S. (2014). *Aircraft propulsion*. Second edition. John Wiley and Sons.

Inoziemcew, A.A., Nichamkin, M.A., & Sandrackij, W.L. (2008). *Osnowy konstruirowania awiacionnych dwigatielej i energeticzeskich ustanowok*. T.2. Maszinostrojenie.

Je-Chin, H., Sandip D., Srinath, V., & Ekkard, D. (2001). *Gas turbine heat transfer and cooling technology*. Taylor & Francis.

Kopeliew, S.Z. (1983). *Ochłażdajemyje łopatki gazowych turbin*. Nauka, Moskwa 1983.

Kopeliew, S.Z. (1984). *Projektirowanie protocznoj czasti turbin awiacionnych dwigatelej*. Maszinostrojenie.

Kopeliew, S.Z., & Tichonow, N.D. (1974). *Rasczet turbin awiacionnych dwigatielej*. Maszinostrojenie.

Kułagin, W.W. i in. (2005). *Teoria, rasczet i proektirowanie awiacionnych dwigatelej i energeticzeskich ustanowok*. Maszinostroenie.

Lakshminarayana, B. (1996). *Fluid dynamics and heat transfer of turbomachinery*. Wiley & Sons Inc.

Łokaj, W.I. i in. (1985). *Tiepłopieredacza w ochłażdajemych detaliach gazoturbinnych dwigatelej letatelnych apparatow*. Maszinostrojenie.

Łokaj, W.I., Maksutowa, M.K., & Strunkin, W.A. (1979). *Gazowyje turbiny letatelnych apparatow*. Maszinostrojenie.

Łokaj, W.I., & Salnikow, G.M. (1979). *Termogazodinamiczeskij rasczet wysokotemperaturnych ochłażdajemych turbin awiacionnych*. G.T.D. KAI.

Madejski, J. (1988). *Wymiana ciepła w turbinach cieplnych*. Ossolineum.

Mamajew, B.I., Musatkin, N.F., Aronow, B.M. (1984). *Gazodynamiczeskoje projektirowanie osiewych turbin awiacionnych*. G.T.D. Ku.A.I.

Nieczajew, Ju.N., & Fiedorow, R.M. (1977). *Teoria awiacionnych gazoturbinnych dwigatielej*. Cz. I. Maszinostrojenie.

Nowak, G. (2011). *Optymalizacja kanałów wewnętrznego chłodzenia łopatek turbiny gazowej*. Wydawnistwo Politechniki Śląskiej.

Okita, Y., Nita, K., & Kubo, S. (2017). Aerodynamic performance of novel lightweight turbine blade. *Transactions of the ASME. Journal of Turbomachinery*, 139(7), 071005-1-071005-7. https://doi.org/10.1115/1.4035604

Pawlenko, G.W., Wołow, A.G. (2007). *Gazodinamiczeskij rasczet osiewoj gazowoj turbiny*. Charkowskij Awiacionnyj Institut.

Sieniawski, J. (1995). *Kryteria i sposoby oceny materiałów na elementy lotniczych silników turbinowych.* Oficyna Wydawnicza Politechniki Rzeszowskiej.

Szczeciński, S. i in. (1984). *Lotnicze silniki turbinowe. Konstrukcja i Eksploatacja*. Wydawnictwa Komunikacji i Łączności.

Young, J.B., & Wilcock, R.C. (2002a). Modeling the air-cooled gas turbine: part 2- coolant flows and losses. *Transactions of the ASME. Journal of Turbomachinery*, 124(2), 214-222. https://doi.org/10.1115/1.1415038

Young, J.B., & Wilcock, R.C. (2002b). Modeling the air-cooled gas turbine: part 1-general thermodynamics. *Transactions of the ASME. Journal of Turbomachinery*, 124(2), 207-213. https://doi.org/10.1115/1.1415037

Ziricki. G.S. i in. (1971). *Gazowyje turbiny dwigatielej letatelnych apparatow*. Maszinostroenie.

METHOD FOR CALCULATION OF COOLED TURBINE STAGE PARAMETERS IN THE CONCEPTUAL DESIGN OF UNIT

S u m m a r y

The paper presents the basic types of turbine cooling systems for aircraft turbine engines as well as the essential methods of cooling turbine rim blades. The main part of the article presents the method of determining the stream parameters in the cross - sections of the output rims of the cooled turbine stage, consisting in the first stage of calculations of thermal and kinematic parameters for the stream and geometric parameters on the mean diameter in the uncooled stage. The second stage of the method includes the correction of the exhaust gas parameters and the geometric parameters of the profiles for the nozzle and rotor rim in a cooled stage. The method can be used during the conceptual design of the axial cooled turbine stage and is based on the energy conservation equation, the Euler's moment of momentum equation, the first law of thermodynamics and definitions of the coefficients used in the theory of turbomachinery. The final part of the work includes recommendations regarding the geometric parameters of the cooled rim profiles and conclusions.

Key words: axial - flow turbine, method for calculation, cooled stage

DOI: 10.7862/rm.2022.1

Submitted/Tekst złożono w redakcji: maj 2022
Accepted / Przyjęto do druku: czerwiec 2022
Published/Tekst opublikowano: grudzień 2022

ZESZYTY NAUKOWE POLITECHNIKI RZESZOWSKIEJ – MECHANIKA
SCIENTIFIC LETTERS OF RZESZOW UNIVERSITY OF TECHNOLOGY – MECHANICS
94 (2022), s. 23-35

Bogdan KRASOWSKI[1]
Andrzej KUBIT[2]

EFFECT OF THE LUBRICATION ON THE FRICTION CHARACTERISTICS OF EN AW-2024-T3 ALUMINIUM ALLOY SHEETS

Abstract: The article presents the results of friction tests conducted on EN AW-2024 Alclad aluminium alloy sheets. The lubrication efficiency of oleic acid, mineral and vegetable oils with the addition of SiO_2 and TiO_2 nanoparticles was determined using the strip drawing test to assess the friction conditions in the flange area in the deep drawing process. The samples in the form of sheet metal strips were pulled between countersamples with a rounded surface at a speed of 2.5 mm/s. Gear oil and oleic acid demonstrated the lowest value of the coefficient of friction (COF) in the whole range of nominal pressures investigated. The lowest efficiency in reducing the COF was shown by hydraulic oil, olive oil and machine oil. A high content of TiO_2 nanoparticles (0.5-0.9%wt%) is beneficial in the friction process involving oleic acid.

Keywords: aluminium alloy, lubrication, nanoparticles, strip drawing test, coefficient of friction

1. Introduction

Sheet metal forming (SMF) processes are one of the most frequently used methods of manufacturing finished sheet metal products. Friction is the phenomenon that determines whether of a product with an appropriate surface finish is obtained (Dou et al., 2020; Dou & Xia, 2019; Seshacharyulu et al., 2018). One of the basic ways of reducing the value of the coefficient of friction (COF) in sheet metal forming (SMF) is the use of lubricants (Sigvant et al., 2019; Zabala et al., 2021). The following requirements are imposed on technological grease: ease of application, resistance to high normal pressures, stability in reducing frictional

[1] Corresponding author: Bogdan Krasowski, Carpatian State School in Krosno, Department of Mechanics and Machine Building, Rynek 1, 38-400 Krosno, Poland, e-mail: bogdan.krasowski@kpu.krosno.pl, ORCID ID: 0000-0003-1346-9476

[2] Andrzej Kubit, Rzeszow University of Technology, Department of Manufacturing Processes and Production Engineering, al. Powstańców Warszawy 8, 35-959 Rzeszów, Poland, e-mail: akubit@prz.edu.pl, ORCID ID: 0000-0002-6179-5359

resistance over a wide range of pressures, ease of removal from the product and biodegradability (Krasowski, 2021). Despite the fact that most of the process lubricants used in SMF operations are based on synthetic oils, Carcel et al. (2005), Idegwu et al. (2019), Rao et al. (2009) indicate that vegetable oils can be an effective alternative.

The mineral and synthetic oils usually used in sheet metal processing can be successfully replaced with vegetable oils, even when stamping galvanised sheets (Więckowski et al., 2020; Yu et al., 2010). The presence of long chains of fatty acids in vegetable oils enables effective separation of the friction surface between the tool and the sheet under boundary friction conditions. In addition, these oils provide sufficient protection against corrosion, have a high viscosity index, and are environmentally friendly and biodegradable (Liñeira del Río et al., 2022). Over the same period that 80% of vegetable oils were degraded, only 15–20% of mineral oils degraded (Padgurskas et al., 2016). The major disadvantage of vegetable oils is weak oxidation (Fox et al., 2007).

To improve the properties of lubricating oils, nanoparticle additives are used (Pang & Ngaile, 2020; Zareh-Desari & Davoodi, 2016). The research of Hernández Battez et al. (2008) and Peng et al. (2009) on the use of nanoparticles ZnO, CuO, ZrO_2, TiO_2, SiO_2 as additives in vegetable oils and paraffin oil showed a reduction in the value of the COF and wear. Cortes et al. (2020) investigated the tribological performance of nanoparticles of titanium dioxide (TiO_2) with a purity of 99.5% and SiO_2 with a purity of 99.9%, which were dosed into oils in the amount of 0.1, 0.5 and 0.9% by weight. The experimental results showed that the COF decreased with the addition of SiO_2 and TiO_2 nanoparticles by 77.7% and 93.7%, respectively when compared to base sunflower oil. Although nanoparticles have proven to enhance lubricant properties, the current issue is compatibility Gulzar et al. (2017). Peng et al. (2008) investigated the tribological properties of liquid paraffin to which diamond and SiO2 nanoparticles, which were prepared by the surface modification method using oleic acid. It was found that both nanoparticles as additives in liquid paraffin have better antiwear and antifriction properties than the pure paraffin oil. A ball-on-ring friction tests conducted by Peng et. al. (2010) indicated that the sizes of the synthesized SiO_2 nanoparticles are distributed uniformly and that the optimal concentrations of SiO_2 nanoparticles in liquid paraffin is associated with better tribological properties than pure paraffin oil.

The strip drawing test (SDT) is commonly used to evaluate the coefficient of friction at the sheet metal-blankholder interface. In this paper, the performance of mineral and biodegradable oils with additions of the SiO_2 and TiO_2 nanoparticles was investigated using the SDT using EN AW-2024-T3 aluminium alloy sheets were used as test material. The effect of nominal pressure and oil type has been presented and discussed.

2. Material and Methods

The experimental tests of friction in the SDT were carried out on a 1-mm-thick EN AW-2024-T3 Alclad aluminium alloy sheet strips. The average surface roughness of the sheets is 0.78 µm. The SDT consists in pulling a sheet strip crimped between two non-rotating countersamples with a radius of working surface R = 200 mm. Surface morphology of the countersamples was measured with the 3D optical profiler Talysurf CCI Lite. The values of basic surface roughness parameters are as follows: arithmetical mean height Sa = 1.53 µm, kurtosis Sku = 2.07, skewness Ssk = -0.014. Views of the test stand and countersamples are shown in Figs. 1a and 1b, respectively. A friction simulator frame was mounted in the lower bracket of the Zwick/Roell Z100 testing machine, and one of the ends of the sheet metal is mounted in the upper bracket of the machine. The value of the COF, which is a reference point for the qualitative assessment of a lubricant in reducing friction, can be determined from the relationship:

$$\mu = \frac{F_T}{2F_N} \tag{1}$$

where: F_T – pulling force, F_N – clamping force.

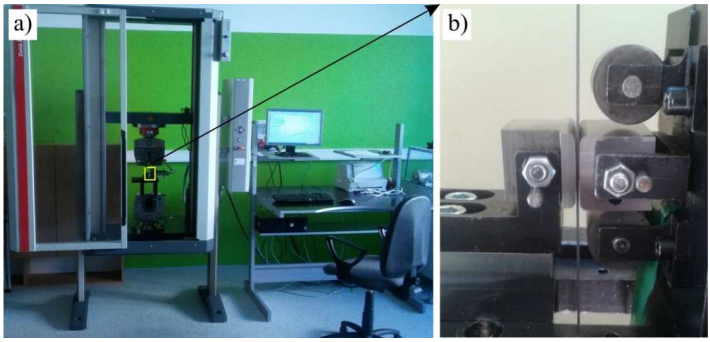

Fig. 1. View of a) the test stand and b) countersamples

The frame (1) of the device (Fig. 2) was mounted in the mounting base of the testing machine. An adjusting screw (6) is used to adjust the clamping (normal) force. The clamping force was determined by tightening the screw (6) with the appropriate torque. The sample (2) was pulled through the fixed countersamples made of cold-work tool steel with a constant sliding speed of 2.5 mm/s. The friction force was recorded continuously by the control system of the testing machine.

Based on the review of articles by Ahmad et al. (2020), Bay et al. (2010), Rodrigues et al. (2020), Zavala et al. (2021), the following lubricants were

selected for testing: L-AN46 machine oil, L-HM 46 hydraulic oil, 75W- 85 gear oil, oleic acid, sunflower oil and olive oil. The basic properties of the lubricants declared by the manufacturers in the product cards are presented in Table 1. The basic physical properties of oleic acid $C_{18}H_{34}O_2$ are as follows: density ρ = 895 kg/m^3, molar mass 283.47 g/mol, boiling point T_w = 360°C. TiO_2 and SiO_2 nanoparticles were added to the two selected oils that showed the lowest COF values during the tests. The following amounts of nanopowders were used: 0.1, 0.5 and 0.9 wt.%. The particle size of TiO_2 was 16 nm and SiO_2 15 nm.

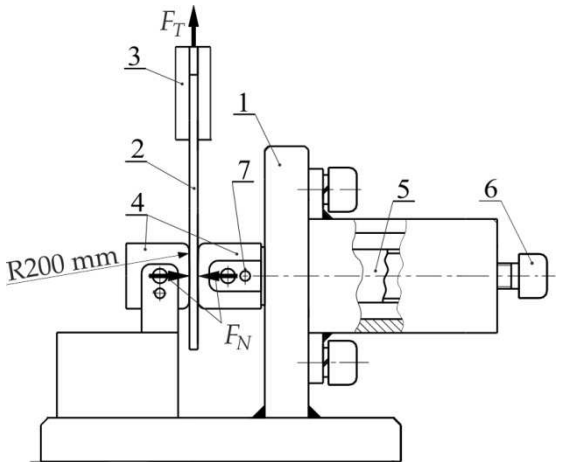

Fig. 2. Diagram of the friction tester: 1 - frame, 2 - sample, 3 - upper bracket of the testing machine, 4 - countersamples, 5 - sleeve, 6 - screw, 7 - blocking pin

Table 1. Basic physical properties of the lubricants used in the tests

Oil	Density ρ, kg/m^3	Kinematic viscosity η_k, mm^2/s
machine oil LAN-46	875	43.9
hydraulic oil L-HM 46	877	44.2
gear oil 75W-85	837	64.6
oleic acid	895	4.50
sunflover oil	883	4.45
olive oil	890	4.50

3. Results and Discussion

For simplification, the following oil acronyms have been adopted: machine oil (MO), hydraulic oil (HO), gear oil (GO), oleic acid (OA), sunflower oil (SO) and olive oil (OO). Under dry friction conditions, EN AW-2024-T3 Alclad sheets exhibited a higher friction coefficient of about 0.2 (Fig. 3). The pressures between the materials of the friction pair (Alclad and cold-work tool steel) are transferred through the micro-areas of real contact. In these areas, the yield point of the

Alclad material is exceeded (50.25 MPa according to Vinay and Vinoth, 2014). This causes an increase in shear stresses and a local increase in temperature in the micro-contact areas. Such a situation - large deformations and high temperature - favours the formation of non-diffusion adhesive tacking, which increases the COF (Abe et al. 2016). Among unmodified oils, GO and OA provided the lowest value of COF in the entire range of nominal pressures investigated (Fig. 3).

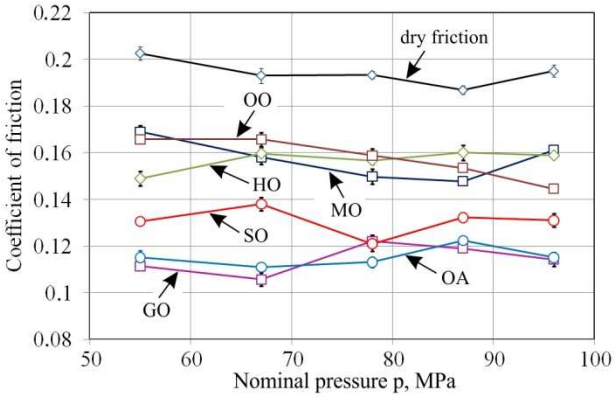

Fig. 3. Effect of nominal pressure on the value of the COF of sheets tested with the use of non-modified oils

The low value of the yield strength of Alclad consisting of technically pure aluminium favours seizing of the coating surface (Fig. 4), also contributing to increasing the value of the COF, especially in conditions of high pressures of 87-96 MPa. The result is a rapid increase in the real contact area by flattening the surface asperities of the Alclad. High pressures combined with intensive flattening of the surface asperities lead to the formation of a network of cracks and discontinuities in the surface layer of the coating (Fig. 5). In order to determine the efficiency with which the oil used reduces the COF by the oil used, the coefficient of lubrication efficiency was introduced:

$$\delta = \frac{\mu_{dry} - \mu_{lub}}{\mu_{lub}} \cdot 100\% \tag{2}$$

where μ_{dry} and μ_{lub} are the COFs determined in dry and lubricated conditions, respectively.

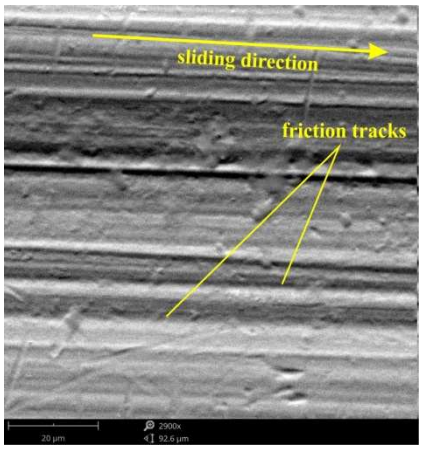

Fig. 4. SEM micrograph of a sheet surface tested under conditions of lubrication with MO at a pressure p = 55 MPa

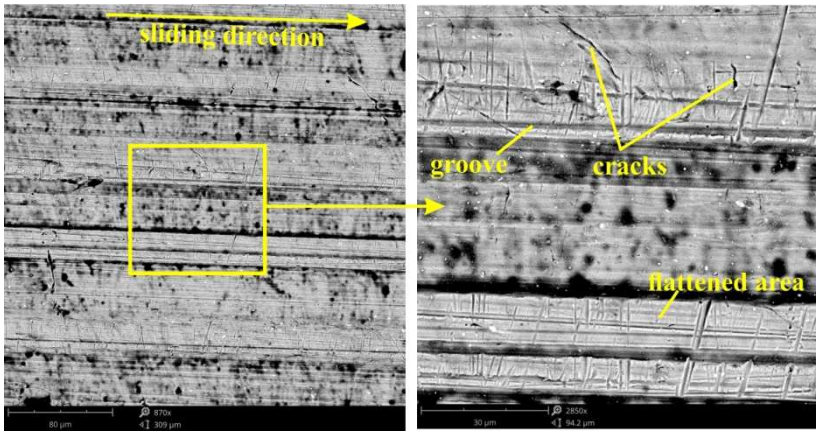

Fig. 5. SEM micrographs of a sheet surface tested under conditions of lubrication with HO at the nominal pressure of 78 MPa

The value of the coefficient lubrication efficiency during the friction process with gear oil and oleic acid fluctuates for both oils in a similar range of 35-45% (Fig. 6). At low pressures, the COF was least effectively reduced by MO and OO, and at high pressures by HO and MO. Under these conditions, these oils ensured a coefficient of lubrication efficiency in the range of 14-26%.

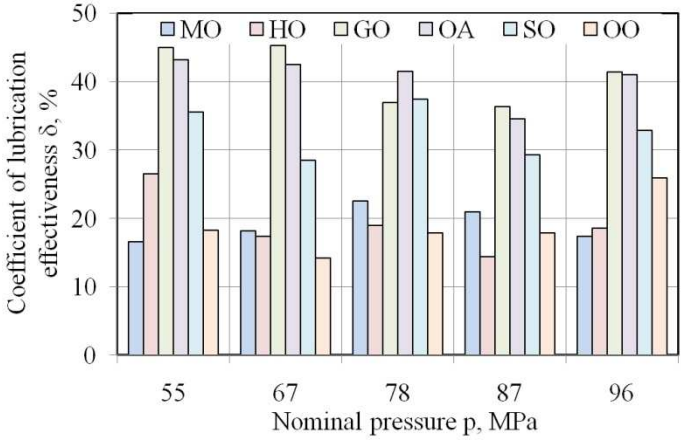

Fig. 6. Influence of nominal pressure on the coefficient of lubrication efficiency on non-modified oils

Under the conditions of lubrication with gear oil, within the range of the nominal pressures considered of 55-67 MPa, a clear tendency was observed for the value of the COF to increase with increasing content of TiO_2 nanoparticles (Fig. 7). A high content of TiO_2 nanoparticles during the friction process is advantageous under the highest of the nominal pressures considered, 87 and 96 MPa, when lubricated with oleic acid containing 0.5-0.9 wt% of TiO_2 nanoparticles. Under these nominal pressures, the values of the COF were reduced by about 10.9% (87 MPa) and 11.1% (96 MPa) in relation to the lubrication with the use of non-modified oils. The most favourable effect of reducing the value of the COF resulting from the addition of SiO_2 nanoparticles was observed for oleic acid with a nanoparticle content of 0.5wt% (Fig. 8a). Modification of oleic acid with SiO_2 nanoparticles reduced the value of the COF by about 1.5% at pressures of 67-78 MPa and 8.9% at pressures of 87-98 MPa. However, in the case of modifying the gear oil with SiO_2 nanoparticles, no significant reduction of COF was found, only a slight decrease was recorded for the nominal pressure of 78 MPa (Fig. 8b).

Additions of nanoparticles of hard materials reduce friction by transferring part of the load in the valleys between the contacting materials. Under high pressure conditions, the particles can disintegrate, which changes the contact conditions. If the surface roughness of the tools is too high in relation to the roughness of the deformed sheet, then the mechanism of mechanical ploughing of the sheet surface is activated. Under such conditions, the lubricant is not able to sufficiently reduce the value of the COF. High pressures acting on the Alclad through the countersample caused the phenomenon of coating material build-up (Fig. 9a) and the formation of adhesive (Fig. 10a) and cohesive cracks (Fig. 9b). The low yield stress of the coating material favours the sticking of the nanoparticles into the Alclad (Fig. 10b).

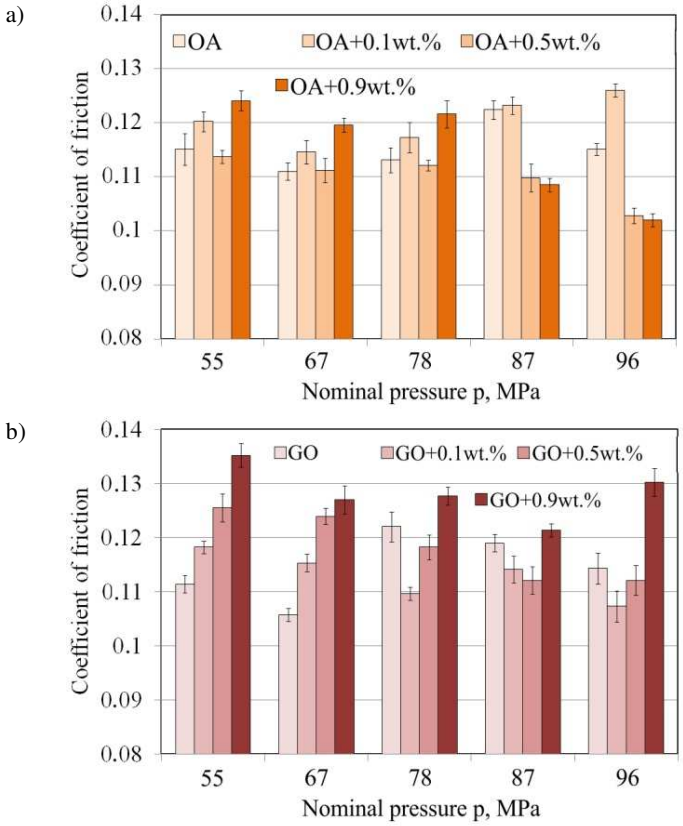

Fig. 7. Influence of nominal pressure on the value of the COF in friction conditions with a) oleic acid and b) gear oil containing TiO_2 nanoparticles

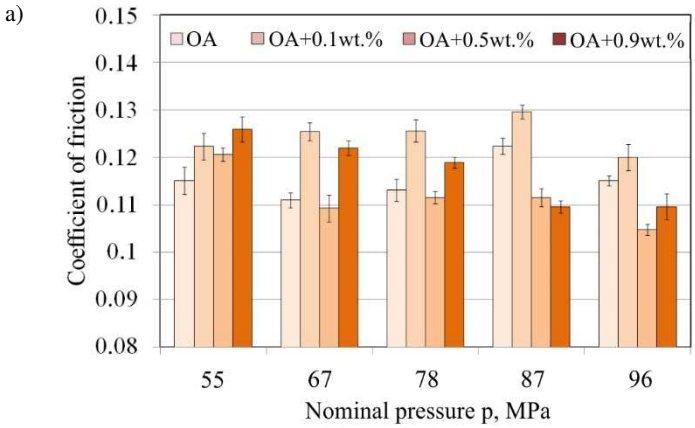

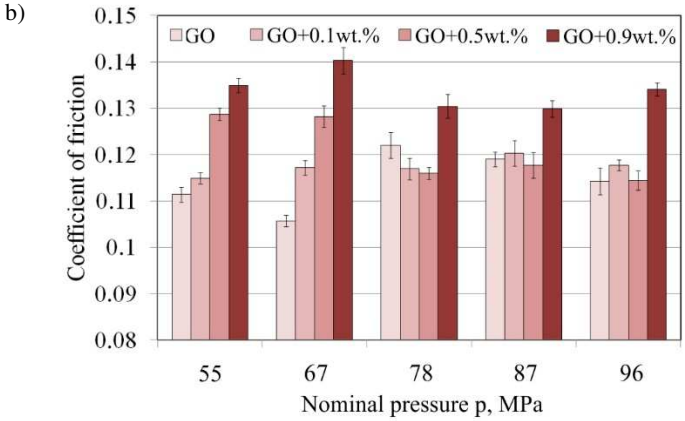

Fig. 8. Influence of nominal pressure on the value of the COF in friction conditions with a) oleic acid and b) gear oil containing SiO_2 nanoparticles

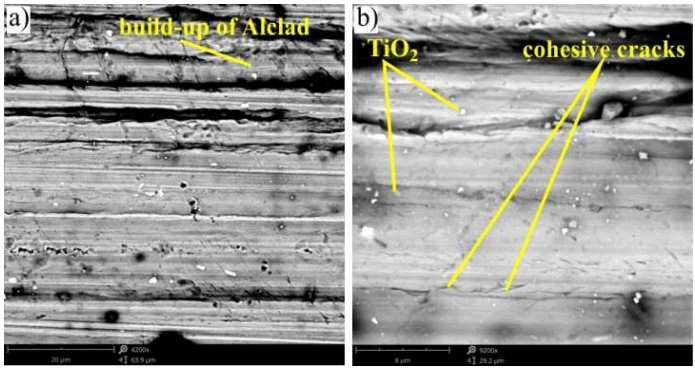

Fig. 9. SEM micrographs of a sheet surface tested under following conditions: a) OA + 0.5wt.% SiO_2, p = 67 MPa, b) OA + 0.1wt .% TiO_2, p = 55 MPa

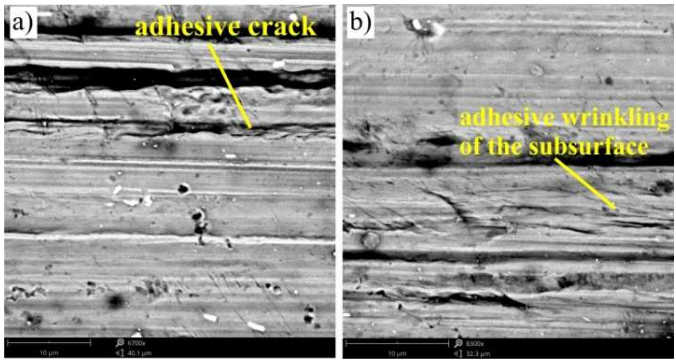

Fig. 10. SEM micrographs of the sheet surface tested in the following conditions: a) GO + 0.5wt.% SiO2, p = 78 MPa, b) GO + 0.9wt.% SiO_2, p = 87 MPa, c) GO + 0.1wt.% TiO_2, p = 55 MPa, c) GO + 0.1wt.% TiO_2, p = 55 MPa

4. Conclusions

This paper examines the effect of lubricant type on the value of the COF of EN AW-2024-T3 Alclad aluminium alloy sheets as determined in the strip drawing test. Based on the research results, the following conclusions can be drawn:

- The influence of the content of nanoparticles in the oil and the grade of nanoparticles on the value of the COF changes with increasing nominal pressure.
- Among non-modified oils, gear oil and oleic acid provided the lowest value of friction coefficient in the entire range of nominal pressures investigated.
- The lowest efficiency in reducing the COF was shown by hydraulic oil, olive oil and machine oil.
- The most favourable effect of reducing the value of the COF resulting from the addition of SiO_2 nanoparticles was observed for oleic acid with a nanoparticle content of 0.5wt%.
- Under the conditions of lubrication with gear oil, within the range of the nominal pressures considered of 55-67 MPa, a clear tendency of increasing the value of the COF with increasing content of TiO_2 nanoparticles was found.

References

Abe, Y., Mori, K., Hatashita, F., Shiba, T., Daodon, W., & Osakada, K. (2016). Improvement of seizure resistance in ironing of stainless steel cup with cermet die having fine lubricant pockets. *Journal of Materials Processing Technology*, 234, 195-207. https://doi.org/10.1016/j.jmatprotec.2016.03.017

Ahmad, N.A., Samion, S., Rahim E.A., & Jamir, M.R.M. (2020). Environmentally approach for enhancing tribological characteristics in metal forming: A review. *Journal Tribologi*, 26, 37-59.

Bay, N., Azushima, A., Groche, P., Ishibashi, I., Merklein, M., Morishita, M., Nakamura, T., Schmid, S., & Yoshida, M. (2010). Environmentally benign tribo-systems for metal forming. *CIRP Annals*, 59(2), 760-780. https://doi.org/10.1016/j.cirp.2010.05.007

Carcel, A.C., Palomares, D., Rodilla, E., & Pérez Puig, M.A. (2005). Evaluation of vegetable oils as pre-lube oils for stamping. *Materials Design*, 26, 587–593. https://doi.org/10.1016/j.matdes.2004.08.010

Cortes V., Sanchez K., Gonzalez R., Alcoutlabi M., & Ortega J.A. (2020). The performance of SiO_2 and TiO_2 nanoparticles as lubricant additives in sunflower oil. *Lubricants*, 8, 10. https://doi.org/10.3390/lubricants8010010

Dou, S., Wang, X., Xia, J., & Wilson, L. (2020). Analysis of sheet metal forming (warm stamping process): A study of the variable friction coefficient on 6111 aluminum alloy. *Metals* 10*,* 1189. https://doi.org/10.3390/met10091189

Dou, S., Xia, J. (2019). Analysis of sheet metal forming (stamping process): A study of the variable friction coefficient on 5052 aluminum slloy. *Metals*, 9, 853. https://doi.org/10.3390/met9080853

Fox, N.J., Stachowiak, G.W. (2007). Vegetable oil-based lubricants—A review of oxidation. *Tribology International*, 40, 1035–1046. https://doi.org/10.1016/j.triboint.2006.10.001

Gulzar, M., Masjuki, H.H., Kalam, M.A., Varman, M., Zulkifli, N.W.M., Mufti, R.A., Zahid, R., & Yunus, R. (2017). Dispersion stability and tribological characteristics of TiO_2/SiO_2 nanocomposite-enriched biobased lubricant. *Tribology Transactions*, 60, 670–680. https://doi.org/10.1080/10402004.2016.1202366

Hernández Battez, A., González, R., Viesca, J.L., Fernández, J.E., Díaz Fernández, J.M., Machado, A., Chou, R., & Riba, J. (2008). CuO, ZrO2 and ZnO nanoparticles as antiwear additive in oil lubricants. *Wear*, 265, 422–428. https://doi.org/10.1016/j.wear.2007.11.013

Idegwu, C.U., Olaleye, S.A., Agboola, J.B., & Ajiboye, J.S. (2019). Evaluation of some non-edible vegetable oils as lubricants for conventional and non-conventional metal forming processes. *AIP Conference Proceedings*, 2113, 030004. https://doi.org/10.1063/1.5112532

Krasowski, B. (2021) *Analiza procesu kształtowania przyrostowego usztywnień w cienkościennych konstrukcjach nośnych wykonanych ze stopów aluminium EN AW-2024-T3 oraz EN AW-7075-T6*. Rozprawa doktorska. Politechnika Rzeszowska.

Liñeira del Río, J.M., Guimarey, M.J.G., Prado, J.L., Lugo, L., López, E.R., & Comuñas, M.J.P. (2022), Improving the tribological performance of a biodegradable lubricant adding graphene nanoplatelets as additives. J*ournal of Molecular Liquids*, 345, 117797. https://doi.org/10.1016/j.molliq.2021.117797

Padgurskas, J., Rukuiža, R., Meškinis, A., Kreivaitis, R., & Spruogis, B. (2016). Influence of manufacturing methods on the tribological properties of rapeseed oil lubricants. *Transport*, 31, 56–62. https://doi.org/10.3846/16484142.2015.1048525

Pang, H., Ngaile, G. (2020). Formulation of SiO_2/oil nanolubricant for metal forming using hydrodynamic cavitation. *Proceedings of the Institution of Mechanical Engineers, Part B: Journal of Engineering Manufacture*, 234, 1549-1558. https://doi.org/10.1177/0954405420933120

Peng, D., Chen, C., Kang, Y., Chang, Y. & Chang, S. (2010). Size effects of SiO_2 nanoparticles as oil additives on tribology of lubricant. *Industrial Lubrication and Tribology*, 62, 111-120. https://doi.org/10.1108/00368791011025656

Peng, D.X., Kang, Y., Hwang, R.M., Shyr, S.S., & Chang, Y.P. (2009). Tribological properties of diamond and SiO_2 nanoparticles added in paraffin. *Tribology International*, 42, 911–917. https://doi.org/10.1016/j.triboint.2008.12.015

Rao, K.P., Xie, C.L. (2006). A comparative study on the performance of boric acid with several conventional lubricants in metal forming processes. *Tribology International*, 39, 663–668. https://doi.org/10.1016/j.triboint.2005.05.004

Rodrigues, J., Costa, I., Farinha, J.T., Mendes, M., & Margalho, L. (2020). Predicting motor oil condition using artificial neural networks and principal component

analysis. *Eksploatacja i Niezawodnosc-Maintenance and Reliability*, 22(3), 440-448. http://dx.doi.org/10.17531/ein.2020.3.6

Seshacharyulu, K., Bandhavi, C., Naik, B.B., SrinivasaRao, S.S., & Singh, S.K. (2018). Understanding friction in sheet metal forming-A review. *Materials Today: Proceedings*, 5(9), 18238-18244. https://doi.org/10.1016/j.matpr.2018.06.160

Sigvant, M., Pilthammar, J., Hol, J., Wiebenga, J.H., Chezan, T., Carleer, B., & van den Boogard, T. (2019). Friction in sheet metal forming: influence of surface roughness and strain rate on sheet metal forming simulation results. *Procedia Manufacturing*, 29, 512-519. https://doi.org/10.1016/j.promfg.2019.02.169

Vinay, K.U., Vinoth, M.A. (2014). Analysis of mechanical properties of pure aluminium based metal matrix composite. *International Journal of Innovative Research & Studies*, 3(5), 702-711.

Więckowski, W., Adamus, J., & Dyner, M. (2020). Sheet metal forming using environmentally benign lubricant. *Archives of Civil and Mechanical Engineering*, 20, 51. https://doi.org/10.1007/s43452-020-00053-x

Yu, Z.Q., Hou, Y.K., Li, S.H., Lin, Z.Q., Zhang, W.G. (2010). Surface damage behavior of galvanized steel sheets in forming process under tension-bending. *International Journal of Modern Physics B*, 24(30), 5877-5884. https://doi.org/10.1142/S0217979210057481

Zabala, A., Galdos, L., Childs, C., Llavori, I., Aginagalde, A., Mendiguren, J., & Saenz de Argandoña, E. (2021). The interaction between the sheet/tool surface texture and the friction/galling behaviour on aluminium deep drawing operations. *Metals*, 11, 979. https://doi.org/10.3390/met11060979

Zareh-Desari, B., Davoodi, B. (2016). Assessing the lubrication performance of vegetable oil-based nano-lubricants for environmentally conscious metal forming processes. *Journal of Cleaner Production*, 135, 1198–1209. https://doi.org/10.1016/j.jclepro.2016.07.040

Zavala, J.M.D., Martínez-Romero, O., Elías-Zúñiga, A., Gutiérrez, H.M.L., de la Vega, A.E., & Taha-Tijerina, J. (2021). Study of friction and wear effects in aluminum parts manufactured via single point incremental forming process using petroleum and vegetable oil-based lubricants. *Materials*, 2021, 14, 3973. https://doi.org/10.3390/ma14143973

WPŁYW SMAROWANIA NA WŁAŚCIWOŚCI TARCIOWE BLACH ZE STOPU ALUMINIUM EN AW-2024-T3

S t r e s z c z e n i e

W artykule przedstawiono wyniki badań tarcia blach ze stopu aluminium EN AW-2024-T3 Alclad. Efektywność smarowania za pomocą kwasu oleinowego, olejów mineralnych oraz roślinnych z dodatkami nanocząstek SiO_2 oraz TiO_2 została określona za pomocą testu przeciągania blachy używanego do oceny warunków tarcia panujących w kołnierzowej części wytłoczki w procesie głębokiego wytłaczania. Próbki w postaci pasów blachy przeciągano pomiędzy przeciwpróbkami o zaokrąglonej powierzchni (R = 200 mm) z prędkością 2,5 mm/s. Olej przekładniowy oraz kwas oleinowy zapewniły najmniejszą wartość współczynnika tarcia w całym zakresie analizowanych nacisków nominalnych. Najmniejszą efektywność zmniejszania współczynnika tarcia wykazały

olej hydrauliczny, oliwa z oliwek oraz olej maszynowy. Najkorzystniejszy efekt zmniejszenia wartości współczynnika tarcia wynikający z dodatku nanocząstek SiO_2 jest widoczny dla kwasu oleinowego przy zawartości nanocząstek 0,5% (wagowo). Wysoka zawartość nanocząstek TiO_2 (0,5-0,9% wagowo) jest korzystna podczas procesu tarcia z udziałem kwasu oleinowego.

Słowa kluczowe: stop aluminium, smarowanie, nanocząstki, test przeciągania blachy, współczynnik tarcia

DOI: 10.7862/rm.2022.2

Submitted/Tekst złożono w redakcji: July 2022
Accepted/Przyjęto do druku: October 2022
Published/Tekst opublikowano: December 2022

ZESZYTY NAUKOWE POLITECHNIKI RZESZOWSKIEJ – MECHANIKA
SCIENTIFIC LETTERS OF RZESZOW UNIVERSITY OF TECHNOLOGY – MECHANICS
94 (2022), s. 37-50

Piotr MYŚLIWIEC[1]

A NEW TOOLING APPROACH FOR FRICTION STIR WELDING OF THIN SHEET AA2024-T3 - OPTIMIZATION OF WELDING PARAMETERS

Abstract: In this study a new ceramics tools with different groove distributions were designed and manufactured in order to enrich technological storage of joining thin-wall structures and obtain sound joint with high quality of Alclad AA2024-T3 alloy of 0.5 mm in thickness. Four types of tools were tested, without grooves, with 1, 2 and 6 grooves. The tools are made of two materials. The straight shank is made from tungsten carbide and tool body made from ceramics strengthened with whiskers. The influence of technological parameters on the strength of FSW joints was tested by the Response Surface Methodology (RSM) and Analysis of Variance (ANOVA) method. The least durable weld is produced by a tool without grooves. The single and double flute tool produces a good quality weld over a wide range of tool speeds. It has been shown that the grooves on the tool shoulder significantly affect the quality of the obtained FSW joint.

Keywords: aluminium alloy AA2024-T3, ANOVA, ceramic tools, friction stir welding, FSW tool geometry, joining of thin sheets, RSM

1. Introduction

Friction stir welding (FSW) is a solid-state welding technique that has evolved as a solution for joining different metal sheets especially dissimilar materials that are difficult to weld. It is currently used as an alternative to riveting for e.g. the assembly of airplane fuselages (Takhakh & Hussein, 2021). FSW uses a rotary pin to locally mix the materials of the two sides of the joint below the melting point temperature (Thomas et al., 1995). Thus, the formation of welding defects such as hot cracking is prevented (Węglowski, 2018). Friction stir welding is a continuous, hot shear, autogenous process involving non-consumable

[1] Corresponding author: Piotr Myśliwiec, Rzeszow University of Technology, Department of Materials Forming and Processing, al. Powstańców Warszawy 8, 35-959 Rzeszów, e-mail: p.mysliwiec@prz.edu.pl, ORCID ID: 0000-0002-9073-2082

rotating tool of harder material than the substrate material (Ahmed et al., 2021). Fig. 1 explains the working principle of FSW process.

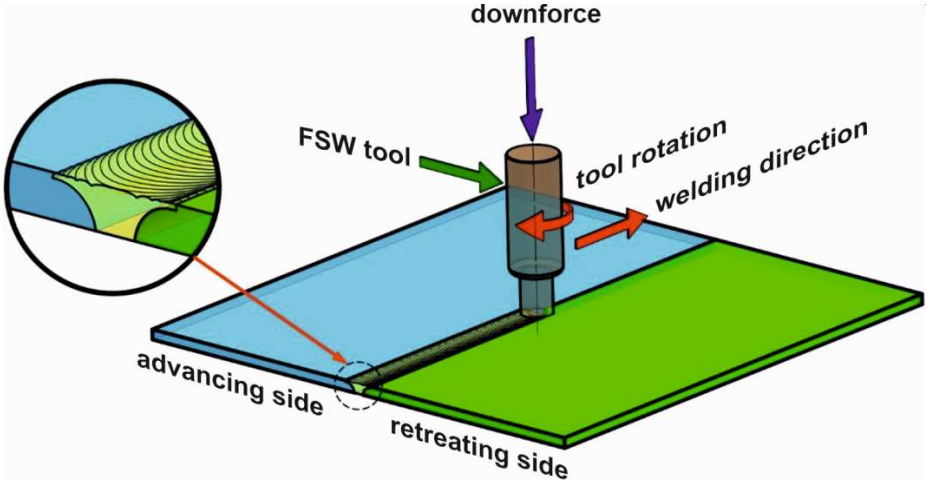

Fig. 1. Schematic representation of FSW principle

In order to increase the efficiency of FSW welding, many different tool variants are being developed. Both the tool material and the tool geometry are subjected to modification. Tool material should be wear-resistant under high thermal stress (Kumar & Kailas, 2008). Tool shoulder plays a key role in generation of surface friction and rise of workpiece temperature. Tool pin generates stirring and therefore materials in processed zone experience sever plastic deformation. Flowing and recrystallisation in processed zone occurs with tool rotation and linear movement. This results in creation of a fine equiaxed microstructure (Elangovan & Balasubramanian, 2007; Zhang et al. 2020).

In this paper, the mechanical properties (tensile strength) of the samples of welded 2024-T3 aluminum alloy sheets were investigated to determine the best rotational speed and welding speeds. The work determines the optimal parameters using one of the optimized methods to ensure proper welding performance based on tensile strength, study the obtained optimal parameters of mechanical properties and performance using the design of experiments (DOE) technique and development of models. It can help designers and engineers to achieve perfect welding. ANOVA techniques were used to identify the relevant factors influencing the ultimate tensile strength (UTS).

2. Material and experimental procedure

The initial material used in this work is a cold-rolled commercial AA2024-T3 aluminum alloy sheet with the 0.5 mm in thickness Alclad covered. In this investigation, the joining region are carefully cleaned prior to welding. After

polished by abrasive paper and cleaning with acetone, several weld plates were subjected to FSW along the rolling direction. The blank sheet dimensions were 180×100 mm (Fig. 2). The FSW experiments were carried out using special prepared CNC milling machine MAKINO PS95 and the welding tools (Fig. 3). Cylindrical tool made from whisker-reinforced ceramic with geometrical features and process inputs are reported in Table 1.

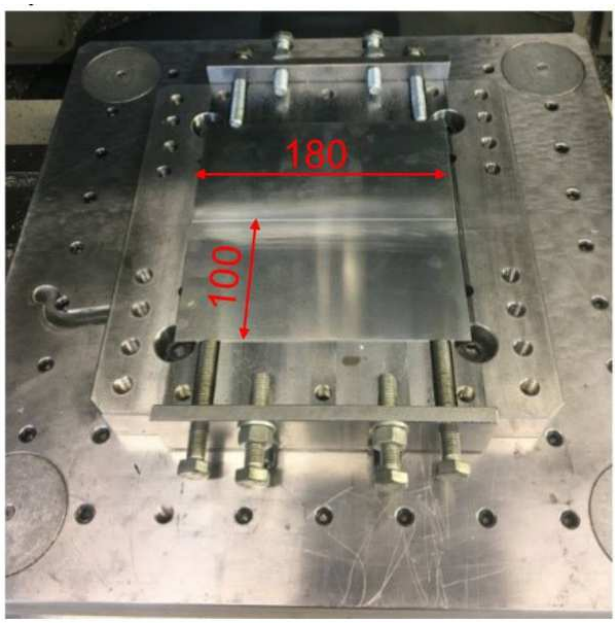

Fig. 2. View of workpiece material installed on fixture device

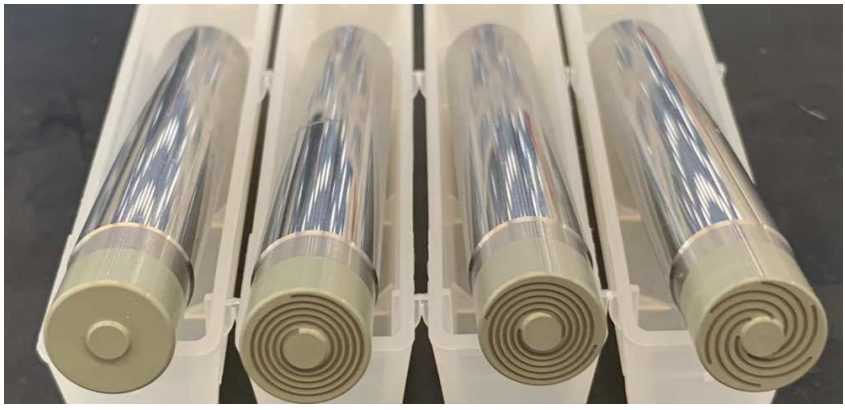

Fig. 3. Different type of shoulder profile of FSW tools with and without groves

Table 1. Inputs used for the experimental set-up of FSW

Tool material	whisker-reinforced ceramics	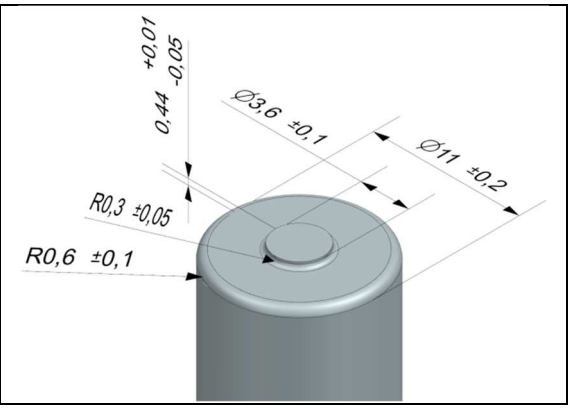
Shoulder diameter D	11 mm	
Pin diameter d	3.6 mm	
Pin height	0.44 mm	
Pin profile	cylindrical	
Shoulder profile	flat	
D/d ratio of the tool	3.05	
Dwell time	1 s	
Penetration depth (tool offset)	0.03 mm	

Tool worked without a tilt angle, perpendicular to the surface of the welded material. The butt joint configuration was prepared to produce the joints. Welding has been done on the 180 mm long section.

A research plan was prepared for the experiment. Design-Expert software by Stat-Ease, Inc. was used. The range for technological parameters was determined for the rotational speed from 1000 to 2000 rpm and the welding speed from 200 to 1000 mm/min (Fig. 4). The last factor was the number of spiral grooves on the tool face. On this basis, a matrix of technological parameters was created. The set of parameters is shown in Fig. 5. Several regression models have been tested. The best results were obtained for the CUBIC model (Table 2).

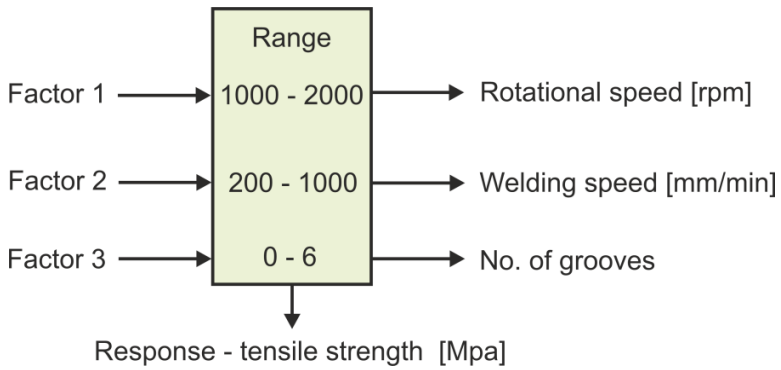

Fig. 4. Ranges of changes in welding parameters

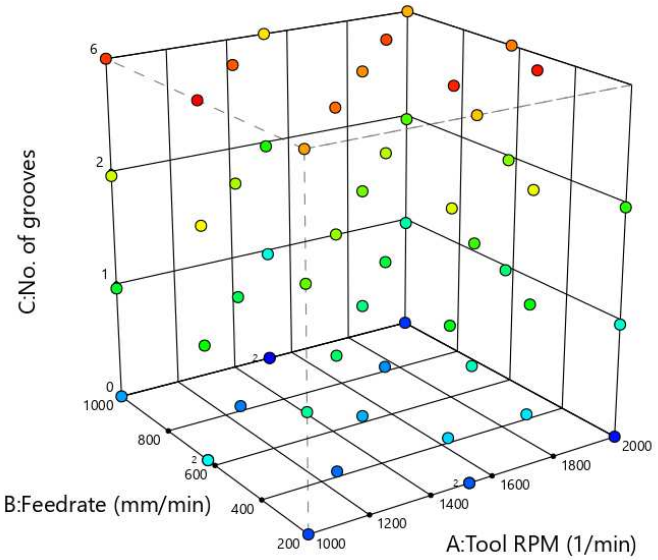

Fig. 5. Matrix of welding parameters

Table 2. Various regression models for the FSW experiment

Source	Model p-value	Lack of fit p-value	Adjusted R^2	Predicted R^2	Recommendation
Design Model	< 0.0001	0.5185	0.6001	0.5637	
Linear	< 0.0001	0.4064	0.4838	0.4091	
2FI	0.0138	0.5060	0.5908	0.4649	
Quadratic	0.0007	0.6467	0.6961	0.5697	Suggested
Cubic	0.0291	0.8023	0.7843	0.3346	Suggested
Quartic	0.2486	0.9016	0.8279	-1.8351	Aliased

Obtained FSW joints were the basis to make specimens for tensile tests. The mechanical properties of the joints were measured during tensile testing. Tensile specimens dimension and a method of preparing was shown on Fig. 6. Static tensile test was performed in accordance with PN-EN ISO 6892-1:2009. The tensile tests were carried out on an Zwick/Roell Z 100 universal testing machine, at room temperature. An extensometer with a gauge length of 50 mm was used for strain data acquisition. The results, given by the nominal stress vs. nominal strain curves, were evaluated in terms of the ultimate tensile strength, yield strength (YS) and ultimate elongation (UE) in percentage. In the purpose of verifying the repeatability of the results each tested samples was repeated at least three times. From each joined metallic plate was cut three samples from the beginning, middle and end of a weld and then the measured values were averaged.

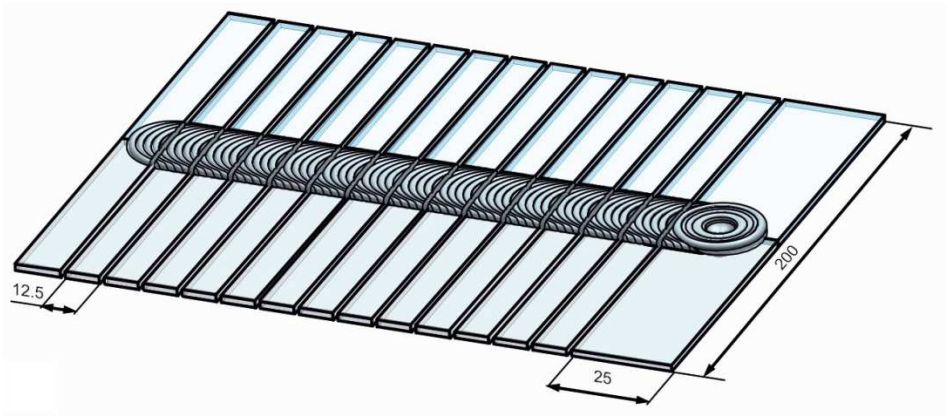

Fig. 6. Geometry of specimens for uniaxial tensile testing (dimension are in mm)

Backward elimination regression model were developed. As an input factors tool rotation per minute, feedrate and number of grooves were selected. Factors were coded -1 for lower and +1 for high limit. Number of grooves was set as categoric 4 levels: 0, 1, 2, 6 (Table 3).

Table 3. Input factors used in experiments

Factor	Name	Units	Type	Min.	Max.	Coded Low	Coded High	Mean	Std. Dev.
A	Tool rotational speed	1/min	Num.	1000	2000	-1 ↔ 1000	+1 ↔ 2000	1500.34	360.59
B	Feed rate	mm/min	Num.	200	1000	-1 ↔ 200	+1 ↔ 1000	586.21	294.66
C	Number of grooves		Categoric	0	6			Levels:	4.00

3. Results

Ultimate tensile strength test results have been taken into account as the response. Performed analysis of variation (ANOVA) and cubic model were selected with regard to fit summary of different models. Then applied backward eliminator algorithm which removes insignificant input factors with p-value less than 0.1 but with hierarchical agreement. Table 4 presents ANOVA for Reduced Cubic Model of UTS. The Model F-value of 19.24 means that model is significant and only a 0.01% chance that this large values could result due to noise. P-value for factors is less than 0.05 which means that model is significant.

Table 4. ANOVA for UTS response for reduced CUBIC model

Source	Sum of Squares	df	Mean Square	F-value	p-value	Signifi-cance
Model	7.572E+05	9	84137.06	19.24	< 0.0001	significant
A-Tool RPM	77165.40	1	77165.40	17.65	0.0001	
B-Feedrate	3.532E+05	1	3.532E+05	80.77	< 0.0001	
C-No. of grooves	1.050E+05	3	35011.94	8.01	0.0002	
AB	1.234E+05	1	1.234E+05	28.22	< 0.0001	
A^2	66868.44	1	66868.44	15.29	0.0003	
B^2	31448.21	1	31448.21	7.19	0.0101	
B^3	41593.47	1	41593.47	9.51	0.0034	
Residual	2.055E+05	47	4372.23			
Lack of Fit	1.881E+05	44	4275.25	0.7378	0.7312	not significant
Pure Error	17383.84	3	5794.61			
Cor Total	9.627E+05	56				
Std. Dev.	66.12			R^2		0.7865
Mean	199.82			Adjusted R^2		0.7457
C.V. %	33.09			Predicted R^2		0.6928
				Adeq Precision		16.7052

Obtained R^2 value is 0.7865 for the UTS model means that it's 78.65% able to predict response values. Predicted R^2 = 0.7457 and adjusted R^2 = 0.6928 are with an acceptable agreement. Precision ratio higher than 4 indicates adequate signal so the model can be applied to operate design space. The equation, which is consistent with the experimental model and describes UTS, is given in Equation (1) with the coded factors:

$$\begin{aligned} UTS = {} & 204.38 - 56.68 \times A - 227.56 \times B - 59.98 \times C[1] \\ & + 43.82 \times C[2] + 35.38 \times C[3] + 87.29 \times AB \\ & - 79.58 \times A^2 + 59.09 \times B^2 + 135.42 \times B^3 \end{aligned} \quad (1)$$

The modified CUBIC model was subjected to a convergence analysis. The following analyzes were performed: externally studentized residuals, predicted vs. actual analysis and Cook's Distance analysis (Vahdati et al., 2020). The obtained results are shown in Fig 7.

The RSM (Eshghi & Lee, 2019) analysis shows the influence of the welding parameters on the strength of the FSW joint (UTS) depending on the used tool and welding parameters (Figs. 8 and 9). The best results were achieved for the C1 and C2 tools. The parameters from the red areas of the graphs correspond to the best strength of the FSW joint. It can be seen that for all tools variants, an increase in the welding speed causes a reduction in the mechanical properties of the FSW joint. Tool without any shoulder modification (C0) produces a FSW joint with the lowest mechanical properties.

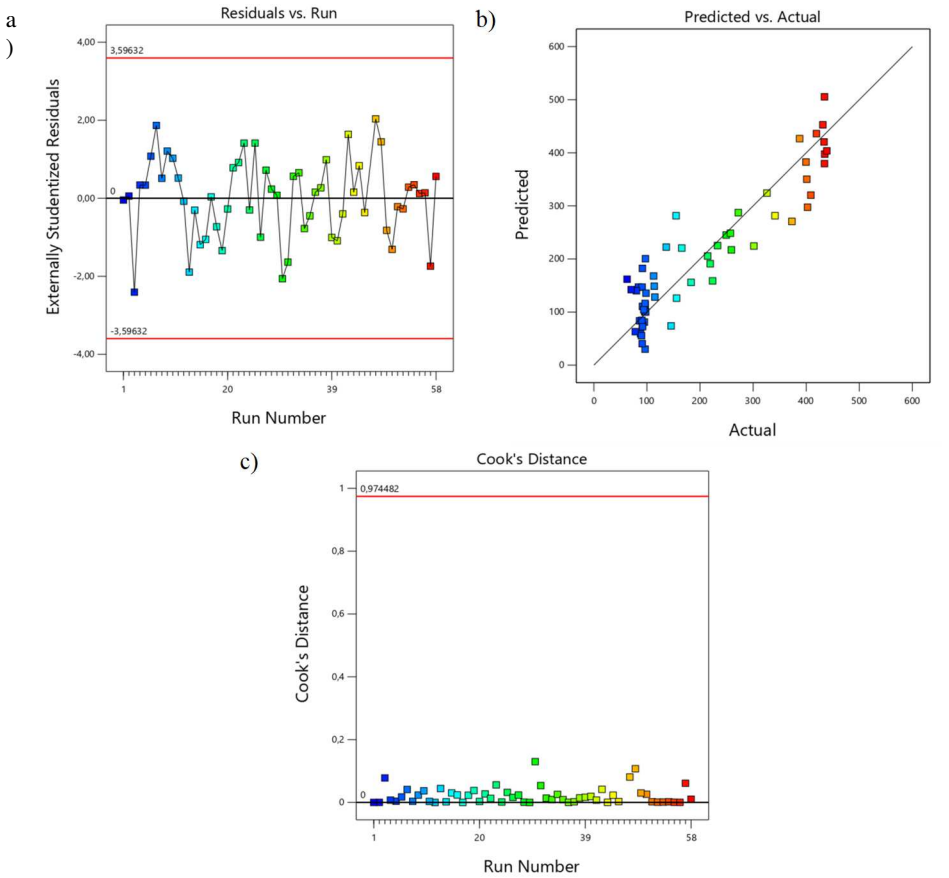

Fig. 7. Analysis of the convergence of the adopted model: a) Externally Studentized Residuals; b) Predicted vs. Actual analysis; c) Cook's distance

For the obtained experimental data, optimization of welding parameters was performed using the hill climbing method. The following optimization criterion was used: rotation speed and welding speed within the scope of the experiment, any tool, UTS max in the range up to 400 ÷ 470 MPa (Fig. 10). As a result of optimization, using the welding parameters of 1000 rpm and 200 mm/min for the tool C1, it is possible to make FSW joints with the best mechanical properties close to the parent material.

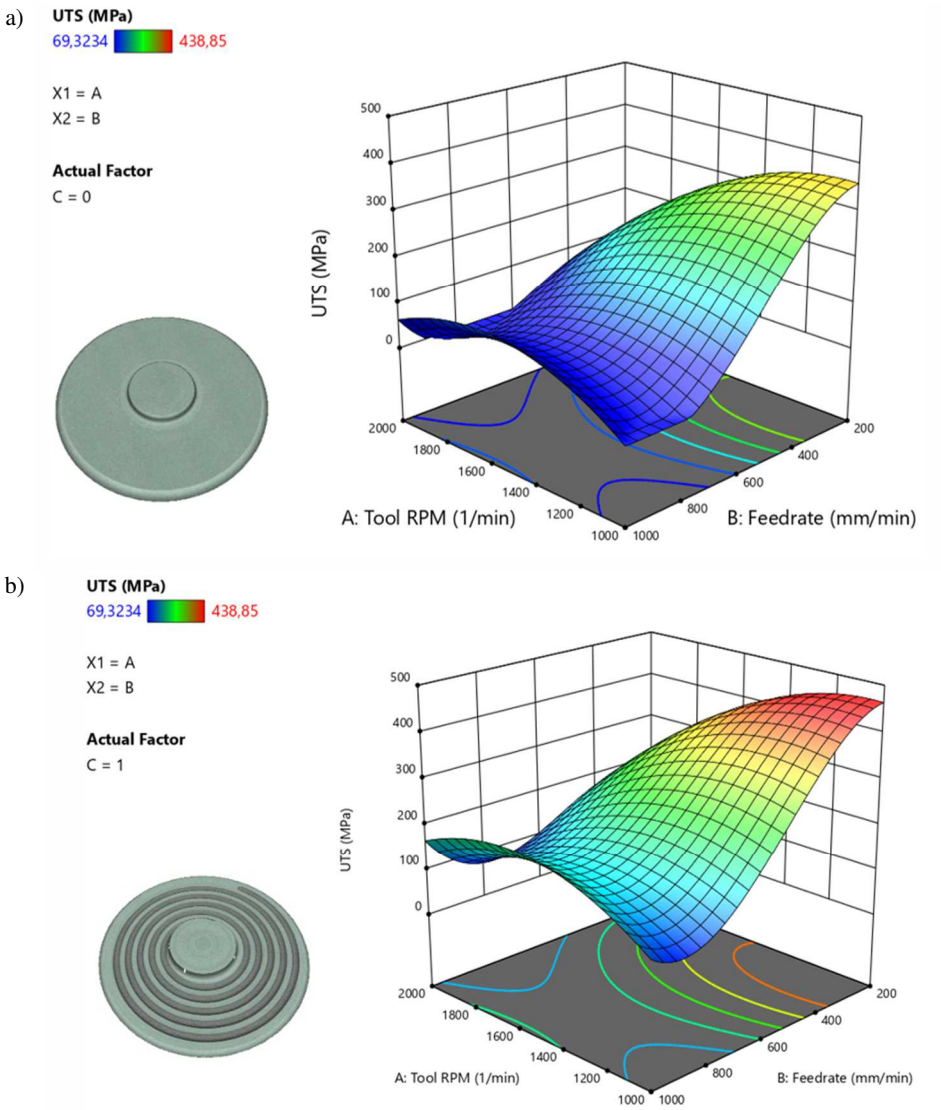

Fig. 8. Response surface plots presenting the interaction between tool rotational speed and feed rate affecting the UTS for a) flat and b) grooved shoulder (number of grooves: 1)

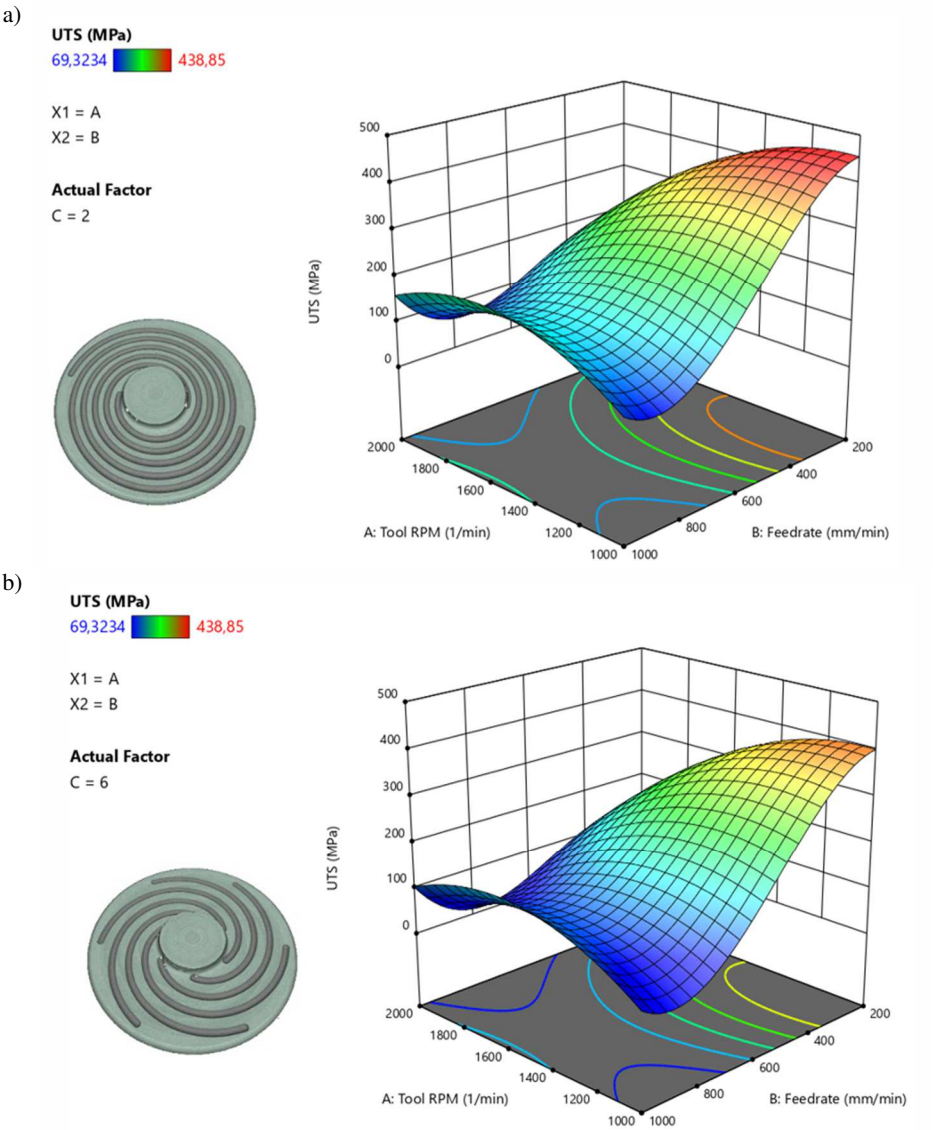

Fig. 9. Response surface plots presenting the interaction between tool rotational speed and feed rate affecting the UTS for grooved shoulder with number of groves: a) 2 and b) 6

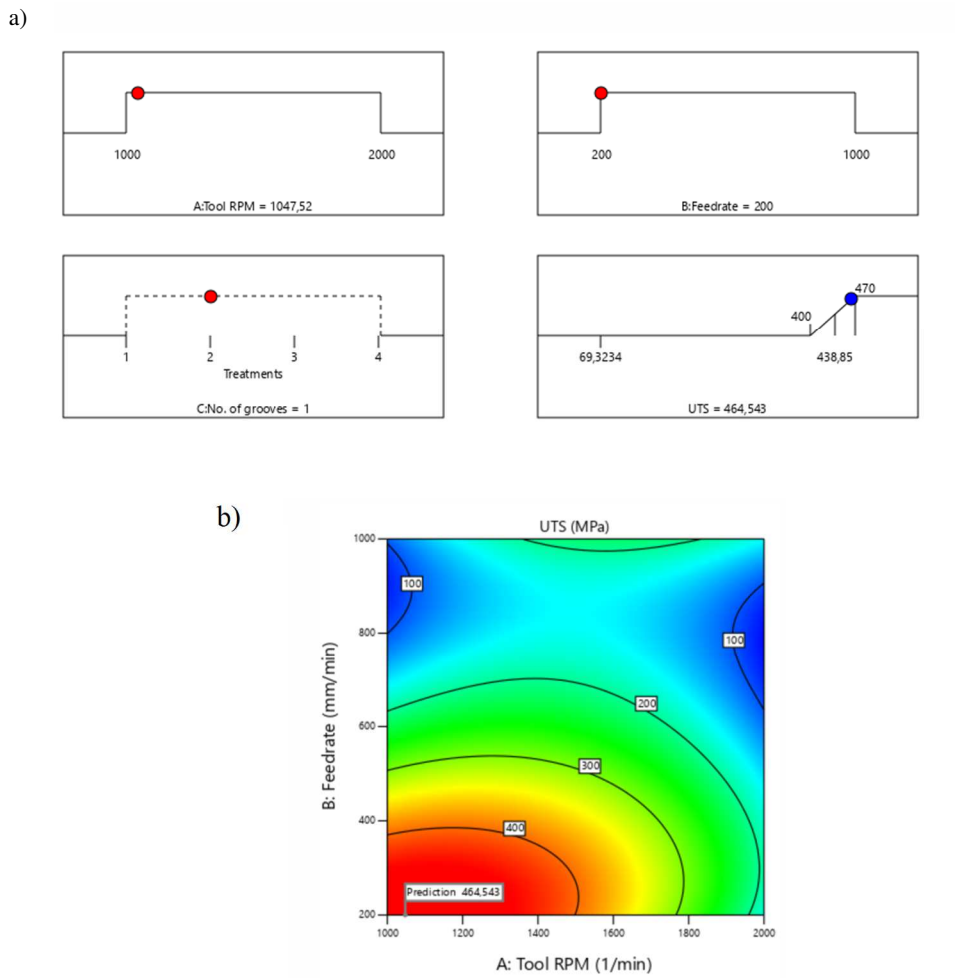

Fig. 10. Hill Climbing optimalization results for FSW process: a) optimization criteria with an indication of the best parameters, b) optimisation results

The tool made of tool whiskers reinforcement ceramics fully meets the expectations regarding the implementation of the FSW process. Tool ceramics are characterized by low thermal conductivity which allows to shorten the dwell time significantly. Another advantage of this approach is high resistance to abrasion and mechanical loads. The manufacturing process of an FSW tool is typical for the manufacture of cutting tools. No problems were encountered in this regard. Moreover, ceramic tools do not shown any signs of wear (Table 5). The geometry of the tool shoulders significantly improves the quality of the weld. A single concentric helix has been shown to help produce the best joint.

Table 5. Tool wear test performed after 10 m of welds

Number of grooves	0	1	2	6
New tools				
Tool used (approx. 10 m of weld)		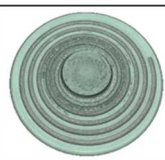	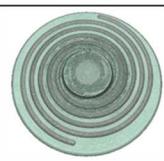	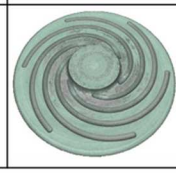

The applied technological parameters of FSW welding allowed for the preparation of regression models with a relatively high convergence of nearly 80% as evidenced by the performed diagnostics of the CUBIC model. Application advanced statistical analyzes to select the optimal technological parameters for welding AA2024-T3 alloy sheets of 0.5 mm in thickness. The results of the experiment confirmed these assumptions.

4. Conclusions

A new tooling approach was proposed for the FSW process based on tool ceramics. The methods used to optimize the technological parameters of the FSW process significantly improved the quality of the obtained joints. Modifying the tools shoulder geometry improves the mechanical properties of the FSW joint and is an important factor for tools design. The following conclusions can be drawn:

- The use of a whisker-reinforcement ceramic tool enables the production of high-quality FSW joints with a strength exceeding 95% compared to the parent material.
- The geometry of the helical grooves on the face of the tool greatly affects the quality of the FSW joint.
- The reduced CUBIC model was characterized by the coefficient of determination $R^2 = 0.7865$.
- For the parameters: 1000 rpm and 200 mm/min and the C1 tool, the best joint was obtained, the strength of which is similar to parent material.
- After realizing approx. 10 m of weld with each tool, no signs of tool wear were observed.

References

Ahmed, M.M.Z., Barakat, W.S., Mohamed, A.Y.A., Alsaleh, N.A., & Elkady, O.A. (2021). The development of WC-based composite tools for friction stir welding of high-softening-temperature materials. *Metals*, 11, 285. https://doi.org/10.3390/met11020285

Elangovan, K., & Balasubramanian, V. (2007). Influences of pin profile and rotational speed of the tool on the formation of friction stir processing zone in AA2219 aluminium alloy. *Materials Science and Engineering: A*, 459, 7–18. https://doi.org/10.1016/j.msea.2006.12.124

Eshghi, A.T., & Lee, S. (2019). Adaptive improved response surface method for reliability-based design optimization. *Engineering Optimization*, 51, 2011–2029. https://doi.org/10.1080/0305215X.2018.1561885

Kumar, K., & Kailas, S.V. (2008). The role of friction stir welding tool on material flow and weld formation. *Materials Science and Engineering: A*, 485, 367–374. https://doi.org/10.1016/j.msea.2007.08.013

Takhakh, A.M., & Hussein, H.K. (2021). Experimental investigation and parametric optimization of FSW for the 2024-O aluminum alloy joints. *IOP Conference Series: Materials Science and Engineering*, 1094, 012134. https://doi.org/10.1088/1757-899X/1094/1/012134

Thomas, W.M., Nicholas, E.D., Needham, J.C., Murch, M.G., Temple-Smith, P., & Dawes, C.J. (1995). Friction welding. US Patent USP1995105460317.

Vahdati, M., Moradi, M., & Shamsborhan, M. (2020). Modeling and optimization of the yield strength and tensile strength of Al7075 butt joint produced by FSW and SFSW using RSM and desirability function method. *Transactions of the Indian Institute of Metals*, 73, 2587–2600. https://doi.org/10.1007/s12666-020-02075-8

Węglowski, M.S. (2018). Friction stir processing – State of the art. *Archives of Civil and Mechanical Engineering*, 18, 114–129. https://doi.org/10.1016/j.acme.2017.06.002

Zhang, C., Qin, Z., Rong, C., Shi, W., & Wang, S. (2020). The preliminary exploration of micro-friction stir welding process and material flow of copper and brass ultra-thin sheets. *Materials*, 13, 2401. https://doi.org/10.3390/ma13102401

NOWE PODEJŚCIE NARZĘDZIOWE DO ZGRZEWANIA TARCIOWEGO CIENKICH BLACH AA2024-T3 - OPTYMALIZACJA PARAMETRÓW ZGRZEWANIA

S t r e s z c z e n i e

W pracy zaprojektowano i wykonano nowe narzędzia ceramiczne o różnym rozkładzie rowków w celu wzbogacenia technologii łączenia konstrukcji cienkościennych i uzyskania wysokiej jakości połączenia blach ze stopu aluminium AA2024-T3 Alclad o grubości 0,5 mm. Przetestowano cztery typy narzędzi, bez rowków, z 1, 2 i 6 rowkami. Narzędzia wykonano z dwóch materiałów. Część chwytową wykonano z węglika wolframu, a korpus narzędzia z ceramiki wzmocnionej whiskerami. Wpływ parametrów technologicznych na wytrzymałość złączy FSW badano metodami analizy powierzchni odpowiedzi (RSM) oraz analizy wariancji (ANOVA). Najmniej trwałą spoinę wytworzyło narzędzie bez rowków. Narzędzie z pojedynczym i podwójnym rowkiem zapewniło

dobrej jakości spoinę w szerokim zakresie prędkości obrotowych narzędzia. Wykazano, że rowki na kołnierzu narzędzia istotnie wpływają na jakość uzyskanego połączenia FSW.

Słowa kluczowe: stop aluminium AA2024-T3, ANOVA, narzędzia ceramiczne, zgrzewanie tarciowe z przemieszaniem, gemetria narzędzia do zgrzewanie tarciowego z przemieszaniem, łączenie cienkich blach, RSM

DOI: 10.7862/rm.2022.3

Submitted//Tekst złożono w redakcji: June 2022
Accepted/Przyjęto do druku: July 2022
Published/Tekst opublikowano: December 2022

ZESZYTY NAUKOWE POLITECHNIKI RZESZOWSKIEJ – MECHANIKA
SCIENTIFIC LETTERS OF RZESZOW UNIVERSITY OF TECHNOLOGY – MECHANICS
94 (2022), s. 51-61

Marek SZEWCZYK[1]
Krzysztof SZWAJKA[2]

ANALYSIS OF THE FRICTION MECHANISMS OF DC04 STEEL SHEETS IN THE FLAT STRIP DRAWING TEST

Abstract: This article presents the use of a specially designed flat strip drawing tester in order to assess the change in surface topography of DC04 steel sheets. The flat strip drawing test simulates friction conditions in the sheet metal-blankholder interface during deep drawing processes. Experimental tests were carried out at various nominal pressures and in dry friction and lubricated conditions. Two widely available gear and engine oils were used in the study. It was found that, in the range of pressures investigated between 3 and 12 MPa, 80W-90 gear oil provided a greater reduction in the value of the coefficient of friction (COF) than 5W-30 engine oil. Gear oil reduced the COF by an average of about 13.4 [%]. The lubrication efficiency depends on the pressure values; the greater the pressure, the lower the lubrication efficiency. A lowering of the value of the main amplitude surface roughness parameters Sa and Sq was generally observed. SEM analysis showed that even under lubrication conditions there was intense flattening of the roughness asperities of the sheet metal.

Keywords: coefficient of friction, friction, sheet metal forming, surface topography

1. Introduction

In the deep drawing process, several areas can be distinguished in terms of the stress state, deformation state, sliding speed and friction conditions: the flange of the drawpiece, the area of the edge of the punch and die, the wall and bottom of the drawpiece. Different friction conditions prevail in these zones due to

[1] Corresponding author: Marek Szewczyk, Rzeszow University of Technology, Department of Integrated Design and Tribology Systems, Faculty of Mechanics and Technology, ul. Kwiatkowskiego 4, 37-450 Stalowa Wola, Poland, e-mail: m.szewczyk@prz.edu.pl, ORCID ID: 0000-0002-3622-6613

[2] Krzysztof Szwajka, Rzeszow University of Technology, Department of Integrated Design and Tribology Systems, Faculty of Mechanics and Technology, ul. Kwiatkowskiego 4, 37-450 Stalowa Wola, Poland, e-mail: kszwajka@prz.edu.pl, ORCID ID: 0000-0002-1038-1148

different sliding velocities and values of normal pressures. The unfavourable effects of friction include, for example, non-uniformity of the drawpiece deformation, increased pressure exerted by the punch and deterioration of the surface finish of the drawpiece (Recklin et al., 2018; Vyboch et al., 2011). Only the friction of the sheet against the surface of the punch is a positive phenomenon because it increases the maximum forming force. The unfavourable phenomenon of friction can be counteracted by, among others factors, using appropriate lubricants, texturing the surface of the tools and applying self-lubricating coatings to the surface of the tools (Antoszewski et al., 2008; Kirkhorn et al., 2012; Sniekers & Smits, 1997). Correct selection of the lubricant is essential to obtain a product with the appropriate surface finish. The lubricant directly influencing the value of the coefficient of friction is a key parameter that determines the maintenance of the lubricating film at elevated temperature, which may occur in the contact zone.

The flange surface under the blankholder is one of the largest areas of friction in the deep drawing process. Too much friction in the flange area can cause the drawpiece to crack prematurely. So, knowing the friction conditions that prevail in this zone is crucial to assuring the appropriate friction conditions. The strip drawing test is used to experimentally determine the value of the coefficient of friction existing in the flange of the drawpiece. This test involves pulling a sheet metal strip between two countersamples, most often of cylindrical (Roizard et al., 2009) or flat (Solfronk et al., 2018) shape. The parameters influencing the change of friction conditions are the countersample clamping force, lubrication conditions, sliding speed and surface roughness of the countersamples.

Over the years, the strip drawing test has been investigated by various researchers. Costa and Emmens (1997) investigated the effect of different contact areas on the friction coefficient, using a vertical strip drawing test. The found that tool length and the contact area has a high influence on friction. Hutchins (2009) studied the effects of die surface patterning on lubrication in strip drawing test. Dies composed of circular pockets and parallel grooves. When the grooves were oriented parallel to the drawing direction, the friction was much greater. On the other hand the grooves oriented perpendicular to the drawing direction greatly reduced the friction. Vollertsen & Hu (2006) studied the tribological size effect in sheet metal forming (SMF) of Al99.5 aluminium sheets using a strip drawing test. They concluded that with miniaturisation of process dimension the tribology within SMF will be greater. Severo et al. (2009) analysed experimentally the tribological behaviour of W–Ti–N coatings in semi-industrial strip-drawing test. The performance of the tester developed has been confirmed. With uncoated tools adhesion always occurred independently of the testing load. In lubricated conditions, the coefficient of friction was always lower with coated tools. Wang et al. (2013) investigated tribological behaviour of diamond-like carbon (DLC) film deposited on female die in strip drawing test. It was found that surface topography

of specimen and the sample dimensions have a little effect on tribological behaviors of DLC film than castor oil. Evin et al. (2021) analysed the friction coefficient in different regions of the die during sheet metal forming in strip drawing test and cup test. DC05 steel sheets for the automotive industry were tested under various friction conditions. It was found that, with increased contact pressure on the contact surfaces, the effectiveness of Anticorit 3802-39 S lubricant with high-pressure EP additives improves. Tevares et al. (2021) analysed the friction mechanisms of thin hard PVD coated forming tools in strip drawing test. The experiments revealed that the VN and CrN/TiN coatings presented low and stable friction coefficient values. This has been attributed to the formation of relatively smooth and partially oxidized transfer layers on the tool. Filali et al. (2022) numerically predicted the galling of 6082 aluminium alloys in cold strip drawing test, with and without lubricant. The developed numerical model was able to predict the onset of galling. Schell et al. (2022) Investigation of oil-, wax-, polymer- and solid lubricants for aluminium warm and hot forming based on a strip drawing test. It was found that mixing different lubricants can greatly improve overall lubrication performance.

In this paper the flat strip drawing test was used to evaluate the coefficient of friction of DC04 steel sheets, commonly used in the automotive industry. Experiments were carried out at various nominal pressures and lubrication conditions. The main friction mechanisms were revealed based on scanning electron microscope micrographs and analysis of the surface topography.

2. Material and methods

2.1. Test material

Deep drawing quality DC04 steel sheet, commonly used in the automotive industry was used as a test material. The mechanical properties of the test material were determined at ambient temperature using a Zwick/Roell Z100 uniaxial tensile testing machine. Three specimens were tested and the average values of the basic mechanical parameters were determined (Table 1).

Table 1. Basic mechanical parameters of the DC04 steel sheet.

Yield stress, [MPa]	Ultimate tensile stress, [MPa]	Elongation , [%]	Percentage reduction of area, [%]	Hardness HV5
165.2	309.3	37.1	45.7	97

The basic height parameters of the geometric structure of the surface were determined using a Hommel-Etamic T8000RC stationary profilometer. The values of basic surface roughness parameters are as follows: arithmetical mean

height Sa = 1.55 [µm], root mean square deviation Sq = 1.26 [µm], kurtosis Sku = 2.68, skewness Ssk = -0.0307, maximum profile peak height Sp = 8.02 [µm], maximum height Sz = 15.0 [µm] and maximum profile valley depth Sv = 6.93 [µm]. The topography of the sheet metal and the flat countersamples are shown in Fig. 1a and Fig. 1b, respectively.

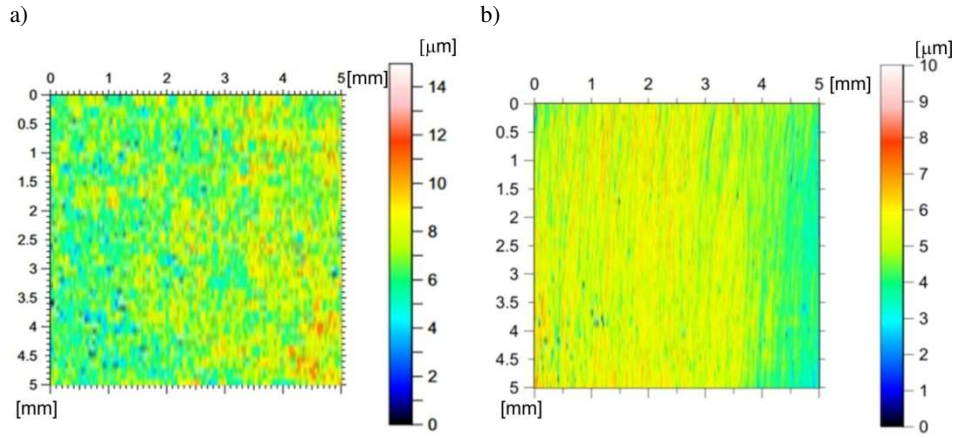

Fig. 1. Topography of the a) sheet surface and b) countersamples.

2.2. Procedure of friction testing

A tester which was specially designed to perform the strip drawing test is shown in Fig. 2. The strip drawing test consists in pulling a sheet metal strip between two countersamples made of 145Cr6 cold-work tool steel with a flat working surface. The device has the advantage that it is a simple structure with uncomplicated measurement of the force parameters during the test. The device was mounted in the lower grip of the Zwick/Roell Z100 testing machine. The upper end of the sample in the form of a sheet metal strip with dimensions of 130 (length) x 20 (width) [mm] was attached in the upper grip of a testing machine. The pulling force was recorded using the measuring system of the testing machine. The contact pressure was recorded by means of the Labview program on the basis of the indications of a Kistler type 9345B force sensor. Values of both friction and normal forces were correlated in the LabVIEW program based on a Megatron Series SPR18 potentiometric linear transducer. On the basis of the values of the pulling force (F_P) and clamping force (F_N), the value of the coefficient of friction was determined in accordance with the relationship:

$$\mu = \frac{F_P}{2F_N} \tag{1}$$

The sliding speed of the specimen was 2 [mm/s]. The friction tests were carried out for four nominal pressures of 3, 6, 9, 12 [MPa] and in conditions of dry friction (in the as-received sheet-metal state) and the sheet surface lubricated with oil. Typical synthetic oils were used, which are generally available and relatively cheap compared to professional deep-drawing greases: Castrol Axle EPX SAE80W-90 gear oil and Castrol Edge SAE5W-30 engine oil with a kinematic viscosity of 134 [mm^2/s] and 70 [mm^2/s], respectively.

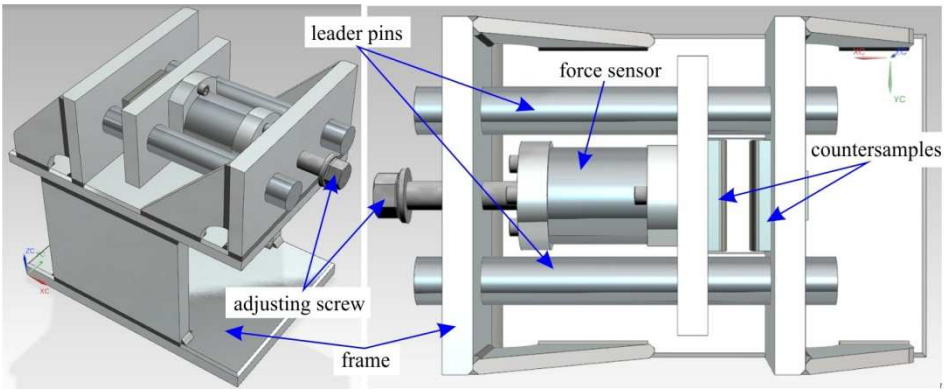

Fig. 2. Model of the friction tester

3. Results and discussion

The value of the COF for all friction conditions investigated decreases with increasing nominal pressure. This is related to the flattening of the roughness asperities and a reduction in the role of the mechanism of interlocking of the asperities in the total resistance to friction. This is a well-known phenomenon that has also been observed by Kirkhorn et al. (2012), Severo et al. (2009), Recklin et al. (2018), Vollertsen & Hu (2006). In the pressure range studied, the coefficient of friction is reduced by 11.5 [%], 15.4 [%], 6.8 [%] for dry friction, lubrication with engine oil and gear oil, respectively. The introduction of a lubricant between the rubbing surfaces changes the external friction into internal friction in this substance. Lubrication with engine oil reduced the coefficient of friction by an average of about 6.1 [%]. in relation to dry friction. The gear oil showed greater lubrication efficiency in reducing the coefficient of friction by an average of about 13.4 [%]. This oil was almost twice as viscous as engine oil.

Low-viscosity oils flow better, so that less energy is lost to overcome internal friction, surface activity and viscosity and this determines the maintenance of the lubricant on the surface under high unit pressures. Liquid lubricants separate the surfaces of the drawpiece and the tool to a to a greater or lesser extent. Due to high unit pressures, it is not always possible to maintain a continuous layer of

lubricant, which results in the activation of the adhesion mechanism. The behaviour of the coefficient of friction in the case of lubrication is illustrated by the so-called Stribeck curve [8].

For the highest value of nominal pressure, the difference in the value of the coefficient of friction for both oils is blurred. The difference in the value of the coefficient of friction determined in the lubrication conditions for the pressure of 12 [MPa] was only 2.6 [%].

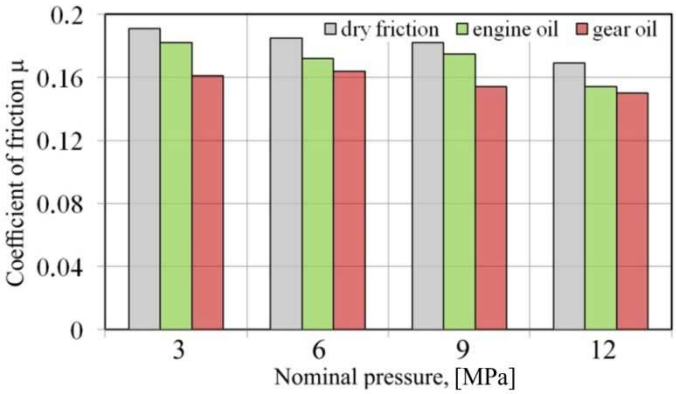

Fig. 3. Effect of nominal pressure on the value of coefficient of friction

Under dry friction conditions, a tendency was observed to decrease the values of the maximum height Sz, maximum profile valley depth Sv and maximum profile peak height Sp (Fig. 4a). The value of the main amplitude parameters (Sa and Sq) determined for the entire surface measured decreases only slightly with increasing nominal pressure. Different behaviour of the friction surface was observed under lubricated conditions (Figs. 4b and 4c). The value of the parameters Sz, Sv and Sp increased only to a certain pressure value of 3-6 [MPa], and then there is a downward trend. In the range of low pressures, the pressure of the lubricant is insufficient to create a "lubricant cushion" completely separating the rubbing surfaces. Thus, there is a significant role of the mechanism of mechanical cooperation of asperities and their flattening. In this way, the values of the parameters Sv and Sz only decrease from a certain pressure value (9 MPa in Figs. 4b and 4c).

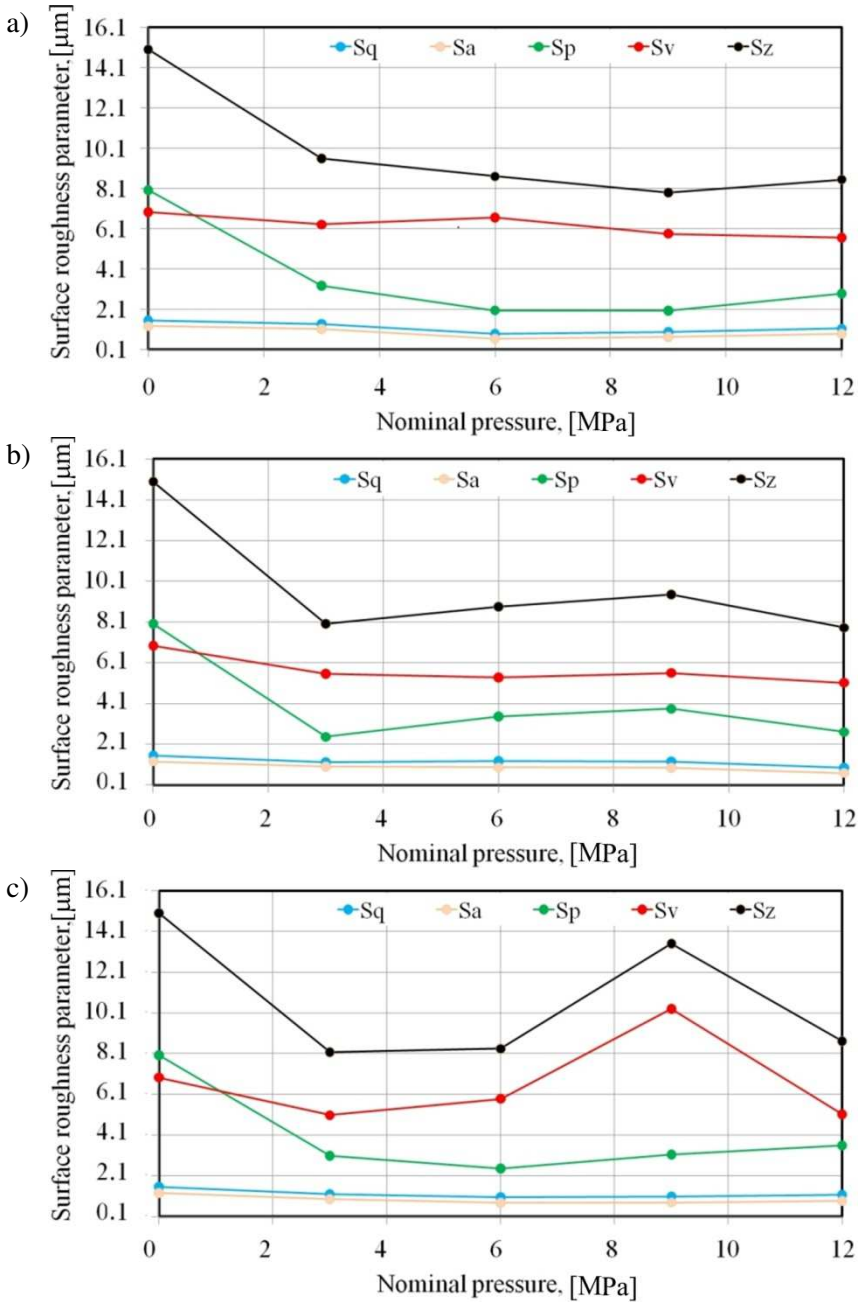

Fig. 4. Influence of nominal pressure on the surface roughness parameters after a) dry friction and lubrication of sheet metal surfaces with b) engine oil and c) gear oil

Due to the large contact area in the flat strip drawing test, the test surface of the sheet is subject to an intensive flattening process, which is visible for all friction conditions investigated (Figs. 5a-5c). It should also be noted that the sheet material is characterised by a much lower yield stress value than the tool material. This distinguishes the friction conditions in metal forming processes from the friction occurring in kinematic pairs, i.e., bearings.

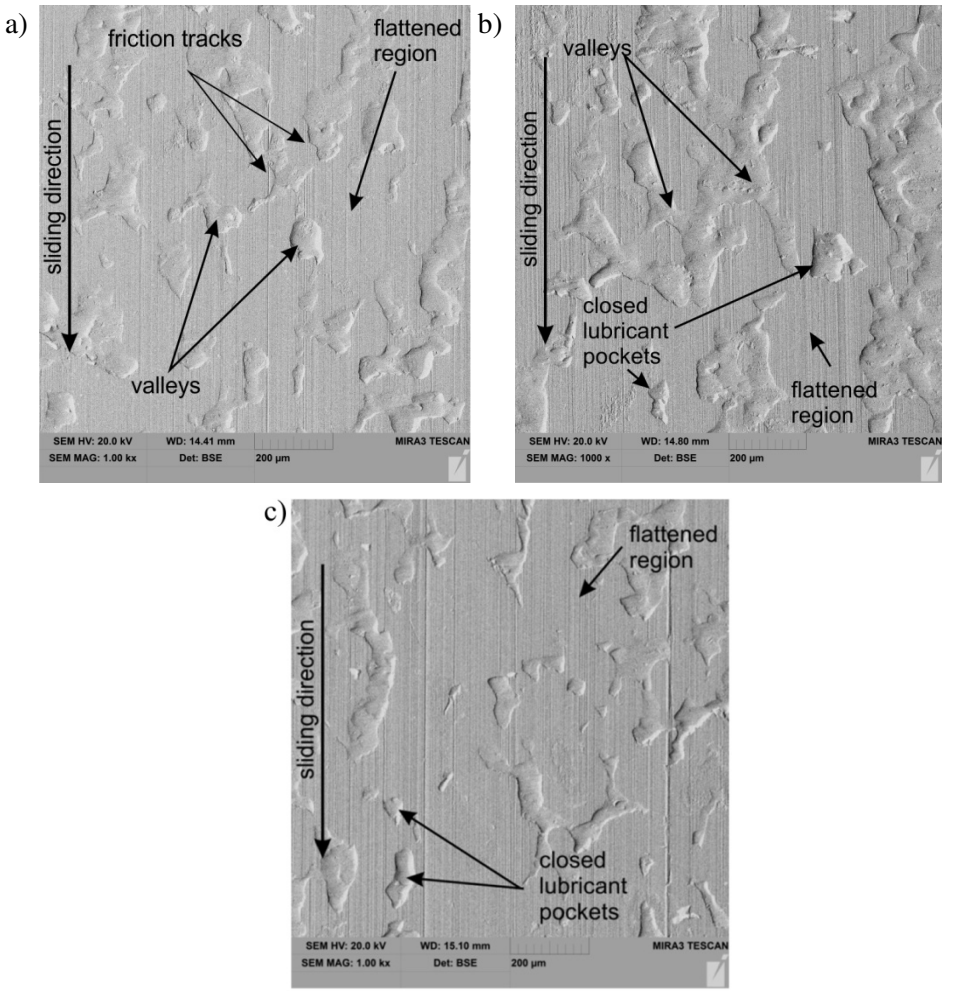

Fig. 5. SEM micrographs of sheet metal surfaces tested under a load of 9 [MPa] in conditions of: a) dry friction, b) lubrication with machine oil and c) lubrication with gear oil

The valleys in the as-received sheet-metal state do not, however, undergo a complete flattening process. However, most of the valleys are connected to each other, which makes it difficult for a "lubricant cushion", consisting of the formation of hydrostatic pressure of the lubricant in closed lubricant pockets (Figs. 5b, 5c), to occur. The lack of deep grooves on the surface of the sheet indicates that the sheet material does not stick to the surface of the tool. Under unfavourable conditions, hard forms build up on the surface of the tools, associated with the phenomenon of adhesive sticking, which forms ridges on the surface of the sheet. The surface of the sheet is subjected to the work hardening phenomenon in places where surface asperities are flattened, which is related to the increase of yield stress of material caused by plastic deformation.

4. Conclusions

In this article, the specially designed flat strip drawing tester was used to investigate friction mechanisms and the change in surface topography of DC04 steel sheets. The values of the COFs of the test material were evaluated in dry friction conditions and with the presence of two commonly available synthetic oils. The experimental tests revealed that, in the range of pressures investigated between 3 and 12 [MPa], 80W-90 gear oil provided a greater reduction in the value of the COF than 5W-30 engine oil. In general, a trend to a decrease of COF with nominal pressure was observed. Lubrication efficiency decreased with increasing pressure. For the highest pressure value (12 [MPa]), the difference in the efficiency of reduction of the COF by both lubricants was equal to about 2.6 [%]. SEM analysis has shown that the friction process causes intensive flattening of the surface asperities, even under lubrication conditions. This can be explained by the cooperation of relatively hard countersamples with the sheet material, characterised by a lower yield stress. Under these conditions, the volumes of the valleys are reduced and, consequently, the lubricant is not able to build up sufficient lubricant pressure.

References

Antoszewski, B., Evin, E., & Audy, J. (2008). A study of the effect of type (Cu+Ti) and (Mo+Ti) electro-spark coatings on friction in pin-on-disc testing. *Journal of Tribology*, 130, 0213031–0213036. https://doi.org/10.1115/1.2842296

Costa, H.L., Hutchings, L.M. (2009). Effects of die surface patterning on lubrication in strip drawing. *Journal of Materials Processing Technology*, 209, 3, 1175-1180. https://doi.org/10.1016/j.jmatprotec.2008.03.026

Emments, W.C. (1997). *Tribology of flat contacts and its application in deep drawing*. Ph.D. Thesis. University of Twente.

Evin, E., Daneshjo, N., Mareš, A., Tomáš, M., & Petrovčiková, K. (2021). Experimental assessment of friction coefficient in deep drawing and its verification by numerical simulation. *Applied Sciences*, 11, 2756. https://doi.org/10.3390/app11062756

Filali, O., Dubois, A., Moghadam, M., Nielsen, C.V., Dubar, L. (2022). Numerical prediction of the galling of aluminium alloys in cold strip drawing. *Journal of Manufacturing Processes*, 73, 340-353. https://doi.org/10.1016/j.jmapro.2021.11.008

Kirkhorn, L., Frogner, K., Andersson, M., & Ståhl, J.E. (2012). Improved tribotesting for sheet metal forming. *Procedia CIRP*, 3, 507–512. https://doi.org/10.1016/j.procir.2012.07.087

Recklin, V., Dietrich, F., & Groche, P. (2018). Influence of test stand and contact size sensitivity on the friction coefficient in sheet metal forming. *Lubricants*, 6, 41. https://doi.org/10.3390/lubricants6020041

Roizard, X., Pothier, J.M., Hihn, J.Y., & Monteil, G. (2009). Experimental device for tribological measurement aspects in deep drawing process. Jour*nal of Materials Processing Technology*, 209(3), 1220-1230. https://doi.org/10.1016/j.jmatprotec.2008.03.023

Schell, L., Emele, M., Holzbeck, A., & Groche, P. (2022). Investigation of different lubricant classes for aluminium warm and hot forming based on a strip drawing test. *Tribology International*, 168, 107449. https://doi.org/10.1016/j.triboint.2022.107449

Severo, V., Vilhena, L., Silva, P.N., Dias, J.P., Becker, D., Wagner, S., & Cavaleiro, A. (2009). Tribological behaviour of W–Ti–N coatings in semi-industrial strip-drawing tests. *Journal of Materials Processing Technology*, 209(10), 4662-4667. https://doi.org/10.1016/j.jmatprotec.2008.11.040

Sniekers, R.J.J.M., Smits, H.A.A. (1997). Experimental set-up and data processing of the radial strip-drawing friction test. *Journal of Materials Processing Technology*, 66, 216–223. https://doi.org/10.1016/S0924-0136(96)02526-5

Solfronk, P., Sobotka, J., Korecek, D., & Kolnerova, M. (2018). Tribological properties of al-alloy designed for drawing stampings in automotive industry. *MM Science Journal*, 6, 2354–2357. http://doi.org/10.17973/MMSJ.2018_06_201757

Stribeck, R. (1902). Die wesentlichen eigenschaften der gleit und rollenlager. *Zeitschrift des Vereines Deutscher Ingenieure*, 36, 1341–1348.

Tavares, A.F., Lopes, A.P.O., Mesquita, E.A., Almeida, D.T., Souza, J.H.C., & Costa, H.L. (2021). Effect of transfer layers on friction and wear mechanisms in strip drawing tests of commercially coated forming tool. *Wear*, 476, 203733. https://doi.org/10.1016/j.wear.2021.203733

Vollertsen, F., Hu, Z. (2006). Tribological size effects in sheet metal forming measured by a strip drawing test. *CIRP Annals*, 55, 1, 291-294. https://doi.org/10.1016/S0007-8506(07)60419-3

Vyboch, J., Evin, E., & Kmec, J. (2011). Tribological aspects of numerical simulation of deep-drawing process. *Manufacturing Engineering*, 3, 38–41.

Wang, C., Guo, B., Shan, D., & Bai, X. (2013). Tribological behaviors of DLC film deposited on female die used in strip drawing. *Journal of Materials Processing Technology*, 213, 323-329. https://doi.org/10.1016/j.jmatprotec.2012.10.011

ANALIZA MECHANIZMÓW TARCIA BLACH STALOWYCH DC04 ZA POMOCĄ TESTU PRZECIĄGANIA PASA BLACHY

S t r e s z c z e n i e

W artykule przedstawiono wyniki oceny zmian topografii powierzchni blach stalowych DC04 za pomocą specjalnie zaprojektowanego testera do realizacji testu przeciągania pasa blachy. Test ten symuluje warunki tarcia na styku blachy z dociskaczem w procesach głębokiego wytłaczania. Badania eksperymentalne przeprowadzono przy różnych naciskach nominalnych oraz w warunkach tarcia suchego i smarowania. Do badań wykorzystano dwa powszechnie dostępne oleje przekładniowe i silnikowe. W zakresie analizowanych nacisków 3-12 [MPa], olej przekładniowy SAE80W-90 zapewnił większe obniżenie wartości współczynnika tarcia w porównaniu do oleju silnikowego SAE5W-30. Olej przekładniowy zredukował wartość współczynnika tarcia średnio o około 13.4 [%]. Efektywność smarowania zależy od wartości nacisków. Im większy nacisk tym efektywność smarowania była mniejsza. Zauważono zmniejszenie wartości głównych parametrów amplitudowych chropowatości powierzchni Sa oraz Sq. Na podstawie mikrofotografii SEM zaobserwowano, że nawet w warunkach smarowania dochodziło do intensywnego wyrównywania wierzchołków nierówności blachy.

Słowa kluczowe: współczynik tarcia, tarcie, kształtowanie blach, topografia powierzchni

DOI: 10.7862/rm.2022.4

Submitted//Tekst złożono w redakcji: July 2022
Accepted//Przyjęto do druku: October 2022
Published//Tekst opublikowano: December 2022

ZESZYTY NAUKOWE POLITECHNIKI RZESZOWSKIEJ – MECHANIKA
SCIENTIFIC LETTERS OF RZESZOW UNIVERSITY OF TECHNOLOGY – MECHANICS
94 (2022), s. 63-75

Marcin SZPUNAR[1]
Maciej BALCERZAK[2]
Krzysztof ŻABA[3]

SHAPE ACCURACY IN SINGLE POINT INCREMENTAL FORMING OF CONICAL FRUSTUMS FROM TITANIUM CP2 SHEETS

Abstract: This paper presents frustum cone drawpiece analysis made of titanium CP2 sheet by a single incremental sheet forming. Central composite design has been adopted to carry out an experiment containing 20 runs, then multi-criteria parameter optimization has been done. Optimal parameters have been validated and responses deviations do not exceed 4% compared to created models. For the drawpiece formed with optimal parameters, AGRUS optical measurement and X-ray tomography has been applied to check the obtained of the part wall thickness and general deviations compared to the CAD model. The wall angle discrepancy of the cone generatrix has also been analyzed. No gaps or ruptures have been confirmed by X-ray. The blank rolling direction has a significant effect on the drawpiece deviations. The measurement results showed deviations of the drawpiece wall angle +0.27°/-0.06°, sheet thickness on the cone +0.012/-0.04 mm and +0.151/-0.096 mm from the reference CAD geometry.

Keywords: incremental sheet forming, titanium, springback, optical forming analysis, X-ray tomography

[1] Corresponding author: Marcin Szpunar, Doctoral School of Engineering and Technical Sciences at the Rzeszow University of Technology, Rzeszow University of Technology, al. Powst. Warszawy 12, 35-959 Rzeszów, Poland, e-mail: d547@stud.prz.edu.pl., ORCID ID: 0000-0003-1580-5357

[2] Maciej Balcerzak, Department of Metal Working and Physical Metallurgy of Non-Ferrous Metals, Faculty of Non-Ferrous Metals, AGH University of Science and Technology, al. Adama Mickiewicza 30, 30-059 Cracow, Poland., e-mail: maciejbalcerzak1@gmail.com

[3] Krzysztof Żaba, Department of Metal Working and Physical Metallurgy of Non-Ferrous Metals, Faculty of Non-Ferrous Metals, AGH University of Science and Technology, al. Adama Mickiewicza 30, 30-059 Cracow, Poland., e-mail: krzyzaba@agh.edu.pl, ORCID ID: 0000-0002-6541-885X

1. Introduction

The widespread use of numerically controlled machines (milling machines, lathes, etc.) enabled the dynamic development of incremental sheet forming (ISF) methods. The effect of this development is the possibility of forming sheet metals with free shapes. In high-volume production, incremental sheet metal forming is used when the desired effect cannot be obtained using conventional methods (Behera et al., 2017). There are several different types of forming approach that use an incremental approach: Single Point Incremental Forming (SPIF) (Martins et al., 2008), Two-Point Incremental Forming (TPIF) (Mostafanezhad et al., 2018), ultrasonic assisted ISF (Cheng et al., 2019), electromagnetic incremental forming (EMIF) (Cheng et al., 2022), water jet incremental forming (Shi et al., 2019) etc. To form hard-to-deform materials, heat-assisted incremental sheet forming was developed by Liu (2018). During the single-point incremental sheet metal forming analysis in this article, the deformation of the material is carried out gradually. The workpiece material and tools are less loaded compared to conventional deep-drawing processes. SPIF has the following advantages (Li et al., 2017; Murugesan et al., 2022; Wang et al., 2022): low force resulting from the incremental character of the process, high flexibility of the process makes it possible to quickly and easily take into account design changes in shaped elements, a conventional CNC machine can be used to carry out the process, the process does not require stamping dies. SPIF has also some disadvantages: requires a longer forming time than a conventional sheet forming process, the process is limited to prototyping and small production batches, poor surface finish.

One of the main problems in ISF are geometric deviations of the workpiece material after unloading which means that the resulting shape is not necessarily the desired shape. Honarpisheh et al. (2019) investigated the incremental forming process of explosively welded Cu/St/Cu multilayer sheets in order to determine the springback phenomenon on different layers. Spindle speed, tool feed, and incremental step depth were found to affect springback in SPIF. Khan et al. (2015) developed a classifier-based intelligent process model and its application to analyse the shape errors of square-based modified pyramids made from DC04 steel sheet. Cédric et al. (2020) proposed a technique to compensate, after the fact, for shape defects related to forming and springback in the micro-single-point incremental forming technique (μ-SPIF). The advantage of this method is to avoid geometric discontinuities by using B-spline curves. Micari et al. (2007) discussed several methods to improve the ability of the SPIF and concluded that tool path optimization approaches are the most promising in reduction of the springback defects. Karim et al. (2021) used a numerical response surface methodology with a Design of Experiments (DOE) to improve thickness reduction and the effects of the springback. Furthermore, the Gurson-Tvergaard-Needleman damage model was used to analyse the damage evolution during deformation of a

truncated pyramid. It was found that the wall angle is the most influential parameter on the springback amount. Jain et al. (2021) investigated the effect of various parameters on springback and thinning while performing SPIF on polypropylene sheets. The springback was found to increase with increasing tool diameter. Rusu et al. (2021) studied the behaviour of different EN AW-2007, EN AW-5754 and EN AW-6060 aluminium alloy sheets deformed through SPIF regarding springback effect. Frustum pyramids made of EN AW-2007 alloy presented the highest springback. Liao et al. (2022) investigated the effects of ultrasonic vibration and temperature on springback of polyether-ether-ketone drawpieces during the incremental forming process. As the temperature rises, the springback of most areas of the drawpiece decreases. They also found that ultrasonic vibration is beneficial to improving the geometric accuracy of SPIFed parts. Mezher et al. (2021) predicted the springback during the SPIF process of DC04 and EN AW1050 aluminium alloy sheet. They concluded that the degree of springback is increased as a result of increasing the wall angle. Wang et al. (2018) tried to reduce the springback for double-sided incremental forming and found that reverse bending and squeezing can decrease the springback of EN AW-7075 aluminium alloy drawpieces. Jung et al. (2020) proposed a procedure to construct the tool path for counter SPIF to decrease shape error. The two-stage SPIF was very effective in increasing the geometric accuracy of the EN AW-5052 aluminium alloy conical drawpieces. Oleksik et al. (2014) predicted springback of DC04 steel parts using the ARAMIS computational system. The lowest amount of springback is found in the opposite corner of the frustum of pyramid, compared to the corner where the maximum value of springback appears. A four camera system designed for measuring the shape variations of a sheet metal part during a SPIF process has been presented by Orteu et al. (2011).

In this paper, optical analysis ARGUS and computer tomography methods have been applied to determine the drawpiece thickness distribution as well as shape deviations caused mainly by a springback effect after the SPIF process of titanium CP 2 sheet. The drawpiece formed with optimized parameters as a result of multi-criteria optimization form central composite design of experiment has been taken into account.

2. Experimental setup

Titanium CP 2 has been selected as the material for a geometry formation of truncated cones. The initial sheet thickness was 0.4 mm and cut for round blanks with a diameter Ø100 mm. The mechanical properties of the material selected are presented in Table 1.

Table 1. Properties of the material selected for the drawpieces – titanium CP2

Density	Hardness	Ultimate Tensile Strength	Tensile Yield Strength	Elastic modulus
4.51 g/cm^3	235 HV	430 MPa	340 MPa	102 GPa

The Makino PS95 3-axis milling machine has been selected for a test stand. To firmly clamp the sheet blanks, a dedicated fixture for the incremental forming process has been produced. The fixture has been located inside the milling machine zone and attached to the CNC working table. A solid carbide hemispherical end tool with diameter Ø8 mm has been selected as a punch tool. The tool was ground from an ISO K30-K40 tungsten carbide rod and mounted in a collet chuck ER32. To reduce the friction coefficient and improve the lubrication between the tool and the formed sheet, 75W85 synthetic oil has been deposited. NX Siemens PLM software has been selected to create a drawpiece CAD shape and to generate CNC paths (Fig. 1a). An experimental stand prepared for the incremental forming process is presented in Fig. 1b. The drawpiece geometry has been assumed as 45° truncated cone ended with radius equal to the tool tip R = 4 mm (Fig. 2).

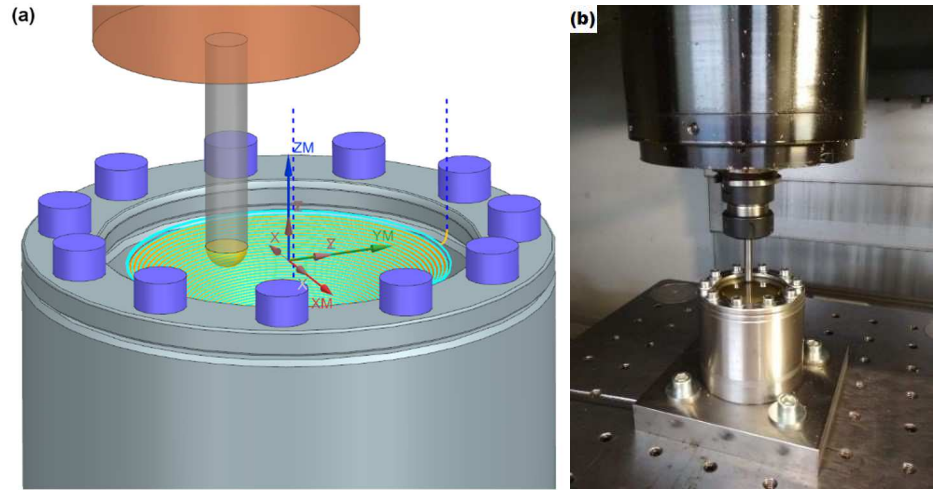

Fig. 1. (a) Programmed CNC tool path in NX Siemens CAM, (b) Test stand – Makino PS95 with SPIF dedicated device

Process input parameters have been determined as following: spindle speed, tool feed and incremental step depth, while incremental step depth means the vertical pitch between the spiral tool path during one loop. The central composite design of the experiment has been developed (Fig. 3) to determine the influence of input parameters on forming outputs such as axial forming force, in-plane forming force, surface roughness Rz parameter and forming success. On the basis of the created models, optimal forming parameters have been determined with

optimization criteria taken into account. Detailed information on the experiment can be found in the previous manuscript (Szpunar et al., 2021).

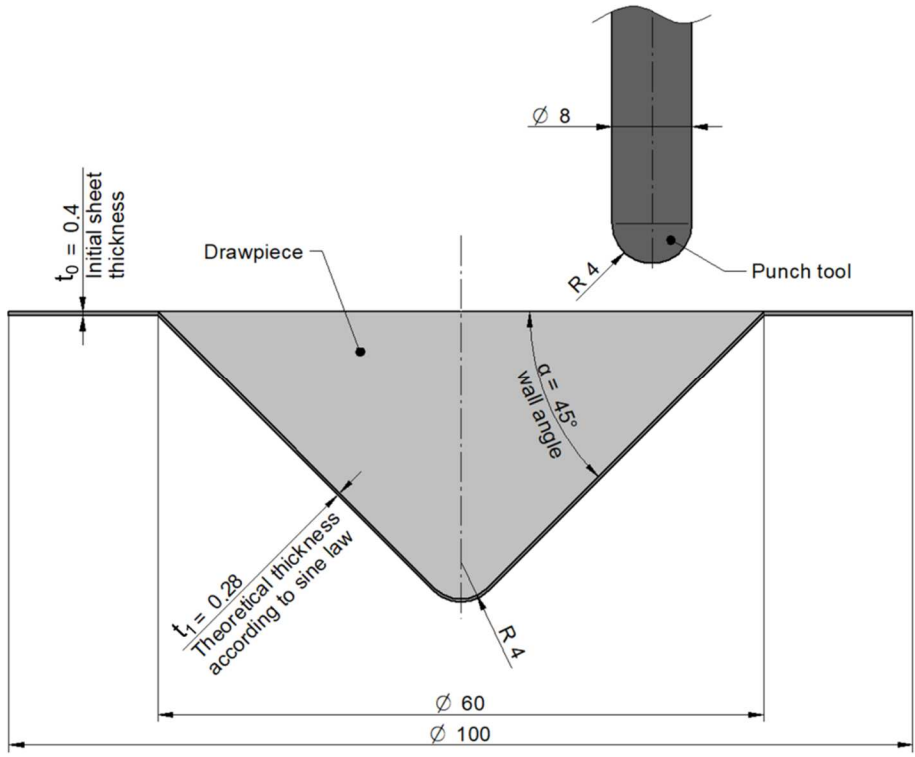

Fig. 2. Cross section of the desired drawpiece intended for deviation analysis

$$t_1 = t_0 \sin(90° - \alpha) \tag{1}$$

where t_1 – sheet thickness in forming stage,
t_0 – initial sheet thickness,
α – drawpiece wall angle.

Optimal forming parameters have been determined and validated with a deviation of outputs less than 4%. Figure 4 presents optimal forming parameters with predictions of the results according to the models obtained. The drawpiece formed using optimal parameters has been selected for further shape analysis (Fig. 5).

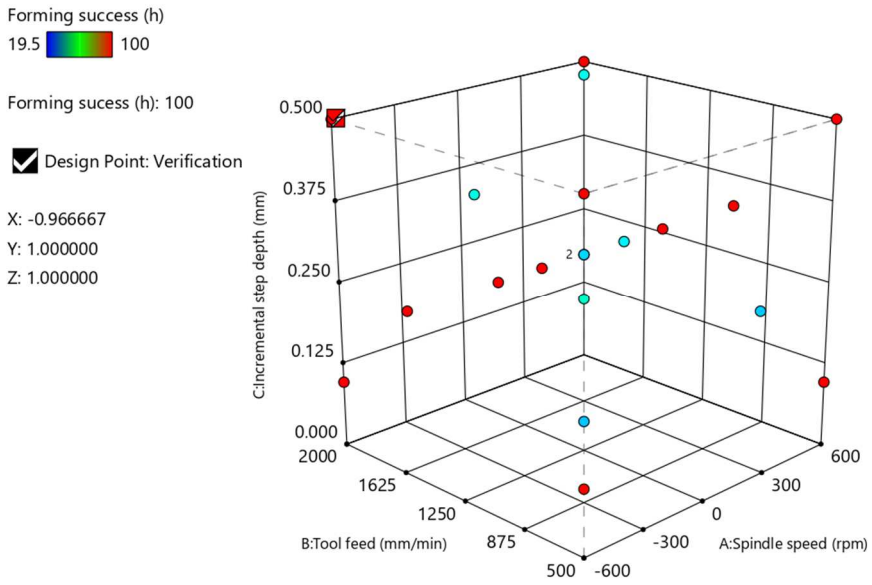

Fig. 3. 3D graph presenting the central composite design with a verification run

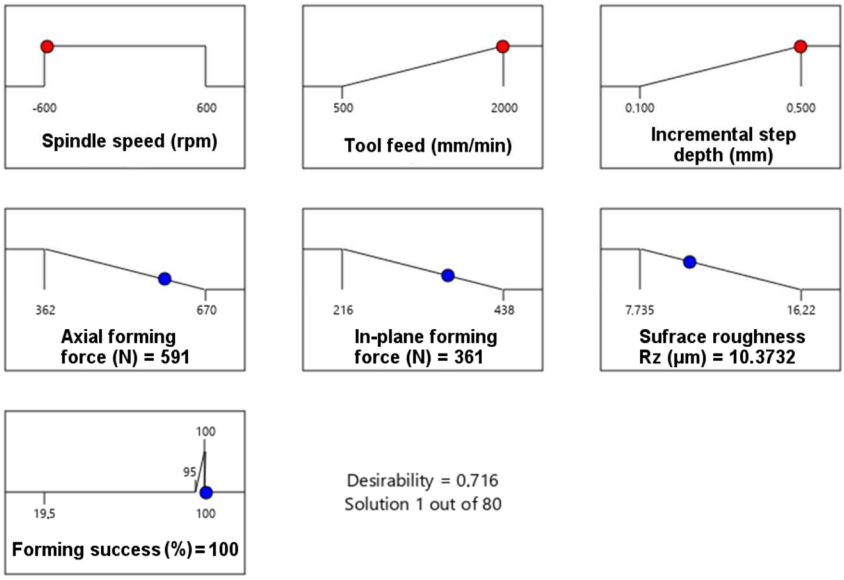

Fig. 4. Optimal ISF parameters with predicted process output received as multi-criteria optimization

Fig. 5. Successfully achieved the drawpiece using optimized parameters

The specimen was analyzed by the ARGUS system, which allows one to create 3D models from the scans. By these possibilities, drawpiece deviations and sheet thickness distribution measurement could be obtained. To be sure that there are no internal cracks, computer tomography using GE V | TOME | X M300 has been performed and several X-ray intersections have been captured. The major advantages of visual scanning methods are rapid analysis of drawpieces and non-destructive form of exploration. The theoretical thickness of the sheet can be described by Equation 1 using the principle of constant volume of material. Figure 2 presents the ideal shape of the drawpiece with the calculation of the sheet thickness (Eq. 1) taken into account. This method of necking estimation has been applied by many researchers (Chen et al., 2017; Harhash & Palkowski, 2021; Su et al., 2021). The CAD model of the drawpiece has been selected as a reference for the analysis of the sheet thickness differences as the well as shape deviations.

3. Results and Discussion

The 3D scan has been analysed in case of wall angle difference. 2D sections in a rolling and perpendicular to rolling direction were extracted and compared by measuring wall angle. Figure 6 presents the drawpiece wall angle determination through the intersection generatrix and the not deformed face. The resulting wall angle was 45.27° and 45.16° in the rolling direction, while 44.94° and 45.03° perpendicular to the rolling direction.

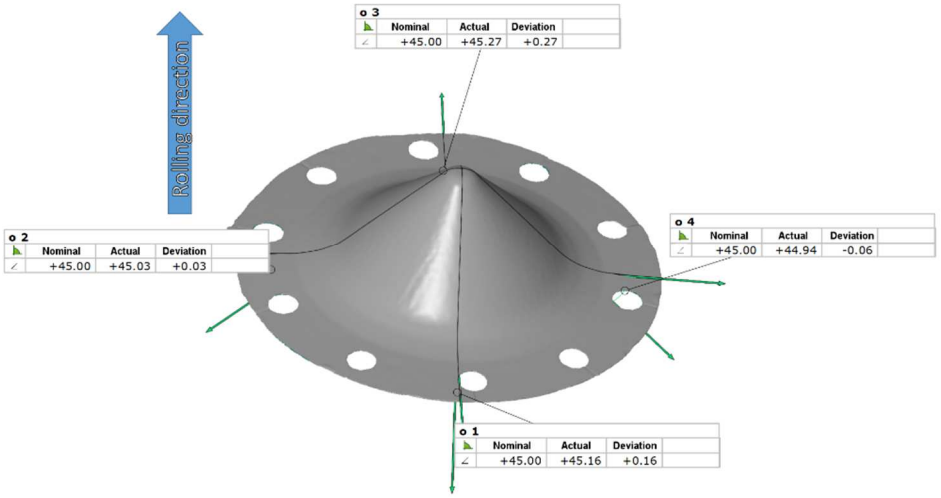

Fig. 6. Drawpiece wall angle scan using the ARGUS device

The ARGUS system allows thickness distribution analysis. The scan presented in Fig. 7 shows multilocation measurement of the drawpiece thickness. Taking into account the initial sheet thickness tolerance ±0.03 mm as well as measurement uncertainty of ARGUS device ±0.02 mm, a 0.357 mm (0,4 mm ± 0,05 mm) initial sheet thickness was obtained. Applying the sine law (Eq.1) theoretical thickness 0.252 mm ±0.05 mm should be achieved on a generatrix. All measurement points located at generatrix meet the criteria of the sine law equation (Fig. 7).

The inaccuracy caused mainly by a springback effect was revealed by analyzing the deviations scanned by ARGUS (Fig. 8). Large discrepancies were located at the initial stage of forming, where the bending zone appears. The bending zone is a part of the sheet where tool-workpiece contact does not exist; however, the sheet bends under the forming forces in the process. The vertex of the drawpiece is also burdened with shape error caused by the tool retraction from the workpiece and also high acceleration demanded by the CNC machine to achieve the set feed rate on a short path. Such a quick change of axis movement direction also causes vibrations of the entire system, which negatively effects accuracy. Lower deviations can be observed at the generatrix located in accordance with the rolling direction +0.09/-0.051 mm, while perpendicular to the rolling direction +0.151/-0.096 mm.

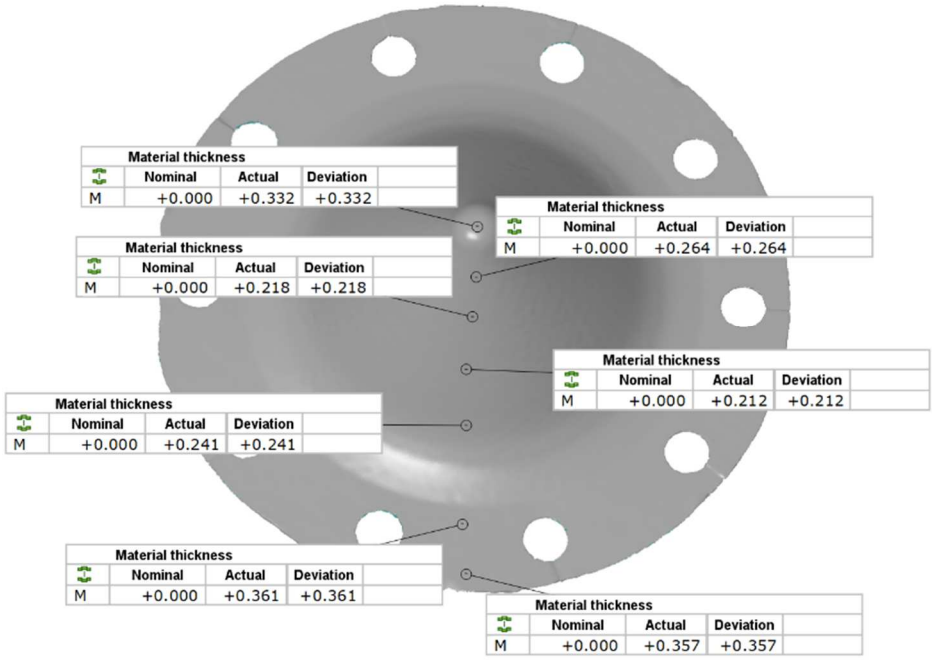

Fig. 7. The sheet thickness distribution measured by ARGUS system

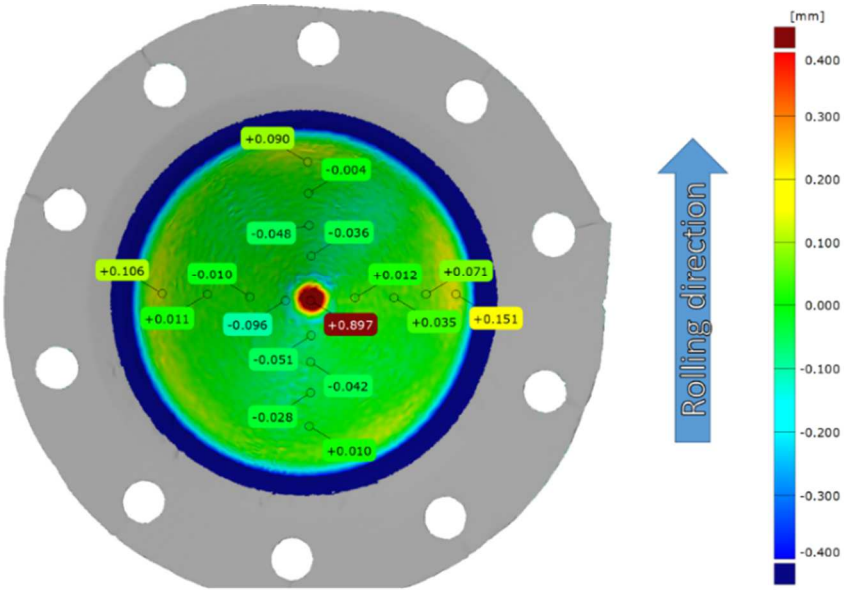

Fig. 8. Drawpiece shape deviations measured using ARGUS system

Tomography X-ray devices has possibilities to obtain multiple high resolution intersections of the measured part. This option allows one to inspect the drawpiece in case of internal cracks or breakages. It is also possible to compare the obtained drawpiece with reference to the CAD geometry. The high resolution intersection analysis of the tomography approved that there was no internal crack or break in the drawpiece. Figure 9 presents deviations of the captured cross section. The maximum shape error is located in a bending zone.

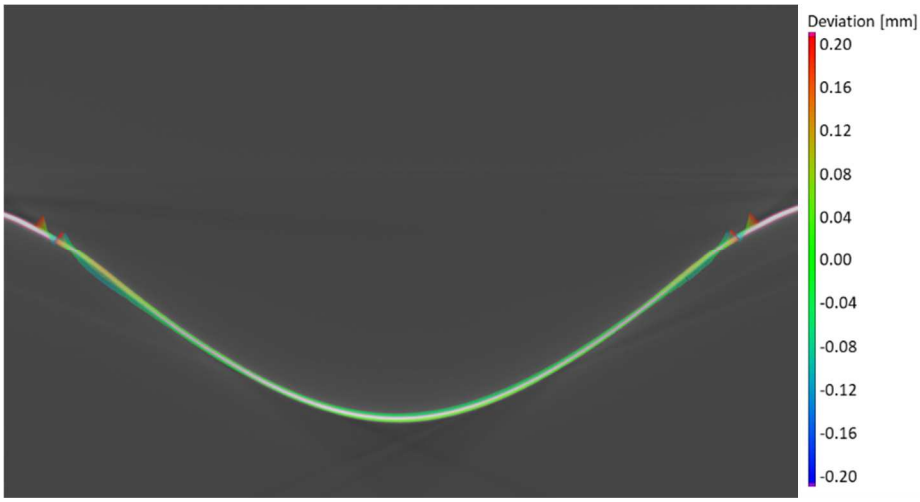

Fig. 9. One of the drawpiece sections with marked deviations captured using X-ray tomography

4. Conclusions

In this research paper, the springback effect on the accuracy of the drawpiece has been investigated. The optical measurement system has been applied to the wall angle discrepancy, drawpiece thinning analysis, as well as deviations from the reference CAD model. The following conclusions can be drawn:

- The blank rolling direction significantly affects the springback, which resulted in a difference in drawpiece deviations.
- The sine law can be applied to predict the wall thickness of the generatrix of the 45° cone drawpiece with optimal parameters.
- X-ray tomography analysis allows for a drawpiece fracture detection as well as deviation analysis. The achieved drawpiece does not contain gaps or breakages in material continuity.
- The measured deviations of the frustum cone formed with optimized parameters are as follows: wall angle +0.27°/-0.06°, generatrix thickness +0.012/-0.04 mm and deviation from the reference CAD geometry +0.151/-0.096 mm.

- To reduce deviations at the vertex of the frustum cone, tool feed reduction may be applied at the end of the forming path or vertical (axial) plunging while the tool axis overlaps the drawpiece axis.

References

Behera, A. K., de Sousa, R. A., Ingarao, G., & Oleksik, V. (2017). Single point incremental forming: An assessment of the progress and technology trends from 2005 to 2015. Journal of Manufacturing Processes, 27, 37–62. https://doi.org/10.1016/j.jmapro.2017.03.014

Cédric, B., Pierrick, M., & Sébastien, T. (2020). Shape Accuracy Improvement Obtained by μ-SPIF by Tool Path Compensation. Procedia Manufacturing, 47, 1399–1402. https://doi.org/10.1016/j.promfg.2020.04.293

Chen, J., Qian, J., & Wang, H. (2017). Study on Wall Thickness Prediction Accuracy by Sine Law for Incrementally Formed Conical Parts. Zhongguo Jixie Gongcheng/China Mechanical Engineering, 28, 2760–2766. https://doi.org/10.3969/j.issn.1004-132X.2017.22.017

Cheng, R., Wiley, N., Short, M., Liu, X., & Taub, A. (2019). Applying ultrasonic vibration during single-point and two-point incremental sheet forming. Procedia Manufacturing, 34, 186–192. https://doi.org/10.1016/j.promfg.2019.06.137

Cheng, Z., Li, Y., Li, J., Li, F., & Meehan, P. A. (2022). Ultrasonic assisted incremental sheet forming: Constitutive modeling and deformation analysis. Journal of Materials Processing Technology, 299, 117365. https://doi.org/10.1016/j.jmatprotec.2021.117365

Harhash, M., & Palkowski, H. (2021). Incremental sheet forming of steel/polymer/steel sandwich composites. Journal of Materials Research and Technology, 13, 417–430. https://doi.org/10.1016/j.jmrt.2021.04.088

Honarpisheh, M., Ebrahimi, M. R., & Mansouri, H. (2019). Investigation of Springback Angle in Single Point Incremental Forming Process on Explosive Welded Cu/St/Cu Multilayer. Journal of Modern Processes in Manufacturing and Production, 8(3), 13–26.

Jain, P. S., Kagzi, S. A., Patel, S., & Vasava, J. (2021). An analysis of the effect of various parameters on surface roughness, springback and thinning while performing single point incremental forming on polypropylene sheet. Proceedings of the Institution of Mechanical Engineers, Part E: Journal of Process Mechanical Engineering, 09544089211047203. https://doi.org/10.1177/09544089211047203

Jung, K.-S., Yu, J.-H., Chung, W.-J., & Lee, C.-W. (2020). Tool Path Design of the Counter Single Point Incremental Forming Process to Decrease Shape Error. Materials, 13(21), 4719. https://doi.org/10.3390/ma13214719

Karim, B., Mohand, O. O., Nasereddine, Z., & Sébastien, T. (2021). Investigation of the influence of incremental sheet forming process parameters using response surface methodology. Metallurgical Research & Technology, 118(4), 401. https://doi.org/10.1051/metal/2021039

Khan, M. S., Coenen, F., Dixon, C., El-Salhi, S., Penalva, M., & Rivero, A. (2015). An intelligent process model: Predicting springback in single point incremental

forming. The International Journal of Advanced Manufacturing Technology, 76(9–12), 2071–2082. https://doi.org/10.1007/s00170-014-6431-1

Li, Y., Chen, X., Liu, Z., Sun, J., Li, F., Li, J., & Zhao, G. (2017). A review on the recent development of incremental sheet-forming process. The International Journal of Advanced Manufacturing Technology, 92(5–8), 2439–2462. https://doi.org/10.1007/s00170-017-0251-z

Liao, J., Zhou, S., & Xue, X. (2022). Twist Springback and Microstructure Analysis of PEEK Sheets in Ultrasonic-Assisted Thermal Incremental Forming [Preprint]. In Review. https://doi.org/10.21203/rs.3.rs-1561711/v1

Liu, Z. (2018). Heat-assisted incremental sheet forming: A state-of-the-art review. The International Journal of Advanced Manufacturing Technology, 98(9), 2987–3003. https://doi.org/10.1007/s00170-018-2470-3

Martins, P. A. F., Bay, N., Skjoedt, M., & Silva, M. B. (2008). Theory of single point incremental forming. CIRP Annals, 57(1), 247–252. https://doi.org/10.1016/j.cirp.2008.03.047

Mezher, M., Barrak, O., Nama, S., & Shakir, R. (2021). Predication of Forming Limit Diagram and Spring-back during SPIF process of AA1050 and DC04 Sheet Metals. Journal of Mechanical Engineering Research and Developments, 41, 337–345.

Micari, F., Ambrogio, G., & Filice, L. (2007). Shape and dimensional accuracy in Single Point Incremental Forming: State of the art and future trends. Journal of Materials Processing Technology, 191(1–3), 390–395. https://doi.org/10.1016/j.jmatprotec.2007.03.066

Mostafanezhad, H., Menghari, H. G., Esmaeili, S., & Shirkharkolaee, E. M. (2018). Optimization of two-point incremental forming process of AA1050 through response surface methodology. Measurement, 127, 21–28. https://doi.org/10.1016/j.measurement.2018.04.042

Murugesan, M., Yu, J.-H., Jung, K.-S., Cho, S.-M., Bhandari, K. S., & Lee, C.-W. (2022). Optimization of Forming Parameters in Incremental Sheet Forming of AA3003-H18 Sheets Using Taguchi Method. Materials, 15(4), 1458. https://doi.org/10.3390/ma15041458

Oleksik, V., Pascu, A., Bondrea, I., Avrigean, E., & Rosca, L. (2014). Comparative Study for Springback Prediction on Single Point Incremental Forming Process. Key Engineering Materials, 622–623, 375–381. https://doi.org/10.4028/www.scientific.net/KEM.622-623.375

Orteu, J.-J., Bugarin, F., Harvent, J., Robert, L., & Velay, V. (2011). Multiple-Camera Instrumentation of a Single Point Incremental Forming Process Pilot for Shape and 3D Displacement Measurements: Methodology and Results. Experimental Mechanics, 51(4), 625–639. https://doi.org/10.1007/s11340-010-9436-1

Rusu, G. P., Bârsan, A., Popp, M. O., & Maroșan, A. (2021). Comparison between aluminum alloys behavior in incremental sheet metal forming process of frustum pyramid shaped parts. IOP Conference Series: Materials Science and Engineering, 1009(1), 012054. https://doi.org/10.1088/1757-899X/1009/1/012054

Shi, Y., Zhang, W., Cao, J., & Ehmann, K. F. (2019). Experimental study of water jet incremental micro-forming with supporting dies. Journal of Materials Processing Technology, 268, 117–131. https://doi.org/10.1016/j.jmatprotec.2019.01.012

Su, C., Lv, S., Wang, R., Lv, Y., Lou, S., Wang, Q., & Guo, S. (2021). Effects of forming parameters on the forming limit of single-point incremental forming of sheet metal. The International Journal of Advanced Manufacturing Technology, 113(1–2), 483–501. https://doi.org/10.1007/s00170-020-06576-0

Szpunar, M., Ostrowski, R., Trzepieciński, T., & Kaščák, Ľ. (2021). Central Composite Design Optimisation in Single Point Incremental Forming of Truncated Cones from Commercially Pure Titanium Grade 2 Sheet Metals. Materials, 14(13), 3634. https://doi.org/10.3390/ma14133634

Wang, H., Zhang, R., Zhang, H., Hu, Q., & Chen, J. (2018). Novel strategies to reduce the springback for double-sided incremental forming. The International Journal of Advanced Manufacturing Technology, 96(1–4), 973–979. https://doi.org/10.1007/s00170-018-1659-9

Wang, Y., Wang, L., Zhang, H., Gu, Y., & Ye, Y. (2022). A Novel Algorithm for Thickness Prediction in Incremental Sheet Metal Forming. Materials, 15(3), 1201. https://doi.org/10.3390/ma15031201

DOKŁADNOŚĆ KSZTAŁTU W JEDNOPUNKTOWYM KSZTAŁTOWANIU PRZYROSTOWYM STOŻKÓW ŚCIĘTYCH Z BLACH TYTANOWYCH CP2

S t r e s z c z e n i e

W pracy przedstawiono analizę wytłoczek w kształcie stożka ściętego wykonanego z blachy tytanowej CP2 metodą jednopunktowego przyrostowego kształtowania. Do przeprowadzenia eksperymentu obejmującego 20 przebiegów przyjęto centralny plan kompozycyjny, następnie dokonano wielokryterialnej optymalizacji parametrów. Dokonano walidacji optymalnych parametrów, a uzyskane wyniki nie przekraczają 4% w odniesieniu do stworzonych modeli. Dla wytłoczki uformowanej z optymalnymi parametrami zastosowano pomiar optyczny AGRUS oraz tomografię rentgenowską w celu sprawdzenia uzyskanej grubości ścianki wytłoczki i odchyłek w porównaniu z modelem CAD. Przeanalizowano również rozbieżność kątów ścian tworzących stożka. Za pomocą skanu rentgenowskiego potwierdzono brak szczelin i pęknięć wytłoczki. Kierunek walcowania półfabrykatu ma istotny wpływ na odchyłki. Wyniki pomiarów wykazały odchylenia kąta ścianki wytłoczki +0,27/-0,06°, grubości ścianki na stożku +0.012/-0.04 mm oraz +0.151/-0.096 mm od geometrii referencyjnej CAD.

Słowa kluczowe: kształtowanie przyrostowe blach, tytan, sprężynowanie, analizy optyczne kształtowania, komputerowa tomografia.

DOI: 10.7862/rm.2022.5

Submitted/Tekst złożono w redakcji: July 2022
Accepted / Przyjęto do druku: September 2022
Published/Tekst opublikowano: December 2022

ZESZYTY NAUKOWE POLITECHNIKI RZESZOWSKIEJ – MECHANIKA
SCIENTIFIC LETTERS OF RZESZOW UNIVERSITY OF TECHNOLOGY – MECHANICS
94 (2022), s. 77-89

Maria TYCHANICZ-KWIECIEŃ [1]

THE APPLICATION OF THE WILSON PLOT METHOD TO CONVECTIVE HEAT TRANSFER – LAST ACHIEVEMENTS

Abstract: The paper discusses and presents the application of the Wilson plot method to the variety of issues related to convective heat transfer. The Wilson plot is a remarkable calculation procedure, which enables the analysis and estimation of convection heat transfer coefficient on the basis of experimental measurements of heat exchanger thermal and flow parameters and the evaluation of corresponding correlation equations. The main facility of the Wilson method is that the heat transfer coefficient can be obtained without the requirement of determining the surface temperature. Much attention was paid to clarify the concept of the standard, original Wilson method as well as its modified versions. The issue was presented in the form of the latest literature review, which featured the investigation of convection coefficients obtained by the Wilson method in the following cases: the flow of nanofluids, refrigerants and other working media in conventional and mini/micro channels and micro-tubes as well as heat transfer under boiling/condensation conditions. The validity of the method utilization has been presented and its future prospects have been specified.

Keywords: Wilson plot, convective heat transfer, thermal characteristics, heat exchanger

Nomenclature

A – heat transfer area
A_c – heat transfer area of the cold side
A_h – heat transfer area of the hot side
c_c – specific heat capacity of cold fluid
c_h – specific heat capacity of hot fluid
d_c – diameter on the inner side of the tube

[1] Corresponding author: Maria Tychanicz-Kwiecień, Rzeszow University of Technology, Faculty of Mechanical Engineering and Aeronautics, Department of Thermodynamics, al. Powstańców Warszawy 12, 35-959 Rzeszów, e-mail: mtychanicz@prz.edu.pl, ORCID ID: 0000-0003-4312-2772

d_h – diameter on the outer side of the tube
h_c – heat transfer coefficient of the cold side
h_h – heat transfer coefficient of the hot side
L – tube length
m – mass
R_c – thermal resistance of the cold fluid
R_h – thermal resistance of the hot fluid
R_{ovr} – overall thermal resistance
R_w – thermal resistance of the wall
U – overall heat transfer coefficient
v_r – reduced velocity
ΔT_c – temperature difference of the cold side
ΔT_h – temperature difference of the hot side
ΔT_{log} – logarithmic mean temperature difference
$\dot{Q}$ – heat transfer rate
λ_w – thermal conductivity of the wall

1. Introduction

Heat transfer occurs by convection, conduction and radiation. As far as convective heat transfer is concerned, the amount of energy transferred between the solid body and surrounded fluid for a certain temperature difference, is described by the Newton's Law of cooling. It states that heat transfer rate is obtained by the temperature difference between the surface and the fluid, surface area and heat transfer coefficient.

Experimental measurements of heat exchangers require the determination of mean heat transfer coefficients on both sides of heat transfer surface area. The description of convection heat transfer is very complex and the analytical solution requires solving of mass, momentum and energy conservation equations for a specified geometry and fluid properties (Fernández-Seara, Uhía, & Sieres, 2007). Due to complexity of this approach, it is restricted to simple geometrical configurations of heat exchangers and flow passages. In the majority of real-life cases, heat exchangers are of advanced geometry and therefore analytical approach in determination of local heat transfer coefficient is no longer applicable.

According to the Newton's Law of cooling, the experimental determination of heat transfer coefficient (HTC) can be accomplished by measuring temperatures of the surface and the fluid for prescribed geometry, flow and heat conditions (Fernández-Seara, Uhía, Sieres, et al., 2007). However, direct determination of HTC is not always a straightforward task. The experimental approach can be troublesome and not always feasible due to practical obstacles concerning precise measurement of the surface temperature, e.g. the measurement limitations of the temperature sensors or the impossibility of accurate measurement of this

temperature. It is also possible that inserting the temperature sensor may disturb the flow field and thereby the temperature distribution. The problem is even more complex with reference to mini- and micro-heat exchangers, where thermal measurements are frequently tough due to small flow passages.

Therefore, an alternative methodologies have been sought, where the experimental determination of surface temperature was not required. These difficulties can be avoided by applying the Wilson plot method, which is characterized by simplicity and widespread application in experimental investigations of heat exchangers.

Wilson method is a technique used for obtaining heat transfer coefficient of individual working fluid, which is based on the determination of overall heat transfer coefficient for variable flow velocity. The Wilson method allows the estimation of convective heat transfer coefficients in a variety of heat transfer problems. It is based on accurate thermal balance of investigated heat exchanger, which requires the evaluation of the overall thermal resistance (Mikielewicz, 2001). From the practical side, it relies on experimental determination of heat exchanger inlet and outlet thermal and flow parameters, while heat transfer coefficient is obtained from corresponding correlation equation and linear regression analysis. Due to the variety of investigated heat transfer cases and extensive development of heat exchangers with progressively more sophisticated geometry, the method has undergone series of modifications in recent years and currently it represents a universal measuring technique applied to broadly defined convective heat transfer.

This paper focuses on the description of research facilities of the Wilson plot method and its application in convective heat transfer research field. The issue was presented on the basis of current open literature and the main focus was put on the determination of thermal characteristics in minichannel heat exchangers and microtubes, also with two-phase heat transfer and during flow of nanofluids and refrigerants. The general concept of the original Wilson method and its validity have been presented and its future prospects have been specified.

2. The description of the standard Wilson method

The development threshold of the Wilson method is dated back to 1915 (Wilson, 1915). It was first applied to the shell and tube heat exchanger in the case of water flow inside a smooth circular tube and vapour condensation on the outer side in order to obtain convective heat transfer coefficients. The main concept of the Wilson method is to separate the overall thermal resistance into individual ones derived from hot and cold fluid convection and conduction through separating wall (Styrylska & Lechowska, 2003), what enables the evaluation of individual heat transfer coefficients. Overall thermal resistance is obtained from experimental measurements, particularly inlet and outlet flow rates and

temperatures, on the basis of which the thermal balance of investigated heat exchanger is performed.

In the first approach, Wilson has made several assumptions regarding his method (Sieres, 2020):

- thermal resistances of the wall R_w and of one fluid are constant,
- the heat transfer correlation equation for other fluid is known,
- variations of fluid properties are neglected,
- fouling effects resistance are neglected.

In order to employ the original Wilson method in practise, it is crucial to schedule a series of measurements in a way to keep the flow rate of cold fluid at a constant level and the flow rate on the shell side can be varied arbitrary. Afterwards the order is reversed, which means that the flow rate of the other fluid is established, while the flow rate of the previously constant fluid is changed. It is assumed that during the variation of flowrate, the variation of overall thermal resistance is influenced by the variation of heat transfer coefficient. The thorough description of the concept of the original Wilson method is presented below.

Thermal energy balance of the heat exchanger can be expressed as:

$$\dot{Q} = m_c \cdot c_c \cdot \Delta T_c = m_h \cdot c_h \cdot \Delta T_h \tag{1}$$

At the same time, heat transfer rate can be written with the use of overall heat transfer coefficient U, heat transfer area A and logarithmic mean temperature difference ΔT_{log}:

$$\dot{Q} = U \cdot A \cdot \Delta T_{log} \tag{2}$$

The product of overall heat transfer coefficient and heat transfer area gives the inverse of overall thermal resistance, which is described by the formula:

$$\frac{1}{R_{ovr}} = U \cdot A \tag{3}$$

Thus, the combination of Eq. (2) and Eq. (3) provides the expression of the overall thermal resistance:

$$R_{ovr} = \frac{\Delta T_{log}}{\dot{Q}} \tag{4}$$

According to Fernández-Seara, Uhía, Sieres et al. (2007) and Sieres (2020), the overall thermal resistance R_{ovr} can be also expressed as a sum of three thermal resistances, which correspond to the cold and hot fluid flow R_c and R_h respectively, and wall thermal resistance R_w, as shown below:

$$R_{ovr} = R_c + R_w + R_h \tag{5}$$

The Eq. (5) can be expanded to the following, more detailed form:

$$R_{ovr} = \frac{1}{h_c \cdot A_c} + \frac{ln\left(\frac{d_h}{d_c}\right)}{2\pi \cdot \lambda_w \cdot L} + \frac{1}{h_h \cdot A_h} \tag{6}$$

It is relevant that Eq. (6) is applicable for cylindrical cross section geometries. If the outer flow is maintained constant, then the corresponding thermal resistances of the hot fluid and the wall, can be also considered constant, which can be written as:

$$R_w + R_h = C_1 \tag{7}$$

Moreover, when assuming constant fluid properties (Fernández-Seara et al., 2005), heat transfer coefficient of the cold fluid during fully developed turbulent flow is proportional to the power function of reduced velocity:

$$h_c = v_r^n \cdot C_2 \tag{8}$$

Therefore, thermal resistance of the cold fluid is proportional to the inverse of the power function of reduced velocity. Hence, the combination of equations (6), (7) and (8), yields to the overall thermal resistance expressed in a form:

$$R_{ovr} = \frac{1}{C_2 \cdot A_c} \cdot \frac{1}{v_r^n} + C_1 \tag{9}$$

Equation (9) has a form of a linear function $y = ax + b$, with a slope equal to $\frac{1}{C_2 \cdot A_c}$ and absolute term b equal to constant C_1 , which is an interception of the line with y-axis. The graphic presentation of the original Wilson plot technique was shown in Fig. 1.

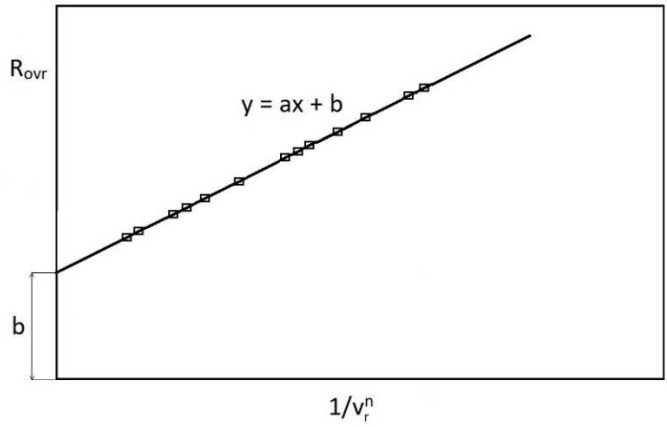

Fig. 1. Graphic interpretation of the standard Wilson plot method

The value of the exponent n in Eq. (9) is selected in such a way that experimentally obtained overall thermal resistance can be represented as a linear function of the expression $\frac{1}{v_r^n}$. The value of n is usually 0.8, however it may be sometimes corrected in order to best fit the experimental results. The straight line equation, which matches the experimental data, is determined analytically by applying linear regression analysis methods. Therefore, constants C_1 and C_2 can be estimated and the inside and outside convection coefficients can be assessed as a function of the cooling liquid velocity (Fernández-Seara, Uhía, Sieres et al., 2007; Fernández-Seara et al., 2005). With the first development of the Wilson method, some general correlations describing the convective heat transfer have appeared in the open literature, which are still in use so far.

Wilson plot method is applicable when thermal resistances on both sides of heat exchanger are of the same order as well as when both fluid flows are uniform. In the original method it is essential to maintain the flow of one fluid constant while altering the flow rate of other fluid, which is often uncomfortable. Moreover, the method is appropriate when the flow on the inner side of the heat exchanger is turbulent and fully developed.

Primary modifications of the Wilson method were characterized by the fact that the mass flow of the fluid was varied as a function of the Reynolds and Prandtl numbers. Nusselt number correlation used to obtain convective coefficients combined the Reynolds and Prandtl numbers, which has a form of Eq. (10):

$$Nu = C \cdot Re^n \cdot Pr^m \tag{10}$$

For simplicity, the values of exponents n and m have to be established first.

Further modifications of the Wilson method resulted from certain limitations imposed by the original version of the method, which is based on number of assumptions, including the consistency of the outside convection coefficient and neglecting the fouling effects as well as prescribed values of n and m exponents of Reynolds and Prandtl numbers in Nusselt number correlation. In the case when either of the condition cannot be accomplished, e.g. the occurrence of surface roughness, which depends on tube design and condition, the parameters initially assumed constant, will vary. Therefore, more advanced mathematical formulations are required to assign thermal parameters for investigated heat exchanger.

Van Rooyen (2012) presented current status and future perspectives of modified Wilson plots and several works have been quoted, in which the modifications of the Wilson plot have been applied. The modified versions of original Wilson plot enabled developing correlations for both the inside and outside heat transfer coefficients (Young, 1957) and the establishing of three parameters: constants C_c and C_h and an exponent in heat transfer coefficient correlation (Briggs, 1969). The prospects of determining two and more constants by applying second

linear regression have been widely described in (Fernández-Seara, Uhía, Sieres et al., 2007).

Many of the existing modifications of the Wilson method are not restricted to individual considered cases and can be successfully applied to other types of heat exchangers and flow conditions.

3. Literature review concerning Wilson plot

The subject of application of the Wilson method to various problems related to convective heat transfer, have been undertaken by many researchers throughout the years. Therefore, a brief overview of selected literature concerning the Wilson method, which covers approximately the last 20 years, was presented below. Particular attention was paid on determination of heat transfer coefficient in mini-, microchannels and conventional size channels with the flow of nanofluid, refrigerants and standard working media.

As far as Wilson plot method is concerned, the works of Fernandez-Seara et al. provided valuable general knowledge referring to this research field. The state-of-the-art review of both the original and modified Wilson plot methods was presented by Fernández-Seara et al., (2007). The fundamentals of Wilson method have been described and its various alternations have been reported. An experimental setup, which enabled the application of the Wilson method in practise and therefore to obtain heat transfer coefficients, was shown by Fernández-Seara et al. (2005). The trial measurements have been conducted and the standard and modified Wilson methods have been employed. It was noticed that the results of heat transfer coefficient obtained experimentally and determined from correlations were consistent. Then, Fernández-Seara, Uhía, & Sieres, (2007) proposed thermal characteristics of smooth and corrugated test tubes obtained by the Wilson method. The tubes have been experimentally investigated on the test stand presented by Fernández-Seara et al. (2005). Also results for both investigated configurations have been compared with standard correlations and satisfactory correspondence was achieved.

In the beginning of the XXI century, Wang et al. (1996) obtained heat transfer coefficients for microfin tubes by means of modified Wilson plot technique. The experiments were performed for several tube geometry inserted in a double-pipe heat exchanger with water as a working fluid. As a result, a general heat transfer correlation equation was suggested and the analysis concerning the selection of the appropriate correlation depending on the Reynolds number range, was presented.

The Wilson plot method was also applied to minichannel aluminium heat exchanger, as reported in (Fernando et al., 2008) for the purpose of determining correlations for single-phase heat transfer coefficients. The investigated heat exchanger had a form of a multiport minichannel tube with square shaped parallel

channels. It was found that experimentally obtained Nusselt number fit well with the Nusselt number predicted from correlation in transition flow regime. However, for the case of laminar flow none of the well-known correlation predicted the Nusselt number properly.

Koo et al. (2016) studied experimentally thermal and hydraulic characteristics of shell and helically coiled tube heat exchangers with two different tube types. Wilson plot method was used for obtaining the overall thermal resistance, which in investigated case was determined as a linear function of inverse Reynolds number to the power of m. The authors also provided a comparison of thermal and fouling characteristics between shell and helically coiled tube heat exchanger and brazed plate heat exchanger.

Baba et al. (2018) employed both original and modified Wilson methods to determine Nusselt number correlation for the case of water nanofluid flow inside double tube heat exchanger with longitudinal fins on internal side. The authors reported that applied Wilson method corresponded well with experimental data.

Convective heat transfer and flow characteristics in helical coil double pipe heat exchanger have been also presented by Sheeba et al., (2019). Wilson plot method was applied to determine heat transfer coefficients on both sides of the inner tube. Experimental measurements of heat exchanger have been supported by numerical investigations and satisfactory results correspondence has been obtained.

In original Wilson method it is assumed that one fluid flow is kept constant, while the other is changed. Rybiński et al. (2018) developed such a modification of Wilson method, where both flows and temperatures may be modified at the same time. The presented method was applied to minichannel heat exchanger in order to obtain its thermal characteristics, which were determined statistically. Experimental measurements have been conducted as well. The new method is based on the determination of regression function of corrected overall thermal resistance, which statistically estimates the experimental overall thermal resistance with the use of linear correction coefficients. It was stated that the method can be successfully applied to other types of heat exchangers.

Another crucial aspect connected to the Wilson plot method is the uncertainty of experimental measurements. According to Rose (2004), theoretical considerations affecting the accuracy of temperature measurements in terms of applicability and usefulness of Wilson plot technique has been conducted. The author has also specified other certain factors essential for validity and accuracy of results obtained.

The uncertainty analysis applied to the results obtained by the Wilson plot method for the case of vapour condensation on horizontal plain tubes has been studied by Uhia et al. (2013). The general uncertainty propagation equation has been used. It was noticed that the influence of uncertainty of water temperature measurement on the experimental heat transfer coefficient obtained by the Wilson

plot method was supreme and slight impact of uncertainty of flow rate measurements and vapour temperature has been observed.

The collective specification of abovementioned references is shown in Table 1.

Table 1. Summary of a brief overview of selected literature concerning the Wilson method

Reference	Subject of study	Type of investigated heat exchanger	Conclusions
(Fernández-Seara, Uhía, Sieres, et al., 2007)	Review of the original and modified Wilson plot methods	-	Wide range of application of the Wilson method, the method can be used to analyse various convective heat transfer problems
(Fernández-Seara et al., 2005)	The presentation of an experimental setup for the application of the Wilson method in practise	Smooth tube and a spirally corrugated tube	The consistency of results of heat transfer coefficient obtained experimentally and determined from correlations
(Wang et al., 1996)	Single-phase heat transfer and pressure drop characteristics	Microfin tubes inserted in a double-pipe heat exchanger	A suggestion of general heat transfer correlation equation depending on the range of Reynolds number

Table 1. *Cont.*

(Fernando et al., 2008)	Determining correlations for single-phase heat transfer coefficients	Multiport minichannel aluminium heat exchanger	In transition flow regime experimentally obtained Nusselt number matched the predicted Nusselt number and for laminar flow compliance was not achieved
(Kyoungmin Koo, 2016)	The studies of experimental thermal and hydraulic characteristics with the use of Wilson plot to obtain overall thermal resistance	Shell and helically coiled tube heat exchangers with two different tube types	The comparison of thermal and fouling characteristics between shell and helically coiled tube heat exchanger and brazed plate heat exchanger
(Baba et al., 2018)	The determination of Nusselt number correlations with the use of original and modified Wilson methods	Double tube heat exchanger with longitudinal fins with water nanofluid flow	Applied Wilson method corresponded well with experimental data
(Sheeba et al., 2019)	Convective heat transfer with the use of Wilson	Helical coil double pipe heat exchanger	Satisfactory correspondence of experimental

	plot and flow characteristics		and numerical results has been achieved
(Rybiński W., 2018)	The development of new modification of the Wilson method to statistically obtain thermal characteristics of heat exchangers	Minichannel heat exchanger	The determination of regression function of corrected overall thermal resistance with the use of linear correction coefficients
(Rose, 2004)	Theoretical considerations affecting the accuracy of temperature measurements in terms of applicability of Wilson method	-	The specifications of determinants essential for validity and accuracy of results in terms of heat transfer measurements
(Uhia et al., 2013)	The uncertainty analysis applied to the results obtained by the Wilson plot method	Horizontal plain tubes	Influence of uncertainty of water temperature measurement, of flow rate measurements and vapour temperature on the experimental heat transfer coefficient

4. Summary

This paper attempted to discuss the application capabilities of the Wilson plot method. The main concept of the original Wilson method has been presented and brief discussion of literature concerning Wilson plot method has been performed. For the purpose of the review featured in this paper, the most scientifically meaningful literature has been encapsulated, which referred to the last 20 years.

Wilson plot method is an outstanding calculation procedure of convective heat transfer coefficients, which constitutes a great potential of applicability in the context of heat exchangers and convective heat transfer in general. From the presented review it can be seen that Wilson method can be applied to both conventional and mini- and microchannel heat exchangers, where both the standard working media are used, as well as nanofluids and refrigerants, what proofs the versatility of the Wilson method. Despite that Wilson plot in its original form was developed over a century ago, it is still a valuable technique used to analyse heat transfer behaviour in simple heat exchanger configurations, both on the industrial and laboratory range. In addition, the modified versions of the Wilson method exceeded its applicability and overcome limitations imposed by primary method.

The greatest benefit of the Wilson technique is its simplicity and usefulness, especially when the temperature inside heat exchanger is impossible to determine, like in minichannel heat exchangers and microtubes. The method can be successfully adapted to almost every considered case with satisfactory accuracy. Due to the fact that there are a lot of modifications of the Wilson method and new

ones keep appearing progressively, it is possible to obtain a dataset of results obtained by this method for the variety of individual cases. The additional potential of the Wilson method lies in the possibility of developing a correlation equation for investigated heat transfer condition, which can be validated by well-known correlations described in literature.

The main disadvantage of the Wilson method is its susceptibility for temperature measurement errors, which implies that even for minor measurement errors, negative values of heat transfer coefficients can be obtained. Another inconvenience pertains to the assumption of keeping one flow constant during one series of measurements, however after so many modifications, this assumption can be withdrawn.

The convergence between experimental data trend and correlation equation used is main determinant of assessing Wilson method accuracy. Certainly, the efforts should be made to ensure that this match is as good as possible, what could be the subject of interest for future researchers.

Taking into account the abovementioned considerations and susceptibility of the Wilson method to various modifications, it can be concluded that Wilson technique belongs to the group of evolutionary research methods with exceedingly broad development prospectives.

References

Baba, M. S., Sita Rama Raju, A. V., & Bhagvanth Rao, M. (2018) Heat transfer enhancement and pressure drop of Fe3O4 -water nanofluid ina double tube counter flow heat exchanger with longitudinal fins. *Case Studies in Thermal Engineering*, 12, 600-607. https://doi.org/10.1016/j.csite.2018.08.001

Briggs, D. E., & Young, E. H. (1969). Modified Wilson plot techniques for obtaining heat transfer correlations for shell and tube heat exchangers. Chemical Engineering Progress Symposium Series: Vol. 65, No. 92 (pp. 35-45). AIChE, New York, NY.

Fernández-Seara, J., Uhía, F. J., Sieres, J., & Campo, A. (2005). Experimental apparatus for measuring heat transfer coefficients by the Wilson plot method. *European Journal of Physics*, *26*(3), N1. https://doi.org/10.1088/0143-0807/26/3/N01

Fernández-Seara, J., Uhía, F. J., & Sieres, J. (2007). Laboratory practices with the Wilson plot method. *Experimental Heat Transfer*, *20*(2), 123-135. https://doi.org/10.1080/08916150601091415

Fernández-Seara, J., Uhía, F. J., Sieres, J., & Campo, A. (2007). A general review of the Wilson plot method and its modifications to determine convection coefficients in heat exchange devices. *Applied Thermal Engineering*, *27*(17-18), 2745-2757. https://doi.org/10.1016/j.applthermaleng.2007.04.004

Fernando, P., Palm, B., Ameel, T., Lundqvist, P., & Granryd, E., (2008). A minichannels aluminum tube heat exchanger – Part I: Evaluation of single-phase heat transfer

coefficients by the Wilson plot method. *International Journal of Refrigeration*, *31*(4), 669-680. https://doi.org/10.1016/j.ijrefrig.2008.02.011

Koo, K., Hwang, J., Hur, H., Lee, J., Na, B., Hwang, Y., Kim, B., Ahn, Y. (2016). An experimental study on the thermal and fouling characteristics in a washable shell and helically coiled heat exchanger by the Wilson plot method. *Journal of Mechanical Science and Technology*, *30*(6), 2805-2812. https://doi.org/10.1007/s12206-016-0540-8

Mikielewicz, J. (2001). Wyznaczanie współczynników przenikania ciepła dla rekuperatorów metodą Wilsona. *Technika Chłodnicza i Klimatyzacyjna*, 10, 387-397.

Rose, J. W. (2004) Heat-transfer coefficients, Wilson plots and accuracy of thermal measurements. *Experimental Thermal and Fluid Sciences*, 28(2-3), 77-86. https://doi.org/10.1016/S0894-1777(03)00025-6

Rybiński, W., & Mikielewicz, J. (2018). Statistical method for the determination of the minichannels heat exchanger's thermal characteristics. *Energy*, 158, 139-147. https://doi.org/10.1016/j.energy.2018.05.175

Sheeba, A., Abhijith, C. M., Jose Prakash, M. (2019). Experimental and numerical investigations on the heat transfer and flow characteristics of helical coil heat exchanger. *International Journal of Refrigeration*, 99, 490-497. https://doi.org/10.1016/j.ijrefrig.2018.12.002

Sieres, J. (2020). Wilson plots and measurement accuracy. In J. Meyer, & M. Da Paepe (Eds.), *The art of measuring in the thermal sciences* (1st ed., pp. 490–497). CRC Press. https://doi.org/10.1201/9780429201622

Styrylska, T. B., & Lechowska, A. A. (2003). Unified Wilson plot method for determining heat transfer correlations for heat exchangers. *Transactions of the ASME*, *125*(4), 752-756. https://doi.org/10.1115/1.1576810

Uhia, F. J., Campo, A., & Fernandez-Seara, J. (2013). Uncertainty analysis for experimental heat transfer data obtained by the Wilson plot method. *Thermal Science*, *17*(2), 471-487. https://doi.org/10.2298/TSCI110701136U

Wang, C. C., Chiou, C. B., & Lu, D. C. (1996). Single-phase heat transfer and fluid flow friction correlations for microfin tubes. *International Journal of Heat and Fluid Flow*, 17(5), 500-508. https://doi.org/10.1016/0142-727X(96)00048-3

Wilson, E. E. (1915). A basis for rational design of heat transfer apparatus. *Transactions of ASME*, 37, 47-70.

Young, E. H., & Wall, J. R. (1957). Development of an apparatus for the measurement of low bond resistance in finned and bare duplex tubing. Engineering Research Institute, University of Michigan. Report No. 48.

ZASTOSOWANIE METODY WILSONA W ZAGADNIENIACH KONWEKCYJNEJ WYMIANY CIEPŁA – OMÓWIENIE

Streszczenie

W artykule omówiono i przedstawiono zastosowanie metody Wilsona w różnorodnych zagadnieniach związanych z wymianą ciepła na drodze konwekcji. Metoda Wilsona pozwala na analizę i określenie konwekcyjnego współczynnika przejmowania ciepła na podstawie eksperymentalnych pomiarów parametrów cieplnych i przepływowych badanego wymiennika ciepła oraz zastosowanie

lub opracowanie odpowiednich zależności korelacyjnych. Szczególnym atutem metody Wilsona jest możliwość określenia współczynnika przejmowania ciepła bez konieczności pomiaru temperatury powierzchni badanego wymiennika ciepła Dużo uwagi poświęcono wyjaśnieniu koncepcji standardowej, oryginalnej metody Wilsona oraz jej zmodyfikowanych wersji. Zagadnienie zostało przedstawione w formie przeglądu literatury, w którym uwzględniono podsumowanie wyników badań współczynników przejmowania ciepła uzyskanych metodą Wilsona w następujących przypadkach: przepływu nanocieczy, czynników chłodniczych i innych mediów roboczych w kanałach konwencjonalnych i mini/mikrokanałach oraz mikrorurkach, jak również wymianę ciepła podczas wrzenia/kondensacji. Przedstawiono zasadność wykorzystania metody oraz określono jej perspektywy na przyszłość.

Słowa kluczowe: metoda Wilsona, wymiana ciepła, charakterystyka cieplna, wymiennik ciepła

DOI: 10.7862/rm.2022.6

Submitted/Tekst złożono w redakcji: October 2022
Accepted / Przyjęto do druku: November 2022
Published/Tekst opublikowano: December 2022

Informacje dodatkowe

1. Lista recenzentów współpracujących będzie zamieszczona na stronie internetowej:

   http://oficyna.prz.edu.pl/pl/zeszyty-naukowe/mechanika/

2. Zasady recenzowania są udostępnione na stronie internetowej:

   http://oficyna.prz.edu.pl/zasady-recenzowania/

3. Informacje dla autorów artykułów są udostępnione na stronie internetowej:

   http://oficyna.prz.edu.pl/informacje-dla-autorow/

4. Formularz recenzji jest udostępniony na stronie internetowej:

   http://oficyna.prz.edu.pl/pl/zeszyty-naukowe/mechanika/

5. Instrukcja dla autorów omawiająca szczegółowo strukturę artykułu, jego układ, sposób przygotowywania materiału ilustracyjnego i piśmiennictwa jest zamieszczona na stronach internetowych:

   http://oficyna.prz.edu.pl/pl/instrukcja-dla-autorow/

   oraz

   http://oficyna.prz.edu.pl/pl/zeszyty-naukowe/mechanika/

   w zakładce „Instrukcja dla autorów".

6. Dane kontaktowe do redakcji czasopisma, adresy pocztowe i e-mail do przesłania artykułów oraz dane kontaktowe do wydawcy są podane na stronie internetowej (Komitet Redakcyjny):

   http://oficyna.prz.edu.pl/pl/zeszyty-naukowe/mechanika/

Zasady recenzowania, informacje dla autorów, formularz recenzji, instrukcja dla autorów i dane kontaktowe do redakcji czasopisma i wydawcy są zamieszczone na stronie internetowej czasopisma:

http://oficyna.prz.edu.pl/pl/zeszyty-naukowe/mechanika/

oraz

https://journals.prz.edu.pl/amme